DNA Origami as a Tool for Single-Molecule Fluorescence Studies

Ingo H. Stein

München 2012

DNA Origami as a Tool for Single-Molecule Fluorescence Studies

Ingo H. Stein

Dissertation

durchgeführt an der Fakultät für Physik

der Ludwig–Maximilians–Universität

München

vorgelegt von

Ingo H. Stein

geboren in Dachau

München, den 27.4.2012

Erstgutachter: Prof. Dr. Philip Tinnefeld

Zweitgutachter: Prof. Dr. Tim Liedl

Tag der mündlichen Prüfung: 5.6.2012

Zusammenfassung

Untersuchungen auf Basis von Einzelmolekülfluoreszenz werden weltweit standardmäßig eingesetzt. Besonders Fluoreszenz-Resonanzenergietransfer (FRET) hat als experimentelles Werkzeug dazu beigetragen Konformationsänderungen und Interaktionen von Biomolekülen aufzudecken. Mit der DNA-Origami-Methode wurde vor Kurzem eine Technik vorgestellt, die es erlaubt auf der Nanoskala Objekte mit DNA als Baumaterial zu formen. Wie in dieser Arbeit gezeigt wird, kann die DNA-Nanotechnologie auf einfache Weise mit Einzelmolekül-FRET-Messungen kombiniert werden, was neuartige wissenschaftliche Entwicklungsmöglichkeiten schafft.

Unter Anbetracht der Fortschritte von Einzelmolekültechniken ist die Qualität der einzelnen Farbstoffmoleküle das Nadelöhr für viele Anwendungen. Gerade deshalb ist ein Verständnis der photophysikalischen Eigenschaften von Farbstoffen unabdingbar um erfolgreich Einzelmolekülexperimente durchführen zu können. Im ersten Teil dieser Dissertation geht es um grundlegende Erkenntnisse in Bezug auf charakteristische Eigenschaften von Fluoreszenzmolekülen. Das typische Phänomen des Blinkens einzelner Moleküle wird für die homologe Reihe der Cyanin-Farbstoffe untersucht. Es wird ein Modell erarbeitet, dass die Vorhersage von Blinkeigenschaften von Fluorophoren auf Basis von Parametern wie dem Redoxpotential und der Größe des Chromophors erlaubt. Die Vorhersagen werden experimentell überprüft durch die Auswertung des zeitlichen Verlaufs der Fluoreszenz einzelner immobilisierter Farbstoffmoleküle.

Um die Abstandsabhängigkeit von FRET zu charakterisieren, wurden bisher verschiedene Ansätze für die Konstruktion eines molekularen Maßstabes durchgeführt, unter anderem basierend auf doppelsträngiger DNA oder dem Polypeptid Polyprolin als Abstandshalter. Es wird gezeigt, dass mit Hilfe der DNA-Origami-Technik maßgeschneiderte molekulare Abstandshalter hergestellt werden können, die spezifisch auf die experimentellen Anfordungen abgestimmt sind. Ein starrer DNA-Origami-Block wurde entworfen, der als verlässlicher FRET-Maßstab auf Einzelmolekülebene einsetzbar ist. Dieses Verfahren bietet eine Reihe von eindeutigen Vorteilen im Vergleich zu bisherigen Systemen, die mit begrenzten Persistenzlängen und Probenheterogenität zu kämpfen hatten.

Das abschließende Projekt dieser Arbeit wurde von der Vorstellung geleitet, DNA-Origami-Strukturen als Steckbrett für molekulare photonische Schaltkreise einzusetzen. In Zukunft könnten lichtbasierte Schaltungen dabei helfen, die Einschränkungen der aktuellen Elektronik zu überwinden. Durch Verwendung der bemerkenswerten Adressierbarkeit von DNA-Origami-Objekten wurden vier spektral verschiedene Farbstoffmoleküle an genau definierten Positionen in ein DNA-Origami-Rechteck eingebaut, um ein spektroskopisches Netzwerk zu erzeugen. Die Besonderheit dieser Anordnung ist die Manipulierbarkeit des Energietransfer-Pfades, wobei ein Vermittler-Farbstoff das Licht zu zwei spektral verschiedenen Ausgängen leitet. Um diese Kontrolle über den Weg des Energietransfers sichtbar zu machen und um Subpopulationen zu sortieren, wurde eine neue experimentelle vierfarbige FRET-Technik entwickelt, die auf alternierender Laseranregung basiert.

Abstract

Single-molecule fluorescence studies have become a routine practice in laboratories worldwide. As an experimental tool, especially fluorescence resonance energy transfer (FRET) has helped to unravel conformational changes and interactions of biomolecules. With the DNA origami method a new technique to create nanoscale shapes with DNA as a building material was recently introduced. As shown in this work, DNA nanotechnology can be readily combined with single-molecule FRET experiments, opening up new scientific prospects.

With the progress of single-molecule techniques, the limiting factor for many applications is the quality of individual dye molecules. For successful single-molecule experiments, an understanding of the photophysical properties of dyes is essential. The first part of this thesis is devoted to providing fundamental insights into characteristic properties of fluorescent molecules. The common feature of single-molecule blinking is studied for the homologous series of cyanine dyes. A model is presented that allows predicting the blinking behavior of fluorophores, based on parameters such as the redox potential and chromophore size. The predictions are experimentally verified by evaluating fluorescence time transients of immobilized dye molecules.

To characterize the distance dependence of FRET, in the past several approaches have been made to build a molecular ruler, including double stranded DNA and the polypeptide polyproline as spacer molecules. It is demonstrated that the DNA origami technique allows creating tailored molecular spacers that are specifically engineered to meet experimental requirements. A rigid DNA origami block was designed that can be used as a reliable FRET ruler on the single-molecule level. This approach offers distinct advantages compared to previous systems that suffered from limited persistence lengths and sample heterogeneity.

The final project in this thesis was guided by the vision to use a DNA origami structure as a breadboard for molecular photonic circuits. In the future, light-based circuitry could help tackling limitations of current electronics. Exploiting the remarkable addressability of DNA origami objects, four spectrally distinct fluorophores were incorporated into a rectangular DNA origami at specific positions to create a spectroscopic network. The unique feature of this arrangement is that the energy transfer path can be manipulated by a mediator dye that guides the light to two spectrally distinct outputs. To visualize this control over the energy transfer path and for sorting of the subpopulations, a new experimental four-color FRET technique is developed, based on alternating laser excitation.

Contents

1 Introduction

Many of the fundamental processes of life occur on the length scale below one hundred nanometers. As a prominent example, the enzyme DNA polymerase that is responsible for replicating genetic information in the form of DNA has a diameter of approximately 10 nm, whereas a single DNA base is less than half a nanometer long. Manipulating and understanding biological processes in this size regime is the endeavor of the emerging field of nanobiotechnology that is at the interface between nanotechnology and biology and is also influenced by physics and chemistry.

Simply looking at structures with conventional microscopes is not possible for these dimensions, because of restrictions by the diffraction limit. For visible light this sets a limit to the achievable resolution of several hundred nanometers. To overcome this barrier, one alternative is to lower the wavelength, which is taken to the limit e.g. by electron microscopy. Therefore, the wavelength of the electrons is reduced up to a factor of 100.000 compared to visible light achieving a remarkable resolution of 50 pm [1]. Nevertheless, these methods are not suited for looking at biomolecules in their native environments, e.g. due to staining requirements of the samples. Another method, X-ray crystallography, also has the potential to yield high resolution structures down to the atomic level. Yet, for the technique to work the molecules of interest need to be crystallized. Although more than 60.000 protein structures have been determined, as currently listed online in the Protein Data Bank (PDB), several classes of proteins such as membrane proteins remain hard to crystallize. However, a more fundamental problem is that these techniques do not allow visualizing the dynamics of interaction processes but mainly give a static picture.

A completely different approach to visualizing biomolecules and their interactions is by fluorescence microscopy. In the last two decades especially single-molecule spectroscopy methods have taken a huge step forward. Fluorescence resonance energy transfer (FRET), which

is based on a distance dependent dipole-dipole interaction between individual fluorophores, is a valuable tool. It is now being routinely used as a 'spectroscopic ruler' in the range of $2-10\,\mathrm{nm}$ and even on the single-molecule level [2, 3]. With the aid of FRET, conformational changes as well as interactions between biomolecules can be studied. In contrast to ensemble techniques, with single-molecule approaches even subpopulations of heterogeneous samples as well as dynamics of tediously synchronizable systems can be investigated.

Furthermore, novel strategies of increasing optical resolution have emerged, based on the opportunities on the single-molecule level. Many of these so-called super-resolution microscopy techniques make use of the unique features of individual fluorophores to reconstruct super-resolved images, thereby braking the optical resolution limit [4, 5, 6, 7, 8].

At the current level, the limiting factor for most experiments relying on single-molecule fluorescence is the quality of the dye molecules. For instance, the maximum time for data acquisition is limited by the time before the molecules are irreversibly photobleached. This is obviously a serious issue for investigating dynamics over extended periods of time. Additionally, blinking of individual fluorophores, i.e. switching between a fluorescent and non-fluorescent state, can yield misleading results for FRET measurements. The photophysical fluctuations in intensity could be misinterpreted as distance changes between donor and acceptor molecules. However, the blinking of molecules can also be valuable for super-resolution techniques, as in Blink Microscopy [7]. Summing up, a fundamental understanding of fluorophore properties and photophysics is crucial for single-molecule experiments [9]. In chapter 3 the blinking behavior of commonly used cyanine fluorophores is investigated and potential implications for super-resolution microscopy are pointed out.

Apart from the task of visualization, a key objective of nanotechnology is the ability of manipulating objects on the nanoscale. For this aim, a new technique was introduced by Paul Rothemund in 2006 [10], termed 'DNA origami', that allows creating structures on the nanoscale by self-assembly using DNA as a building material (see section 2.5 for details). Apart from a mere assembly of the structures, diverse components such as fluorophores, biomolecules or nanoparticles can be incorporated at specific positions. Originally presented for the construction of two-dimensional objects with lateral dimensions on the order of 100 nm, the technique was quickly advanced to also create three-dimensional objects, even allowing for curved and pre-stressed nanoscale shapes [11, 12, 13].

A nanoscale DNA box with a controllable lid was described by Andersen et al. in 2009 [14] pushing the vision of targeted drug delivery with the aid of DNA origami. Just recently, Douglas et al. [15] demonstrated the functionality of a DNA nanorobot that can transport molecular payloads, with a triggered release by an aptamer-encoded logic gate.

In the field of DNA nanotechnology, the most common techniques for visualizing and examining the correct folding of the nanostructures are gel-based analysis, electron microscopy (TEM or cryo-EM) and AFM imaging (see e.g. refs. [16, 17]). In many applications it is desirable to monitor the structure of the objects in solution and especially to follow reactions in real time and on the level of individual molecules. The opening of the DNA box mentioned above, was determined by ensemble FRET [14]. For a breakthrough in the area of targeted drug delivery, obviously the molecular designs need to be very refined. Following such conformational changes on the single-molecule level could yield valuable insights in the kinetics and heterogeneity of the process that may contribute to functional enhancements.

In chapter 4 a novel molecular ruler for investigating the distance dependence of FRET on the single-molecule level is introduced. The strengths of the DNA origami technique in creating DNA nanostructures with tailored properties are demonstrated with the design of a rigid DNA origami block. A series of these blocks with varying inter-dye distances was assembled, each incorporating a donor and acceptor dye. Accurate distance measurements of these structures were performed in solution using single-molecule FRET. Considering the capabilities of this measurement technique, it could be used as a tool for characterizing the folding of complex three-dimensional DNA nanostructures, yielding complimentary data to the established techniques mentioned in the previous paragraph.

A further potential of the DNA origami technique is the downscaling of lab-on-a-chip devices, possibly down to the level of interactions between single molecules. For the creation of complex and functional machines on the nanoscale, the precise and efficient incorporation of 'guest' molecules is required, which is a major challenge for the community [19].

This notion of a DNA origami as a 'molecular breadboard' for the assembly of biomolecules in the nanometer range is elaborated in chapter 5. The accurate positioning of fluorophores allows building a spectroscopic network with alternative pathways for the energy transfer. In figure 1.1 a schematic of the designed DNA origami rectangle is shown, with four spectrally distinct fluorophores incorporated. For the switching of energy-transfer paths on the structure

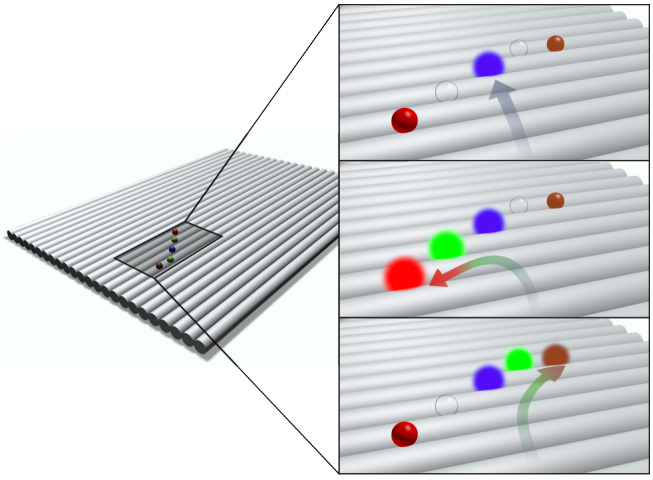

Figure 1.1: *Schematic of a DNA origami rectangle used as breadboard for molecular photonics: The precise addressability of the DNA self-assembly technique allows building a spectroscopic network with nanometer dimensions. The alternative FRET pathways are mediated by a green 'jumper' dye that guides the light from the blue input dye to either the red or IR output. Reprinted with permission from ref. [18]. Copyright 2011 American Chemical Society.*

to work, the presence and exact placement of all four fluorophores is essential. The functionality of this photonic device thus is a demonstration of the power of the origami technique to position objects with subnanometer precision. To visualize the control over energy-transfer paths on the level of individual DNA nanostructures and to sort subpopulations a novel single-molecule four-color FRET technique is introduced in chapter 5.

2 Theoretical and Experimental Basics

2.1 Single-molecule fluorescence

Fluorescence microscopes and fluorometers are commonly used in labs worldwide for a variety of applications in medical research, biology and the life sciences in general. Most of these techniques are based on ensemble fluorescence, and all of them make use of the fluorescence principle that the emitted light is red-shifted with respect to the excitation light. By only collecting the fluorescence light of the sample and blocking the excitation light by appropriate filters, images of the fluorescently labeled structure can be made with low background. E.g. by staining the actin filaments and the nucleus of a cell with different colored fluorescent markers, the individual components of the cell can be visualized.

In the last decades a large number of single-molecule techniques have been developed that have unique advantages and can unmask details that stay hidden in ensemble measurements [20]. For heterogeneous populations single-molecule techniques offer the possibility to study and quantitatively analyze individual subpopulations. Especially, dynamics and reaction pathways over time can be investigated for systems that are difficult or even impossible to synchronize, whereas ensemble measurements can only give insights on average properties.

Fluorescence on the single-molecule level shows several unique features. In contrast to the ensemble fluorescence, of e.g. fluorophores in a vial, that decays exponentially over time, the fluorescence intensity of an individual molecule instantly drops to zero when it is destroyed. This is often termed single-step bleaching. Another characteristic is blinking, i.e. fast and repeated switching between a fluorescent and non-fluorescent state. Blinking can have several different origins and is discussed in more detail in chapter 3.

With advances in single-molecule techniques the requirements on the dyes are becoming more and more demanding. Individual fluorophores are not simple light-emitting probes,

but have a variety of different attributes. For successful measurements, understanding the photophysical properties is essential [9]. In most cases 'bright' fluorophores are desirable, i.e. exhibiting a high extinction coefficient and a high quantum yield, that also show stable and long-lived fluorescence. Furthermore, the spectral properties have to be matched with the experimental excitation and detection. However, there is still a number of other properties that can have a large influence in an experiment, such as redox properties, size and the interaction with the local environment. The fluorophores used in this thesis are listed in table 2.1 along with the most important optical properties.

Table 2.1: *Dye properties; λ_{max}^{ab} and λ_{max}^{em} are the wavelengths at the maximum of the absorption and emission spectra respectively, ϵ_{max} is the maximum extinction coefficient and ϕ is the quantum yield*

Dye	λ_{max}^{ab} (nm)	λ_{max}^{em} (nm)	ϵ_{max} $(\frac{1}{mol \cdot cm})$	ϕ	used in
ATTO 488	501	523	$9.0 \cdot 10^4$	80 %	publication P3
ATTO 565	563	592	$1.2 \cdot 10^5$	90 %	publication P3
ATTO 647N	644	669	$1.5 \cdot 10^5$	65 %	publication P3
Alexa Fluor 750	749	775	$2.9 \cdot 10^5$	12 %	publication P3
Cy3	550	570	$1.5 \cdot 10^5$	-	publication P1, P2
Cy5	649	670	$2.5 \cdot 10^5$	-	publication P1, P2
Cy7	752	778	$2.5 \cdot 10^5$	-	publication P1

2.2 FRET - Fluorescence Resonance Energy Transfer

In addition to direct fluorescence emission, if adequate dyes are in immediate proximity (typically closer than 10 nm), energy can be transferred non-radiatively from one dye to the other based on a dipole-dipole interaction. This effect is called fluorescence resonance energy transfer (FRET) [21].

In general, there are two dyes involved in this process: the donor (D) and the acceptor (A), where the donor is always the fluorophore of higher energy, i.e. shorter wavelength. Cy3 and Cy5 are a common FRET pair and are also used in associated publication P2. After laser excitation of the donor fluorophore Cy3, it can - instead of directly emitting a photon - transfer its energy via FRET to Cy5, which then ultimately releases this energy by emitting a photon itself. These two cases can be distinguished, since the emission spectrum of Cy5 is shifted towards longer wavelengths compared to Cy3.

What is interesting for most studies that employ FRET is the distance dependence of this energy transfer process: The closer the respective dyes are, the more effective the energy transfer takes place. In this context, FRET is often referred to as 'spectroscopic ruler' [2] as it can detect distances in the regime of less than 10 nm. A decisive advantage of this technique is that distances are measured directly within a molecule or molecular complex which rules out the problem of sample drift compared to the setup.

For the quantitative determination of distances between dyes, it is important to take a closer look at the efficiency E of the energy transfer process. Thereby $E = 0$, if no energy transfer occurs and $E = 1$, if the donor always relaxes into the ground state by FRET. According to Theodor Förster, who investigated this effect as early as 1948 [21], the energy transfer efficiency can be written as:

$$E = \frac{1}{1 + (\frac{R}{R_0})^6} \tag{2.1}$$

where R_0 is the so-called Förster radius, for which the E-value is exactly 50%. In a quantum mechanical derivation Förster determined R_0 as:

$$R_0 = \sqrt[6]{\frac{9\,\phi_D\,ln(10)\,\kappa^2\,J}{128\,\pi^5\,n^4\,N_A}} \tag{2.2}$$

where ϕ_D is the quantum yield of the donor in absence of the acceptor, n the refractive index of the medium, N_A the Avogadro constant, J the spectral overlap integral of donor emission and acceptor absorption, and κ^2 is the dipole orientation factor. When the dyes are freely rotating and can be considered to be isotropically oriented during the lifetime of the excited state, κ^2 has a value of 2/3. Even if the dyes are not completely free to rotate $\kappa^2 = 2/3$ is still a good approximation and in most cases does not lead to a large error in the calculated distances due to the sixth power dependence. For any configuration κ^2 is always in the following range: $0 < \kappa^2 < 4$.

According to equation 2.2 a considerable FRET between two dyes only occurs if the donor emission and the acceptor absorption spectrum overlap, i.e. $J > 0$. In addition, the dyes should not be too far apart - typical R_0-values are around 5 nm. For an optimal detection sensitivity of conformational changes within a molecular structure, the FRET samples should be designed such that the minimal and maximal distances correspond to E-values below

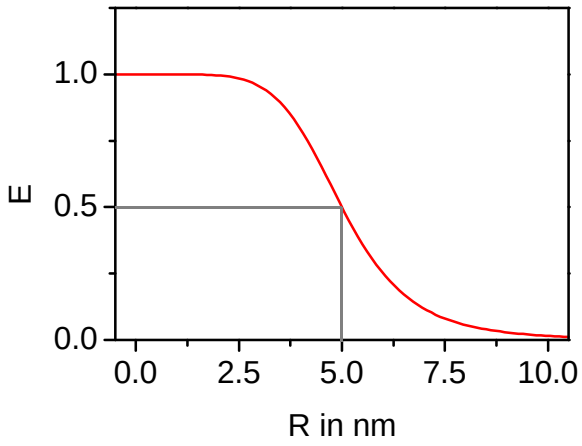

Figure 2.1: *Energy transfer efficiency E plotted against R according to equation 2.1, with* $R_0 = 5$ *nm*

and above 50%, i.e. distances below and above the R_0-value. This is due to the specific R-dependence of E and can be seen from equation 2.1 as well as in figure 2.1.

Experimentally it is possible to determine the energy transfer efficiency via ratiometric measurements of the acceptor and donor emission which was introduced in 1999 by Deniz et al. and Dahan et al. [22, 23]:

$$E^* = \frac{I_A}{I_A + I_D} \tag{2.3}$$

where I_D and I_A are the respective fluorescence intensities of the donor and acceptor molecules observed during donor excitation. The * in E^* indicates that this is the simplest expression for the energy transfer efficiency which does not include any crosstalk, or corrections that take effects such as differences in the quantum yields and detection efficiencies of the dyes into account. Therefore it is sometimes referred to as 'proximity ratio' to emphasize that it is only an approximation of the energy transfer efficiency. The importance of corrections for the determination of accurate distances is discussed in chapter 4.

2.3 Confocal microscope for single-molecule studies

For all of the fluorescence measurements described in this thesis, a custom-built confocal microscope was used. The basic design of the setup is shown in figure 2.2. For flexible wavelength selection, a pulsed white light laser (SuperK Extreme, NKT Photonics) in com-

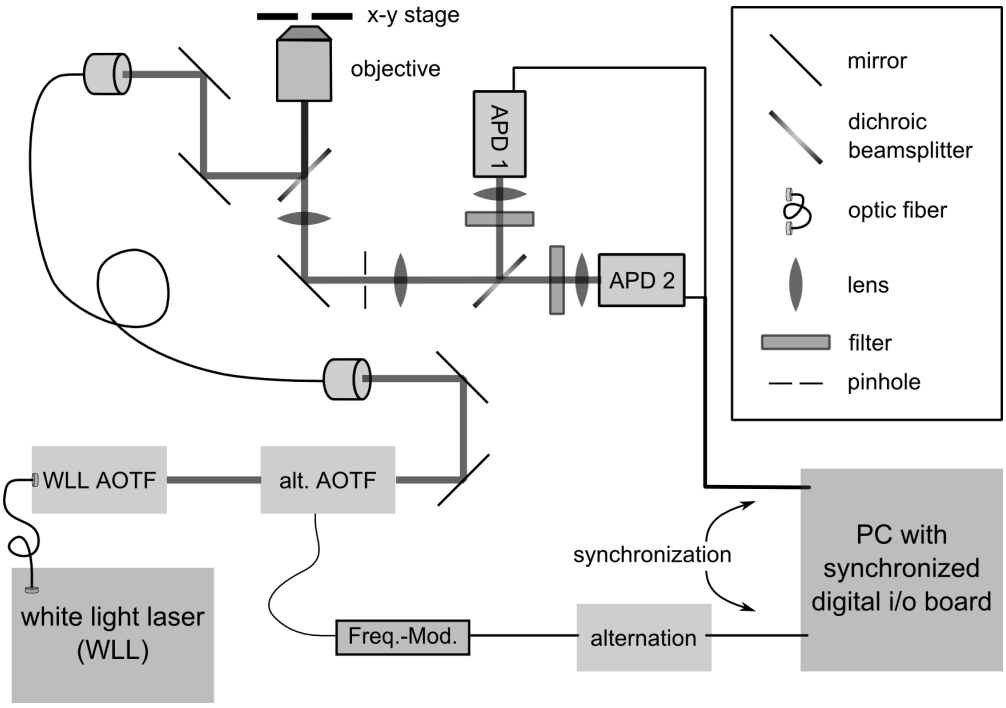

Figure 2.2: *Confocal single-molecule fluorescence microscope with alternating laser excitation (ALEX)*

bination with an acousto-optic tunable filter (AOTF) was used as excitation source. The second AOTF in the beam path (AOTFnc-VIS, AA optoelectronic) enables alternating laser excitation (ALEX) in the μs range. After passing the AOTF the beam is coupled into a fiber and finally adjusted to enter the microscope (Olympus IX 70) where it is reflected off a dichroic mirror and focused into the sample volume by the objective.

The fluorescence light of the sample is collected with the same objective, with the exact placement of the pinhole defining the confocal detection volume. Then the light is split onto two avalanche photo diodes (SPCM, AQR 14, Perkin Elmer) by a dichroic mirror and filtered by appropriate emission filters. The detection signal of the APDs is synchronized with the laser alternation.

For solution measurements a water objective (60x, NA 1.20, UPlanSApo 60XW, Olympus) and for surface scanning measurements an oil immersion objective (60x, NA 1.35, UPLSAPO 60XO, or 100x, NA 1.45, PLAPO100XO/TIRFM-SP, both from Olympus) was used. For surface scanning a piezo stage (E-501.00, Physik Instrumente (PI)) was controlled to move the sample relative to the objective.

Specific changes to the setup configuration as needed for the individual measurements are

outlined in the experimental sections of the associated publications. Particularly, the extensions for the four-color excitation and detection scheme developed for investigating alternative FRET pathways as described in chapter 5 are specified in detail in the supporting information of associated publication P3 (see appendix).

All data was acquired and analyzed with custom-made LabVIEW software.

2.4 ALEX - Alternating Laser Excitation

In 2004 Kapanidis et al. introduced an improved scheme for measuring FRET at the single-molecule level that "serves as a general tool for monitoring structure and interactions simultaneously" [24]. The key idea is to obtain the fluorescence of the single molecules after donor- as well as acceptor-excitation individually, which is achieved by employing an alternating laser excitation scheme (ALEX) with periodic switching between the excitation wavelengths. Naturally, the period of alternation has to be short enough to be able to probe the diffusing molecules numerously during their passage through the laser focus. In the ALEX measurements alternation periods between 50 and 100 μs were used, whereas typical sojourn times of small molecules are on the order of milliseconds.

Table 2.2: *Photon counts obtained in ALEX measurements*

	Detection Channel	
Excitation Laser ↓	Donor	Acceptor
Donor	F_D^D	F_D^A
Acceptor	F_A^D	F_A^A

In table 2.2 the photon counts that are obtained during ALEX measurements are summarized. F_X^Y stands for the number of photons that are collected by detector Y while exciting with laser X. For example, F_D^A indicates the number of photons that arrive in the detection channel of the acceptor during excitation with the donor laser wavelength. An appreciable contribution to F_D^A only occurs, if there is FRET in the observed sample. Therefore, F_D^A is often referred to as the 'FRET channel'.

With the aid of the newly introduced photon counts in table 2.2 two important parameters can be determined: the stoichiometric parameter S and the proximity ratio E^*, that are

defined as follows[1]:

$$E^* = \frac{F_D^A}{F_D^A + F_D^D} \tag{2.4}$$

$$S = \frac{F_D^A + F_D^D}{F_D^A + F_D^D + F_A^A} \tag{2.5}$$

It is important to note that these parameters are evaluated for every burst of fluorescence, i.e. for every molecule that diffuses through the laser focus. The S-value yields information about the stoichiometry of the dyes that are bound to the molecule. For example, for donor-only molecules S $\approx$ 1, because the contribution from F_A^A is negligible due to the absence of an acceptor dye (compare equation 2.5). Similarly, for acceptor-only $S \approx 0$ and for a 1:1 dye stoichiometry the S-value should be $S \approx 0.5$. The critical last value can be achieved by adjusting the relative intensities of the excitation laser wavelengths and a value close to 0.5 is desirable for optimal distinction between the subpopulations. There are several reasons why it can be necessary to deviate from an intensity ratio of the laser wavelengths of 1:1, for example different absorption coefficients of the dyes at the respective excitation wavelengths. Other factors can be due to differing intrinsic properties of the dyes (quantum yield, maximum extinction coefficient) and varying detection efficiencies.

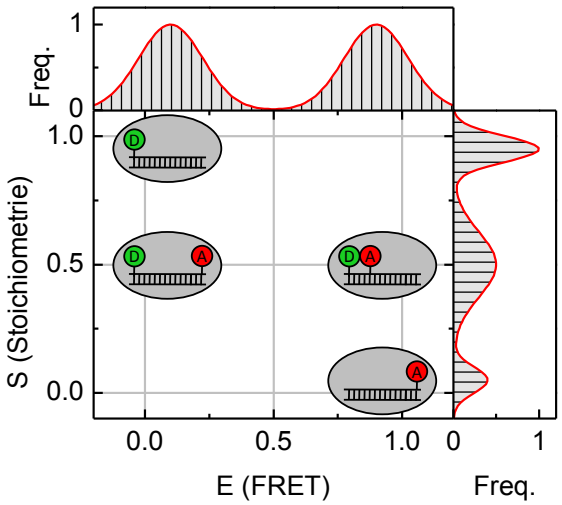

Figure 2.3: *Schematic E-S histogram for an ALEX measurement of a low and high FRET dsDNA sample. This two-dimensional histogram allows distinguishing between the individual subpopulations present in the sample solution. Experimentally the acceptor-only population is not as clearly localized as shown, but spread over a broader E-range. [24]*

[1]To explain the basic principle, correction factors are not considered here

An especially useful illustration of the above parameters is achieved by generating so-called E-S histograms of the obtained data. With these two-dimensional histograms the collected bursts can be evaluated regarding their dye stoichiometry as well as their energy transfer efficiency. Kapanidis et al. [24] introduced this technique of data analysis and defined it as fluorescence-aided molecule sorting (FAMS or ALEX-FAMS in combination with the described laser alternation scheme). An illustration of a schematic E-S histogram of a dsDNA sample with a low and high FRET fraction is given in figure 2.3, where the different populations can be clearly separated. Even if only the low and the high FRET populations are of interest, due to the labeling process the presence of donor-only and acceptor-only populations can often not be avoided. Using the ALEX excitation and detection scheme the populations of interest can be selected by S and individually analyzed for their E-values.

2.5 The DNA origami technique

The field of structural DNA nanotechnology took a huge leap forward when Paul Rothemund introduced the DNA origami technique in 2006 [10]. This technique allows creating objects on the nanometer scale with DNA as a building material. By means of self-assembly a long single stranded DNA (typically by the phage M13mp18 with around seven kilobases, termed 'scaffold' strand) is folded into shape by around 200 so-called 'staple' strands as shown schematically in figure 2.4, driven by the energy minimization of base complementarity. The exact sequences of these artificial DNA strands encode for the shape of the final structure.

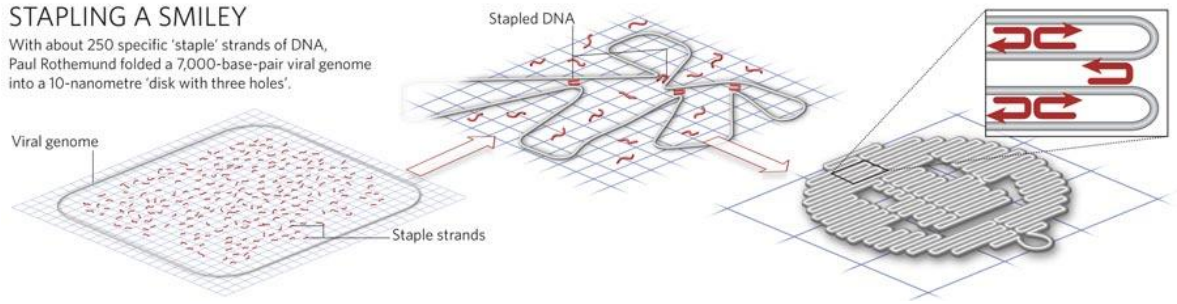

Figure 2.4: *Schematic of the DNA origami method. Reprinted by permission from Macmillan Publishers Ltd: Nature News, ref. [25], copyright 2010.*

For the folding process several nanomole of the scaffold strand are mixed in a vial with an excess of staple strands and heated to just below boiling. In the subsequent cooling process

the structures anneal by self-assembly. Depending on the complexity, structures can form in as fast as one or two hours with high yields of above 90 %.

The unique feature of the DNA origami method is the precise addressability of every part of the created structure, by simply modifying the respective staple strands. For example, to incorporate a fluorophore at a desired position, the corresponding strand is replaced by a labeled strand before the folding process. Strands with specific sequences as well as with a variety of different modifications are commercially available facilitating the process of making custom-made structures. Both associated publication P2 and P3 rely on this capability of localized modifications and the incorporation of fluorophores at precisely defined positions.

3 Linking Single-Molecule Blinking to Chromophore Structure and Redox Potentials

Single-molecule methods displayed a remarkable development in the last decades. With ever more sophisticated approaches the demands on individual fluorophores have increased. Most notably, it has become evident that understanding the intrinsic properties of fluorescent probes is a crucial prerequisite.

3.1 Characteristics of single-molecule blinking

From the beginnings of single-molecule experiments unpredictable blinking had been a major nuisance. Empirically, it was found that several chemical additives can strongly reduce the blinking, although the underlying principle remained mostly unclear [26, 27]. In 2008 Vogelsang et al. introduced a new approach to minimize blinking and bleaching, a reducing and oxidizing system (ROXS) [28], which can be understood in terms of a relatively simple model. To assess the implications of associated publication P1 a basic understanding of the underlying photophysical principle is required and is hence discussed here in some detail [29].

For visualizing the concept of ROXS, figure 3.1 shows the Jablonski diagrams corresponding to different buffer conditions in the left column. In general, exciting a fluorophore leads to a transition from the singlet ground state S_0 into the first excited state S_1. Relaxation into the ground state can then either occur non-radiatively (not shown), through fluorescence or by infrequent intersystem crossing via the triplet state T_1. Since excited state reactions with singlet oxygen are known to cause rapid photobleaching, in all cases oxygen was removed by an enzymatic oxygen scavenging system. If oxidizing and reducing agents are present in the buffer, they can cause electron transfer reactions. In figure 3.1 in the upper panel oxida-

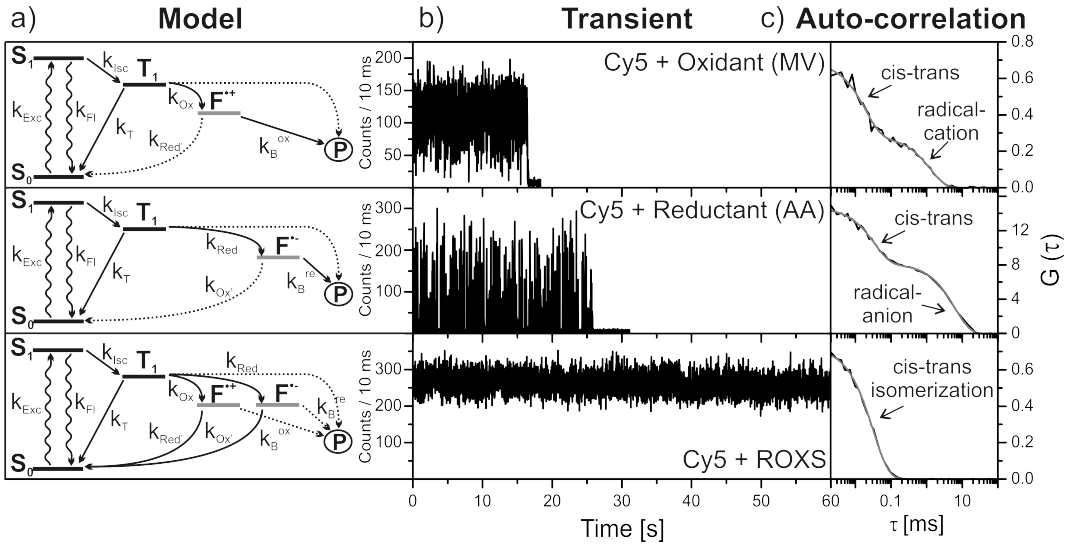

Figure 3.1: *Concept of the reducing and oxidizing system (ROXS) which enables stable and long-lived fluorescence: a) Jablonski diagrams describing the underlying photophysical models for varying buffer conditions b) the resulting fluorescence transients for Cy5 molecules immobilized via dsDNA c) auto-correlation function of the transients shown in b).*
In all cases PBS buffer was used and oxygen was removed by an enzymatic oxygen scavenging system, to prevent rapid bleaching. The oxidant methylviologen (MV) and the reductant ascorbic acid (AA) were added as indicated. Reproduced with permission from ref. [31]. Copyright 2010 WILEY-VCH.

tion leads to frequent formation of a long-lived radical cation F^{*+}, which is seen as frequent intermittence in the fluorescence transient, also shown in the autocorrelation function. In the middle panel a radical anion F^{*-} is formed via reduction, which leads to a similar transient. In both cases bleaching of the molecules is shown in the traces which corresponds to a transition into the photobleached state P as indicated by the black arrow in the model.

In the lower panel of figure 3.1 both oxidant and reductant are present, enabling successive oxidation and reduction reactions which lead to a fast recovery into the ground state. Therefore, blinking is removed and also the bleaching pathway is strongly suppressed. In the autocorrelation curve only the characteristic feature for the cis-trans isomerization of the Cy5 molecule remains [30]. The key to stable fluorescence according to the ROXS principle is that all intermediate states that either cause an intermission of the fluorescence signal or favor bleaching are quickly recovered to the ground state S_0. Using ROXS, the photostability is greatly increased while simultaneously blinking is strongly suppressed. Moreover, it is applicable to different classes of organic fluorescent dyes that are commonly used.

3.2 The importance of blinking for super-resolution microscopy

In the previous section the phenomenon of single-molecule blinking was discussed and a concept was introduced that allows removing it. Not in all cases, however, blinking is an unwanted effect. On the contrary, it has been shown that pronounced blinking can even be beneficial for optical super-resolution microscopy. This new field of techniques (e.g. PALM, STORM, GSDIM or Blink Microscopy, see refs. [4, 5, 6, 7]) is devoted to surpassing the optical diffraction limit, which is on the order of several hundred nanometers for visible light. Most super-resolution techniques rely on preparing a large number of fluorescent molecules into a dark state, whereas only a subset is active. In repetitive cycles the stochastically active fraction of molecules is individually localized, eventually leading to a reconstructed image with increased resolution. At any time only a single molecule should be active within each diffraction limited spot for successful localization. Therefore, long OFF-times are important to enable high labeling densities, which are needed for valuable images. As an example for the capability of these super-resolution techniques, in figure 3.2 an image of labeled actin filaments is shown that was acquired with a) total internal reflection microscopy (TIRF) and b) Blink Microscopy [31].

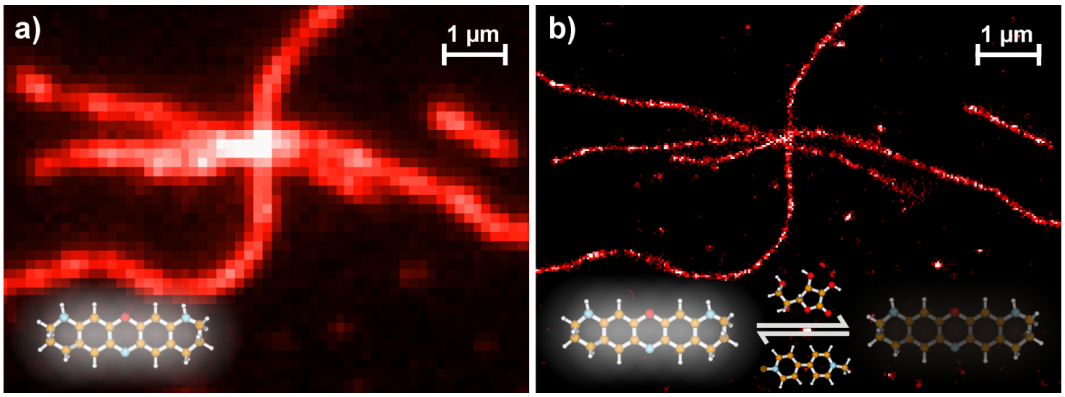

Figure 3.2: *Images of ATTO565-phalloidin-labeled single actin filaments using a) TIRF microscopy and b) Blink Microscopy of the same structure yielding sub-diffraction resolution. The images were recorded with reductant and oxidant concentrations optimized for imaging speed, fluorophore density and excitation intensity (*100 mM *AA,* 100 mM *MV and* 50 kWcm^{-2}*). Adapted with permission from ref. [31]. Copyright 2010 WILEY-VCH.*

The underlying model of the ROXS scheme that was introduced in the previous section as a solution to prevent blinking can also be used to induce pronounced blinking. As shown in the middle panel of figure 3.1, the addition of a reductant (in this case ascorbic acid (AA))

with simultaneous removal of oxygen leads to strong blinking of the Cy5 molecules. The induced radical anion state F^{*-} is long-lived as there is no oxidant present in solution to accelerate a transition back into the ground state. Optimizing the AA concentration to make the OFF-times as long as possible yields OFF-times up to 60 ms that are well suited for super-resolution Blink Microscopy [7].

In principle, generating even longer OFF-times is desirable as this would make higher labeling densities possible that could in turn enhance achievable resolution. Coming back to the previous example of the blinking of Cy5, the question remains what limits the maximum OFF-time to 60 ms. According to the Jablonski diagram in figure 3.1, OFF-times should increase with suppression of the relaxation pathway from the radical anion state F^{*-} back into the ground state. This pathway is mediated by oxidizing agents. As there are no oxidizing species in the PBS buffer, the natural assumption is that the remaining oxygen in the solution, due to incomplete removal by the scavenging system, limits the maximum OFF-times.

Another factor that should influence the OFF-state lifetime is the intrinsic energetic driving force of the fluorophore from the radical state back into the ground state. Specifically, fluorophores with higher reduction potential, i.e. a better stabilized radical ion, should exhibit longer OFF-times [32]. According to this hypothesis, the reduction potential might be the parameter of choice to evaluate dyes for localization-based super-resolution microscopy techniques that rely on the formation of radical OFF-states.

In associated publication P1, the influence of redox potentials and chromophore structure on single-molecule blinking is investigated in detail. For a systematic study, the homologous series of cyanine dyes was chosen, that can be well described by a simple particle-in-the-box model.

3.3 Associated publication P1

Linking Single-Molecule Blinking to Chromophore Structure and Redox Potentials

By

Ingo H. Stein, Stella Capone, Jochem H. Smit, Fabian Baumann, Thorben Cordes and Philip Tinnefeld

published in

ChemPhysChem 2012, 13, 931–937

CPCHFT 13 (4) 881–1096 (2012) · ISSN 1439-4235 · Vol. 13 · No. 4 · March 19, 2012

A EUROPEAN JOURNAL

CHEMPHYSCHEM

OF CHEMICAL PHYSICS AND PHYSICAL CHEMISTRY

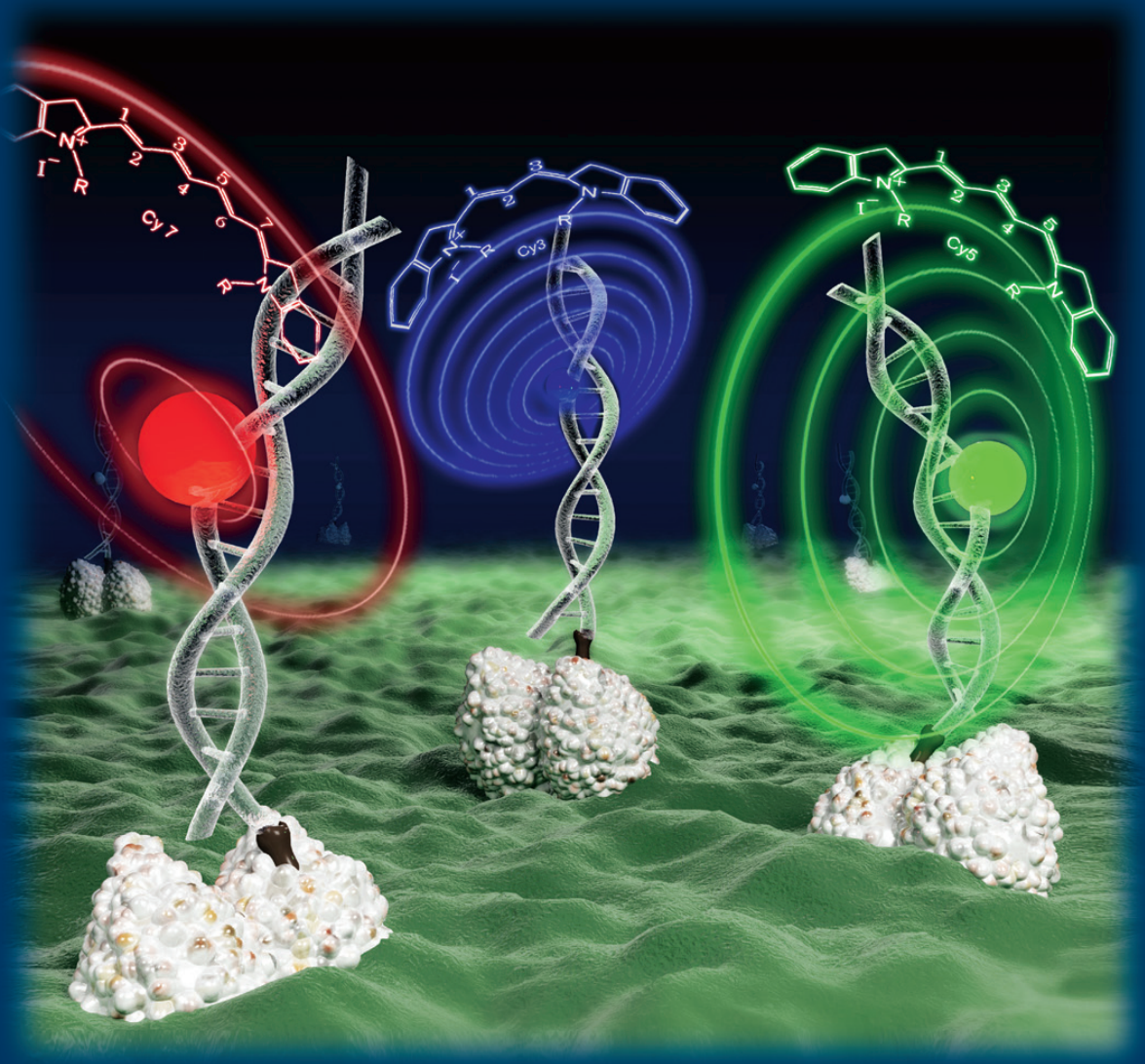

4/2012

A Journal of

ChemPubSoc Europe

Concepts: Chromophores in Conjugated Polymers (J. M. Lupton)

Original Contributions: Single-Molecule Blinking Linked to Chromophore Structure and Redox Potentials (T. Cordes, P. Tinnefeld et al.), Surface-Enhanced Fluorescence on Nanoparticles (H. Uji-i et al.)

www.chemphyschem.org

Special Issue: Single-Molecule Studies

Cover Picture

Ingo H. Stein, Stella Capone, Jochem H. Smit, Fabian Baumann, Thorben Cordes*, and Philip Tinnefeld*

Intensity fluctuations of individual fluorophores, also termed blinking, are studied at the single-molecule level by T. Cordes, P. Tinnefeld et al. on p. 931. Therefore, dye molecules of the homologous series of cyanines were immobilized through double-stranded DNA on BSA-coated cover slips. The OFF-times due to radical-ion formation increase for larger chromophore size and correlate with redox potentials.
Cover artwork by Christoph Hohmann, Nanosystems Initiative Munich (NIM).

DOI: 10.1002/cphc.201100820

Linking Single-Molecule Blinking to Chromophore Structure and Redox Potentials

Ingo H. Stein,[a, b] Stella Capone,[b] Jochem H. Smit,[c] Fabian Baumann,[b] Thorben Cordes,*[c] and Philip Tinnefeld*[a, b]

This paper is contributed in honor and admiration of Professor Christoph Bräuchle's outstanding scientific contributions

Intensity fluctuations between an ON-state and an OFF-state, also called blinking, are common to all luminescent objects when studied at the level of individuals. We studied blinking of three dyes from a homologous series (Cy3, Cy5, Cy7). The underlying radical anion states were induced by removing oxidants (i.e. oxygen) and by adding the reductant ascorbic acid. We find that for different conditions with distinct levels of oxidants in solution the OFF-state lifetime always increases in the order Cy3 < Cy5 < Cy7. Longer OFF-times are related to higher reduction potentials of the fluorophores, which increase with the size of the chromophore. Interestingly, we find reaction rates of the radical anion that are unexpectedly low at the assumed oxygen concentration. On the other hand, reaction rates meet the expectations of similar Rehm–Weller plots when methylviologen is used as oxidant, confirming the model of photoinduced reduction and oxidation reactions. The relation of OFF-state lifetimes to redox potentials might enable predictions about the nature of dark states, depending on the fluorophores' nano-environment in super-resolution microscopy.

1. Introduction

On the single-molecule level, essentially all fluorophores exhibit intensity fluctuations between an ON-state and an OFF-state that is referred to as blinking. Blinking is often caused by transitions into the triplet state or radical states.[1,2] Triplet states result from intersystem crossing and have a typical lifetime in the microsecond to lower millisecond range. Recently, it has been shown that radical ions formed as a result of one-electron transfer reactions can have a much longer lifetime of up to minutes (redox blinking).[3,4]

For a long time unpredictable blinking had been plaguing single-molecule experiments. Only in recent years, has blinking become more controllable and even valuable for optical super-resolution microscopy.[5–12] For microscopy techniques based on subsequent localization of single molecules, such as PALM, fPALM, STORM, GSDIM, dSTORM or Blink Microscopy, the majority of molecules has to be shelved to a transient dark state and the stochastically active molecules successively localized.[6–11] By repeating this procedure, all molecule positions are determined and super-resolved fluorescence images are reconstructed. For this method to work efficiently, the lifetimes of the dark states of the molecules have to be long enough so that a sufficient number of molecules can be co-localized within one diffraction-limited spot.[13] Presumed radical ion states have proven to be well-suited for super-resolution microscopy because they are generic dark states of all fluorophores.[10,13] On the other hand, single-molecule studies showed that the lifetimes of these dark states vary significantly between different dyes at otherwise identical conditions, indicating that some dyes are better suited for super-resolution microscopy than others.[10,11,14]

It has been argued that a higher reduction potential of the fluorophores, that is, a better-stabilized radical ion, should be accompanied by a longer OFF-state lifetime.[4] Accordingly, the reduction potential might be the parameter to evaluate dyes for localization-based super-resolution microscopy. This is why certain oxazine dyes with high reduction potentials have been chosen for super-resolution microscopy.[4] On the other hand, very recently, it has been shown that these oxazine dyes can undergo a second reduction, leading to a long-lived leuko form.[15] Then there is the general question about the nature of the underlying dark states in localization based super-resolution microscopy using the blinking of dyes.[10,11,16] To advance blinking-based super-resolution imaging, the understanding of the underlying dark states is crucial. In addition, the ability to predict the properties of dyes at the single-molecule level will foster further developments. A systematic study of chromo-

[a] I. H. Stein, Prof. Dr. P. Tinnefeld
NanoBioScience Group
Institute for Physical and Theoretical Chemistry
TU Braunschweig
Hans-Sommer-Str. 10, 38106 Braunschweig (Germany)
E-mail: p.tinnefeld@tu-braunschweig.de

[b] I. H. Stein, S. Capone, F. Baumann, Prof. Dr. P. Tinnefeld
Applied Physics-Biophysics & Center for NanoScience (CeNS)
Ludwig Maximilian University
Amalienstr. 54, 80799 München (Germany)

[c] J. H. Smit, Dr. T. Cordes
Molecular Microscopy Research Group & Single-molecule Biophysics
Zernike Institute for Advanced Materials
University of Groningen
Nijenborgh 4, 9747 AG Groningen (The Netherlands)
E-mail: t.m.cordes@rug.nl

phore properties and blinking is required to test the hypothesis of the correlation of blinking kinetics and reduction potentials.

Herein, we study the dependence of redox blinking on the electronic properties of dyes with a focus on the absorption wavelength and the reduction potential. To minimize other influences such as chromophore structure, for example due to chemical substituents, differing hydrophobicity or steric constraints, we used dyes from the homologous series of cyanine fluorophores. Cy3, Cy5, and Cy7 exhibit a systematic increase of their chromophore system and the energetic properties can be described well by the simple particle-in-the-box model (i.e. absorption wavelength and chromophore size are quantitatively connected by the number of delocalized π electrons, see Figure 1, $n = 1,2,3$). According to the Kuhn model,[17] the reduction potentials increase with the number of π electrons, that is, larger dyes within one series are reduced more easily than fluorophores with smaller conjugated π systems.

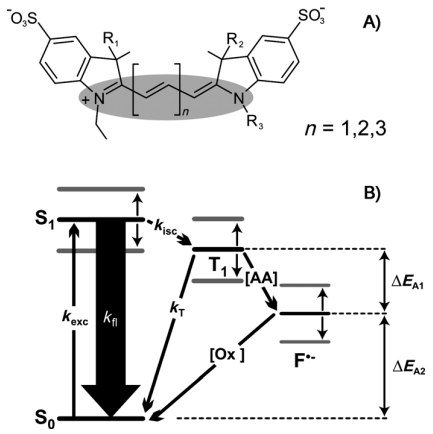

Figure 1. A) Overview of the chemical structures of the cyanine dyes used [$n = 1$ (Cy3), $n = 2$ (Cy5), $n = 3$ (Cy7)]. Residues are $R_1 = R_2 = CH_3$ and $R_3 = (C_5H_{10})$-CO_2NH-(C_6H_{12})-PO_4^--DNA for Cy3/Cy5; $R_1 = R_3 = (C_3H_6)$-SO_3^-, and $R_2 = (C_3H_6)$-CO_2-DNA for Cy7. The basic chromophore is highlighted in grey. B) Jablonski diagram of the fluorophores from one homologous series. One single molecule is excited from its singlet ground state S_0 into the first excited state S_1 by appropriate laser light with the excitation rate k_{exc}, fluorescence is observed with k_{fl}. Intersystem crossing occurs with the rate constant k_{isc} populating the triplet state T_1. The triplet has the intrinsic lifetime of $1/k_T$ but can also be depopulated by a photoinduced electron transfer originating from a reaction with ascorbic acid (AA). This reaction forms a radical anion (assuming a neutral fluorophore before the reaction) which is recovered to the electronic ground by an oxidation process mediated by molecular oxygen or MV. The energy levels of Cy5 are shown in black as a reference; Cy3 has blue-shifted absorption/emission while Cy7 shows a red-shifted absorption/emission. The energy of the triplet state and radical anion change accordingly.

We carried out single-molecule spectroscopy of cyanine dyes that were attached to DNA and immobilized with neutravidin/biotin on BSA-coated cover slips. We developed an assay to ensure comparable conditions in the experiments with different dyes, especially with respect to oxygen concentration. Redox blinking was induced by removing oxygen with the glucose oxidase/catalase (GOC) oxygen scavenging system and adding 75 μM of the reductant ascorbic acid (AA).[10] Single molecules were placed in the laser focus of a confocal microscope and fluorescence transients of redox blinking molecules were recorded. From these transients we extracted the OFF-state lifetime for the three cyanine derivatives. A strong correlation of chromophore size and OFF-state lifetime corroborates the idea that the simple model is able to predict qualitatively the OFF-state lifetime of cyanines, substantiating that the redox potentials are a crucial parameter for dye selection in super-resolution microscopy. In the future, deviations from such predictions might point towards a different nature of observed OFF-states.

2. Results and Discussion

We used three dyes from the homologous series of cyanine fluorophores, Cy3 ($\lambda_{max} = \sim 550$ nm), Cy5 ($\lambda_{max} = \sim 650$ nm), and Cy7 ($\lambda_{max} = \sim 750$ nm). These fluorophores are commonly used to label proteins and nucleic acids and also in demanding applications such as single-molecule FRET and super-resolution microscopy.[9,18–20]

As a basis for our experiment we make a simple qualitative prediction on the blinking properties of fluorophores from one homologous series. The absorption properties of cyanines can be described well by Kuhn's free-electron gas model.[17] The model also allows estimating redox potentials assuming that certain energy contributions such as the solvation energy do not change within the homologous series. In this case the LUMO energy is related to the redox potential by Equation (1):

$$-E_{red} = \frac{A}{F} + k \approx -\frac{E_{LUMO}}{F} + k \qquad (1)$$

where A is the electron affinity, F is Faraday's constant and k is a constant that includes the free energy change for solvation.[21] Since the LUMO energy decreases with increasing size of the box, the reduction potential increases. That is, larger fluorophores within a homologous series are reduced more easily. Since the reaction rates of non-diffusion-limited processes are linked to the Gibbs free energy of the reaction, we expect that the re-oxidation of the radical anion will be faster in the order Cy7 > Cy5 > Cy3 under otherwise identical experimental conditions.[22] This means that the OFF-state lifetime of the radical anion should increase in the order Cy3 < Cy5 < Cy7 in a reducing buffer and low concentrations of oxidant. We used molecular oxygen and 1,1′-dimethyl-4,4′-bipyridinium dichloride hydrate (methylviologen, MV) as oxidants.

To study the OFF-state lifetime of the homologous series of cyanines, fluorophores bound to biotinylated DNA were immobilized with BSA-biotin/neutravidin on glass cover slips. For excitation of the fluorophores from different spectral regions, we used a multi-colour single-molecule setup equipped with a supercontinuum laser and acousto-optical components for free wavelength selection. The detection is carried out by avalanche photodiodes and the spectral windows are selected using dichroic mirrors and appropriate filters. For details of the setup see the Experimental Section and refs. [23, 24]. After recording

fluorescence images (Figure 2A), fluorescence intensity transients were recorded and analysed using custom-made LabVIEW code and OFF-times were determined by autocorrelation analysis as described in ref. [4]. For the analysis only transients that showed a distinct single bleaching step at the end were selected, which allows for individual background correction. A section of an exemplary transient is depicted in Figure 2B together with the corresponding autocorrelation function (Figure 2C). Besides the component for redox blinking ($\tau_{OFF2}=41$ ms and $\tau_{ON2}=3.8$ ms), a short bunching term ($\tau_{OFF1}=180$ μs and $\tau_{ON1}=20$ μs) is visible that is assigned to *cis–trans* isomerisation common to cyanine dyes.[25] At the conditions used, the average ON- and OFF-times of *cis–trans* isomerisation are τ_{OFF1} (Cy3) = 37 μs and τ_{ON1} (Cy3) = 47 μs, τ_{OFF1} (Cy5) = 165 μs and τ_{ON1} (Cy5) = 22 μs, and τ_{OFF1} (Cy7) = 227 μs and τ_{ON1} (Cy7) = 34 μs for the different dyes, respectively.

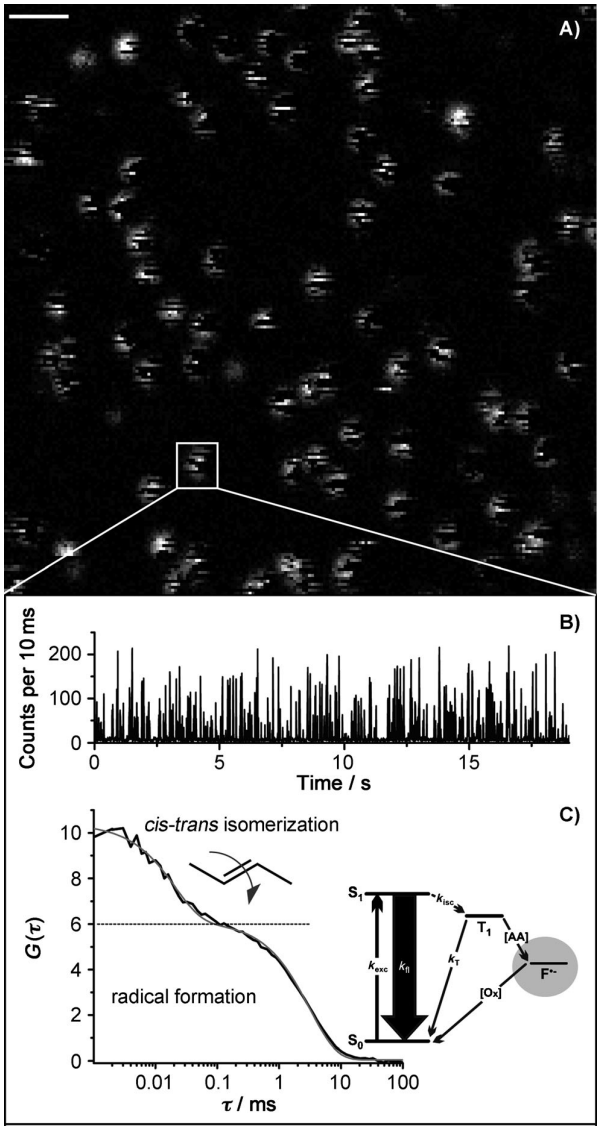

Figure 2. A) Confocal fluorescence intensity image showing immobilized dsDNA-Cy5 molecules in aqueous PBS buffer at pH 7.4. The shown area (10×10 μm, 2 ms/pixel) was scanned by excitation at 640 nm with an average intensity of 3 μW. The scale bar at upper left is 1 μm. Single-molecule blinking due to oxygen removal and the presence of AA ([AA] = 75 μM) is observed as dark pixels in single point spread functions. B) Fluorescence intensity transient recorded under identical experimental conditions. C) Autocorrelation function and biexponential fit of the fluorescent transient shown in (B). The short component, assigned to *cis–trans* isomerization has an OFF-time of $\tau_{OFF}=180$ μs and an ON-time of $\tau_{ON}=20$ μs while the long component, which is assigned to the formation of a radical anion, has an OFF-time of $\tau_{OFF}=41$ ms and an ON-time of $\tau_{ON}=3.8$ ms.

3. Influence of Oxygen on Single-Molecule Blinking

The concentration of the reductant ascorbic acid is chosen to maximize the OFF-state lifetime and is much higher than the oxidant concentration.[10] In the presence of oxygen at atmospheric pressure corresponding to ~500 μM dissolved oxygen, no blinking of Cy5 is observed because triplet as well as radical anionic states are rapidly depleted by reactions with oxygen. Additionally, the molecules bleach quickly due to the formation of singlet oxygen. To also exclude initial photoinduced oxidation by the oxidant we used a significantly lower oxidant than reductant concentration. We can thus safely assume that all observed dark states that cannot be assigned to *cis–trans* isomerisation but represent radical anionic states (with respect to an assumed neutral ground state chromophore). The assumption is justified for two reasons. First, due the concentration difference, reduction from an excited state is more likely than the oxidation. Second, the oxidized state would be too short-lived to be detected at the AA concentration used.

When using oxygen as oxidant, its concentration has to be controlled in a reproducible fashion. To this end, we developed a protocol for oxygen removal by the GOC system that we calibrated with the aid of an oxygen meter. The GOC system allows the removal of dissolved oxygen down to an equilibrium concentration of ~10 μM.[26] To check the oxygen concentration in the single-molecule experiments and to ensure that equilibrium is achieved, we studied the oxygen concentration as a function of time for different glucose oxidase concentrations by monitoring the blinking kinetics of the cyanines. Figures 3A,C show the progression of the OFF-times of Cy5 for two concentrations of glucose oxidase starting directly after addition of GOC and sealing of the chamber (1% v/v vs 10% v/v, see the Experimental Section for details). Each data point represents the average OFF-time obtained for the transient of a single cyanine molecule. The data shown in Figure 3A represent ~400 molecules and Figure 3C ~200 molecules. Both graphs exhibit an initial increase in the OFF-times. Saturation, however, occurs much faster for the higher glucose oxidase concentration after about 10 min whereas saturation is reached after more than 90 min for 1% v/v. In addition, at a lower concentration of the enzyme (1% v/v,) a higher oxygen concentration is indicated by lower mean OFF-times for 1% v/v (12 ± 10 ms) compared to 10% v/v (41 ± 20 ms). Figures 3B,D show the corresponding OFF-time histograms derived after saturation was reached. These results show the importance of a sufficient concentration of glucose oxidase to reach the highest possible OFF-time and also the need to wait for

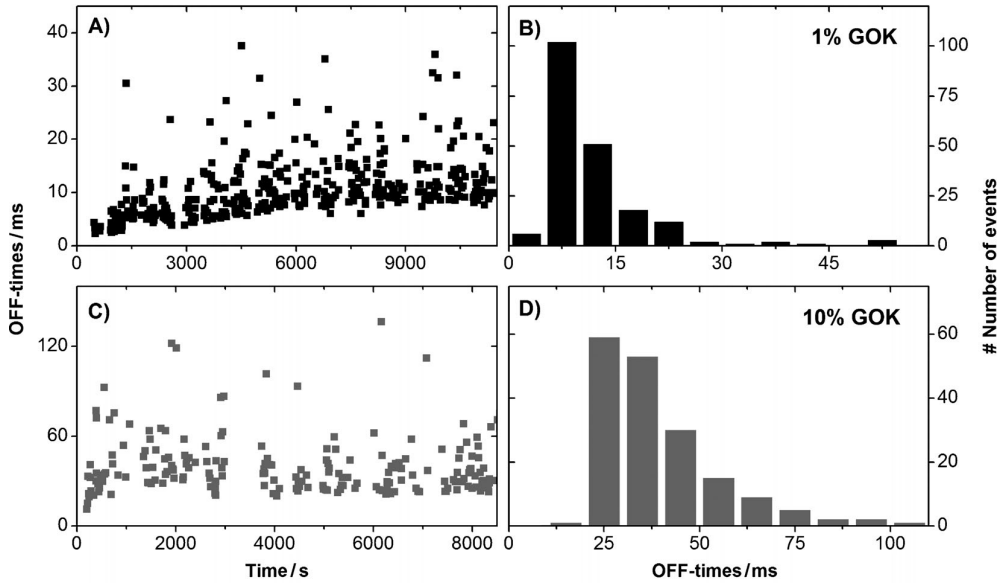

Figure 3. Single-molecule analysis of the OFF-time distribution of immobilized Cy5 molecules at two different concentrations of GOC: A) and C) show the temporal development of the OFF-times after addition of 1% or 10% GOC and sealing of the chamber ($t=0$). The steady state of OFF-times is reached at around $t=6000$ s for 1% GOC and around $t=500$ s for 10% GOC. B) and D) show histograms of the OFF-time distribution after the steady state is reached. The mean value of the distribution is 12 ± 10 ms for 1% GOC and 41 ± 20 ms for 10% GOC.

the system to reach equilibrium. As a consequence we used 10% v/v glucose oxidase for reaching the steady state quickly and reproducibly in all subsequent experiments.

A more subtle detail of the plots in Figures 3 A,C is the asymmetric shape of the distribution. Initially, the OFF-times are quite homogenous and short. With decreasing oxygen concentration the distribution of OFF-times broadens with a remarkably sharp edge for shorter OFF-times. This distribution might reflect sample inhomogeneity with some fluorophores being more exposed to the solution (short OFF-times) and other being better shielded from oxygen by the BSA coating of the surface. A small fraction of individual fluorophore time transients showed switching between distinct OFF-times, which could be an indication of a discrete rearrangement of one fluorophore's specific nano-environment. Moreover, measurements of dsDNA structures with Cy5 at the 5′-end yielded ~50% longer OFF-times for comparable experimental conditions (data not shown, see ref. [10]), indicating the environmental sensitivity of OFF-state lifetimes.

4. Blinking in the Homologous Series Cy3/Cy5/Cy7

The dyes of the homologous series Cy3/Cy5/Cy7 exhibit an increase in chromophore size and number of π electrons that goes along with systematic changes of their spectroscopic and electrochemical properties. Some of these properties are listed in Table 1.

Investigating more than 100 single-molecule transients for each dye reveals a mean OFF-time of 18 ± 8 ms for Cy3 (Figure 4 A), 41 ± 20 ms for Cy5 (Figure 4 B) and 71 ± 23 ms for Cy7 (Figure 4 C). We ascribe the broad distributions to the mentioned variation of the molecules nano-environment, causing a

Table 1. Spectroscopic and electrochemical properties of cyanine dyes.[a]

	Cy3	Cy5	Cy7
Abs. (max)	550 nm	649 nm	752 nm
Fl. (max)	570 nm	670 nm	778 nm
E_{red} vs SCE	−1.0 V[28]	−0.84 V[29]	−0.72 V*
τ_{OFF}	18 ms	47 ms	67 ms

[a] *E_{red} for Cy7 was estimated by linear extrapolation of the values for Cy3 and Cy5 according to the absorption energy.[27]

shoulder in the histograms displayed in Figure 4. Nevertheless, the average values of the OFF-time distributions are reproducible within several milliseconds when repeating the experiment, including new surface preparation, immobilization of dye molecules and oxygen removal. Table 1 shows the average OFF-time for multiple repeats ($n\geq3$) consisting of at least 100 evaluated transients per experiment. We also studied the excitation intensity dependence and found that OFF-times slightly decrease for higher excitation powers.[35] For the given conditions, Cy5, for example, exhibits ~25% shorter OFF-times at 5-fold higher excitation intensity. To reduce the influence of sample heterogeneity in addition to calculating the mean values of the distributions we investigated the behaviour of the mentioned sharp edge for shorter OFF-times for the different cyanine dyes. As a quantitative measure for this lower bound we calculated the lowest decile for the distributions and obtained τ_{OFF} (Cy3) = 11 ms, τ_{OFF} (Cy5) = 23 ms, and τ_{OFF} (Cy7) = 52 ms, which additionally confirms the expected trend of OFF-times.

The data allow an estimation of the rate constants of these electron transfer reactions using $\tau_{off}^{-1}=k_{on}=k_{ox}$ [Ox], that is,

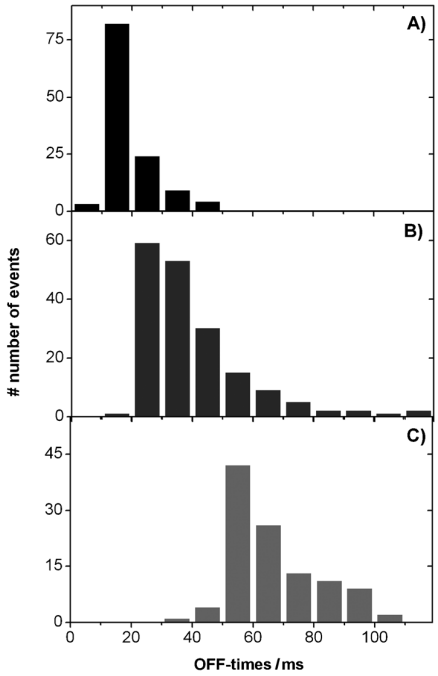

Figure 4. OFF-time histograms of immobilized cyanine molecules at 10% GOC with fully equilibrated oxygen removal. Only time transients showing a single bleaching step at the end are selected. A) Cy3 with a mean value of 18 ± 8 ms, B) Cy5 with a mean value of 41 ± 20 ms, C) Cy7 with a mean value of 71 ± 23 ms.

the rate constant for switching the molecule back ON by the electron transfer to the oxidant k_{ox}. Assuming an oxygen concentration of 10 μM, we obtain k_{ox} in the range of (10^6–10^7) $s^{-1}\,M^{-1}$ for the three dyes. The driving force for the reaction is estimated by the reduction potentials of the fluorophores and the reduction potential of oxygen.[29] The Gibbs energy is $\Delta G = -0.60$ eV for Cy3, $\Delta G = -0.44$ eV for Cy5, and $\Delta G = -0.32$ eV for Cy7, assuming a redox potential of $E_{red}(O_2) = -0.40$ V vs SCE for 1 mol L^{-1} oxygen concentration.[30] Comparing to typical Rehm–Weller plots,[22,31] the expected order of magnitude for the rate constant of these Gibbs energies is between (10^9–10^{10}) $s^{-1}\,M^{-1}$, that is, several orders of magnitude larger than the observed values. While our data qualitatively meet expectation, we cannot explain the large deviation with respect to the absolute expected values. Possibly, the oxygen concentration is much lower than the measured ~10 μM because this concentration is close to the detection limit of the employed oxygen meter. Additionally, the large increase in OFF-times for many fluorophores from <1 μs in the presence of oxygen to >30 ms after enzymatic oxygen removal, that is, by a factor of 3×10^4 can hardly be explained by an oxygen reduction of only 50-fold from 500 μM to 10 μM (see for example refs. [4,29]).

To test whether an overestimation of the oxygen concentration can be the reason for the deviations or whether there might be a more fundamental problem with our model, we used methylviologen (MV) as an alternative oxidant whose concentration is better controlled. We measured the OFF-times of the three dyes at various concentration of MV keeping the AA concentration constant at 75 μM. Oxygen was removed as in previous experiments. For all dyes, the OFF-time already decreases at nanomolar concentrations although MV ($E_{red} = 0.69$ V vs SCE) has less oxidative potential than oxygen (Figure 5). At

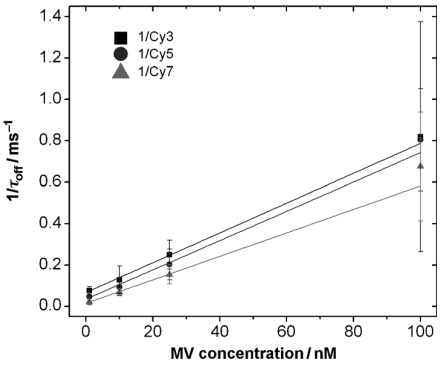

Figure 5. Plot of the dependence of the inverse OFF-times on MV concentration for Cy3 (■), Cy5 (●) and Cy7 (▲). Fits are according to Equation (2): k_{ox} (Cy7) $= 5.68\times10^9\ s^{-1}\,M^{-1}$, k_{ox} (Cy5) $= 7.08\times10^9\ s^{-1}\,M^{-1}$, and k_{ox} (Cy3) $= 7.20\times10^9\ s^{-1}\,M^{-1}$.

concentrations greater than 100 nM the OFF-times become so short that they cannot clearly be distinguished from blinking due to *cis–trans* isomerisation. To determine the rate constants for this system, we fitted the data in Figure 5 by Equation (2):

$$1/\tau_{off} = k_{ox}[MV] + k'_{ox}[O_2] = k_{ox}[MV] + \text{constant} \qquad (2)$$

The offset in the equation accounts for the fact that the remaining oxygen concentration also contributes to the shortening of the OFF-state lifetime, that is, the OFF-state lifetime is not infinite in the absence of MV. The fits yield the reaction rate constants k_{ox} (Cy7) $= 5.68\times10^9\ s^{-1}\,M^{-1}$, k_{ox} (Cy5) $= 7.08\times10^9\ s^{-1}\,M^{-1}$, and k_{ox} (Cy3) $= 7.20\times10^9\ s^{-1}\,M^{-1}$. Taking into account a Gibbs energy for the reaction with MV ($E_{red} = 0.69$ V vs SCE) of $\Delta G = -0.31$ eV for Cy3, $\Delta G = -0.15$ eV for Cy5, and $\Delta G = -0.03$ eV for Cy7, these values match expectations from Rehm–Weller plots very well.[22] The stronger driving forces for Cy5 and Cy3 yield similar values for their quenching constant since the values approach the diffusional plateau. Cy7 only has a small driving force explaining the larger difference between Cy7 and Cy5 compared to Cy5 and Cy3. Considering the small driving force for Cy7 the observed value for k_{ox} is still relatively high. In summary, the kinetics of the oxidation of radical anions by MV corroborates the proposed model and suggests the tight connection between OFF-states of single-molecule redox blinking and chromophores' electronic properties. In addition variations by different local environments of the fluorophores are indicated.

5. Conclusions

We have studied redox blinking of a homologous series of cyanine dyes. The underlying radical anionic states were induced

by removing oxidants (i.e. oxygen) and by adding the reductant ascorbic acid. We found that for different conditions the OFF-state lifetime was increasing in the order Cy3 < Cy5 < Cy7. The behavior was related to the reduction potential of the fluorophores which increases with the size of the chromophore. Thus, we could qualitatively predict blinking properties of fluorophores on the simple basis of the free-electron gas model that a better stabilized radical anion yields longer OFF-state lifetimes. Interestingly, we found reaction rates of the radical anion that were unexpectedly low at the assumed oxygen concentration. On the other hand, reaction rates met the expectations of similar Rehm–Weller plots when methylviologen (MV) was used as oxidant confirming the model of photoinduced reduction and oxidation reactions.[29] The deviation between the results obtained with oxygen and MV as oxidants might be explained by overestimated oxygen concentrations. On the other hand, assuming similar quenching constants for MV and oxygen, oxygen exhibits an activity as if it was present at an effective concentration between 1–10 nM as estimated from the fits in Figure 5. Our data also shed new light on the nature of the underlying dark states in super-resolution microscopy that relies on the successive localization of single molecules. Tetramethylrhodamine (TMR), for example, was used in live-cell super-resolution imaging and exhibited pronounced blinking with long OFF-states.[32,33] TMR has an estimated reduction potential of E_{red} (TMR) = −0.95 V vs SCE,[34] yielding a driving force for the back electron transfer between that of Cy3 and Cy5. From these values, OFF-states long enough for imaging at 50 Hz in living cells are not expected. This either indicates that the nature of the underlying OFF-state might be different. Alternatively, the oxygen activity might be reduced or oxygen is heavily consumed due to the irradiation in the presence of thiols.[15]

Experimental Section

Sample Preparation

Samples for single-molecule experiments were prepared based on DNA oligonucleotides. A 40-mer oligonucleotide labelled with a single fluorophore at position 24 (TAC GAT TCG ATT CCT TAC ACT TA*X* ATT GCA TAG CTA TAC G; *X* = T-Cy3/Cy5/Cy7; as received from IBA, Germany compare Figure 1) was hybridized to a biotinylated counter-strand (also from IBA, Germany). All experiments were carried out at room temperature (22 °C) under the following buffer conditions. Standard phosphate-buffered saline (PBS) with a pH of 7.4 was used in combination with enzymatic oxygen removal (PBS, pH 7.4, containing 10% (wt/v) glucose was mixed with either 10% (v/v) or 1% (v/v) of a prior prepared glucose oxidase solution. This solution was prepared according to the following protocol: 40 μL Tris(2-carboxyethyl)phosphine hydrochloride (TCEP), 40 μL catalase and 10 mg glucose oxidase type VIII were added to 5 mL of TRIS buffer [100 mM TRIS(HCl) pH 7.5, 25 mM KCl] and mixed with 5 mL of glycerine (all purchased from Sigma). Additionally, 75 μM of the reductant ascorbic acid (AA) were added. Surface scans and transients were performed in a chambered cover slide (LabTek, NUNC) with a volume of ~750 μL sealed with microseal adhesive seals (MSB 1001, Bio-Rad, Germany).

Calibration of Oxygen Removal

To calibrate the oxygen removal of the GOC system described above we used a dissolved-oxygen meter (OxyScan light, equipped with a micro oxygen sensor for low sample volumes, UMS GmbH, Germany). Due to the size and characteristics of the sensor, higher sample volumes of around 8 mL had to be used and a magnetic stir bar was employed to ensure a constant flow. Sealing of the small beaker glass was also performed with microseal adhesive seals. For measurements with 10% GOC an equilibrium concentration of ~10 μM oxygen was reached after approximately 10 min, which is in good agreement with prior published data under similar conditions.[26]

Single-Molecule Spectroscopy

Double-stranded DNA (dsDNA) was immobilized on a glass substrate coated with BSA/biotin-streptavidin according to published procedures. By homogenizing the environment through immobilization of fluorophores in solution the static heterogeneity of the molecules is greatly reduced and thus allows the extraction of detailed kinetic information through the analysis of single-molecule fluorescence transients. To study fluorescence on the level of single molecules, a custom-built confocal microscope was used as described in refs. [1,23] (detection of Cy3/Cy5: ref. [1], detection of Cy7: ref. [23]). The laser beam of a pulsed supercontinuum source (SuperK Extreme, Koheras, Denmark) was coupled into a single-mode fiber and appropriate excitation light was chosen by an acoustic-optical tunable filter (AOTFnc-VIS, AA optoelectronic). The following excitation wavelengths were chosen: 533 nm (excitation of the Cy3), 640 nm (excitation of Cy5) and 725 nm (excitation of Cy7). The spatially filtered beam entered an inverse microscope and was coupled into an oil immersion objective (60×, NA 1.35, UPLSAPO 60XO, or 100×, NA 1.45, PLAPO100XO/TIRFM-SP, both from Olympus) by a dual-band dichroic beam splitter (Dualband z532/633 rpc for Cy5/Cy7 and a 740 DCXXR for Cy7, AHF Analysentechnik, Germany). Fluorescence transients and confocal images (size of 10 μm × 10 μm, integration time 2 ms per pixel, 50 nm per pixel) were recorded under the following conditions: 1.5 kW cm^{-2} at 533 nm, 3 kW cm^{-2} at 640 nm, and 8 kW cm^{-2} at 725 nm. The resulting fluorescence was collected by the same objective, focused onto a 50 μm pinhole, and split spectrally at 640 nm onto two APDs for Cy3/Cy5 by a dichroic beam splitter (640DCXR, AHF Analysentechnik, Germany) or onto a 120 μm pinhole and directly imaged onto only one APD for Cy7. Fluorescence was detected by avalanche photodiodes (SPCM-AQR-14, PerkinElmer) with appropriate spectral filtering (Brightline HC582/75 for Cy3, ET-Bandpass 700/75 M and Razoredge longpass for Cy5, Brightline HC 785/62 for Cy7, AHF Analysentechnik, Germany).

Data Evaluation and Analysis

The detector signal was registered and evaluated using custom made LabVIEW software. Single-molecule traces and autocorrelation analysis was performed according to published procedures.[4]

Acknowledgements

We thank Jan Vogelsang, Frederik Becher, Christian Steinhauer and Andreas Gietl for experimental assistance. I. H. Stein is grateful to the Elite Network of Bavaria (International Doctorate Program in NanoBioTechnology) for a doctoral fellowship. T. Cordes was supported by the Centre of Synthetic Biology (University of

Groningen) and the Center for NanoScience (CeNS, LMU München). P. Tinnefeld was supported by the DFG (Ti329/5-1), Biophotonics IV program of the German Ministry of Research and Education (BMBF/VDI), the Center for NanoScience (CeNS, LMU München) and the excellence cluster Nanosystems Initiative Munich.

Keywords: dyes/pigments · fluorescence spectroscopy · photophysics · single-molecule studies · super-resolution microscopy

[1] J. Vogelsang, T. Cordes, P. Tinnefeld, *Photochem. Photobiol. Sci.* **2009**, *8*, 486 – 496.
[2] M. Orrit, *Photochem. Photobiol. Sci.* **2010**, *9*, 637 – 642.
[3] R. Zondervan, F. Kulzer, S. B. Orlinskii, M. Orrit, *J. Phys. Chem. A* **2003**, *107*, 6770 – 6776.
[4] J. Vogelsang, T. Cordes, C. Forthmann, C. Steinhauer, P. Tinnefeld, *Proc. Natl. Acad. Sci. USA* **2009**, *106*, 8107 – 8112.
[5] S. W. Hell, M. Kroug, *Appl. Phys. B* **1995**, *60*, 495 – 497.
[6] E. Betzig, G. H. Patterson, R. Sougrat, O. W. Lindwasser, S. Olenych, J. S. Bonifacino, M. W. Davidson, J. Lippincott-Schwartz, H. F. Hess, *Science* **2006**, *313*, 1642 – 1645.
[7] M. J. Rust, M. Bates, X. Zhuang, *Nat. Methods* **2006**, *3*, 793 – 795.
[8] S. T. Hess, T. P. Girirajan, M. D. Mason, *Biophys. J.* **2006**, *91*, 4258 – 4272.
[9] M. Heilemann, S. van de Linde, M. Schuttpelz, R. Kasper, B. Seefeldt, A. Mukherjee, P. Tinnefeld, M. Sauer, *Angew. Chem.* **2008**, *120*, 6266 – 6271; *Angew. Chem. Int. Ed.* **2008**, *47*, 6172 – 6176.
[10] C. Steinhauer, C. Forthmann, J. Vogelsang, P. Tinnefeld, *J. Am. Chem. Soc.* **2008**, *130*, 16840 – 16841.
[11] J. Fölling, M. Bossi, H. Bock, R. Medda, C. A. Wurm, B. Hein, S. Jakobs, C. Eggeling, S. W. Hell, *Nat. Methods* **2008**, *5*, 943 – 945.
[12] T. Dertinger, R. Colyer, G. Iyer, S. Weiss, J. Enderlein, *Proc. Natl. Acad. Sci. USA* **2009**, *106*, 22287 – 22292.
[13] J. Vogelsang, C. Steinhauer, C. Forthmann, I. H. Stein, B. Person-Skegro, T. Cordes, P. Tinnefeld, *ChemPhysChem* **2010**, *11*, 2475 – 2490.
[14] T. Cordes, J. Vogelsang, M. Anaya, C. Spagnuolo, A. Gietl, W. Summerer, A. Herrmann, K. Mullen, P. Tinnefeld, *J Am Chem. Soc.* **2010**, *132*, 2404 – 2409.
[15] S. van de Linde, I. Krstic, T. Prisner, S. Doose, M. Heilemann, M. Sauer, *Photochem. Photobiol. Sci.* **2011**, *10*, 499 – 506.
[16] S. van de Linde, R. Kasper, M. Heilemann, M. Sauer, *Appl. Phys. B* **2008**, *93*, 725 – 731.
[17] H. Kuhn, *Helv. Chim. Acta* **1949**, *32*, 2247.
[18] M. Levitus, S. Ranjit, *Q. Rev. Biophys.* **2011**, *44*, 123 – 151.
[19] S. Lee, J. Lee, S. Hohng, *PLoS ONE* **2010**, *5*, e12270.
[20] M. Bates, B. Huang, G. T. Dempsey, X. Zhuang, *Science* **2007**, *317*, 1749 – 1753.
[21] M. J. S. Dewar, J. A. Hashmall, N. Trinajstic, *J. Am. Chem. Soc.* **1970**, *92*, 5555 – 5559.
[22] A. Rosspeintner, D. R. Kattnig, G. Angulo, S. Landgraf, G. Grampp, *Chem. Eur. J.* **2008**, *14*, 6213 – 6221.
[23] I. H. Stein, C. Steinhauer, P. Tinnefeld, *J. Am. Chem. Soc.* **2011**, *133*, 4193 – 4195.
[24] J. Ross, P. Buschkamp, D. Fetting, A. Donnermeyer, C. M. Roth, P. Tinnefeld, *J. Phys. Chem. B* **2007**, *111*, 321 – 326.
[25] J. Widengren, P. Schwille, *J. Phys. Chem. A* **2000**, *104*, 6416 – 6428.
[26] C. E. Aitken, R. A. Marshall, J. D. Puglisi, *Biophys. J.* **2008**, *94*, 1826 – 1835.
[27] E. S. Pysh, N. C. Yang, *J. Am. Chem. Soc.* **1963**, *85*, 2124 – 2130.
[28] J. Lenhard, *J. Imaging Sci.* **1986**, *30*, 27 – 35.
[29] J. Vogelsang, R. Kasper, C. Steinhauer, B. Person, M. Heilemann, M. Sauer, P. Tinnefeld, *Angew. Chem.* **2008**, *120*, 5545 – 5550; *Angew. Chem. Int. Ed.* **2008**, *47*, 5465 – 5469.
[30] P. M. Wood, *Biochem. J.* **1988**, *253*, 287 – 289.
[31] D. Rehm, A. Weller, *Isr. J. Chem.* **1970**, *8*, 259 – 271.
[32] I. Testa, C. A. Wurm, R. Medda, E. Rothermel, C. von Middendorf, J. Folling, S. Jakobs, A. Schonle, S. W. Hell, C. Eggeling, *Biophys. J.* **2010**, *99*, 2686 – 2694.
[33] T. Klein, A. Loschberger, S. Proppert, S. Wolter, S. van de Linde, M. Sauer, *Nat. Methods* **2011**, *8*, 7 – 9.
[34] J. R. Unruh, G. Gokulrangan, G. S. Wilson, C. K. Johnson, *Photochem. Photobiol.* **2005**, *81*, 682 – 690.
[35] P. Tinnefeld, V. Buschmann, K. D. Weston, M. Sauer *J. Phys. Chem. A* **2003**, *107*, 323 – 327.

Received: October 16, 2011
Published online on December 8, 2011

4 Single-Molecule FRET Ruler Based on Rigid DNA Origami Blocks

The impact of fluorescence resonance energy transfer (FRET), with a seminal publication by Theodor Förster in 1948 can best be evaluated decades afterwards [21]. On the occasion of the 100th anniversary of his birth Sun et al. reviewed the development of Förster's scientific contribution [33]. The authors assess that over a broad scientific area, including cell biology, the understanding of signaling and regulation and medical research, the use of FRET as a tool has increased rapidly in recent years. This is attributed to the fact that proper instrumentation as well as suitable fluorophores and analytical tools have become available and also affordable in the last two decades leading to an exponential growth in FRET publications. Nevertheless, obtaining accurate distance information has remained a challenging task. In this chapter a new type of molecular ruler for FRET measurements on the single-molecule level is introduced.

4.1 Accurate distance determination with single-molecule FRET

FRET has been widely used as a tool for determining structural properties of biomolecules. A crucial prerequisite for meaningful FRET measurements is stable fluorescence of the fluorophores, as otherwise fluctuating intensities of the dyes could be misinterpreted as distance changes. As shown by Vogelsang et al. by adding reducing and oxidizing agents to the sample solution the stability of fluorescence of common fluorophores can be greatly improved (see ref. [28] and section 3.1). When looking at biomolecular dynamics, typically between a designated low and high FRET state, the switching between these two states is monitored and

exact distances often play a minor role. On the other hand, for exact structural determination measuring accurate distances is desired.

Using FRET for acquiring exact distances is challenging for a number of reasons. Anyhow, an understanding of the photophysical properties of the fluorophores and the conditions in the experiment is essential to ensure valid results. Even with an experimental setup optimized towards a given dye pair by the choice of filters and excitation wavelengths, several corrections need to be taken into account. First of all, the crosstalk of the detected fluorescence signals needs to be considered: i) leakage, the detection of the donor dye in the acceptor channel and ii) direct excitation of the acceptor dye by the donor excitation wavelength. Additionally, with the aid of advanced single-molecule techniques, e.g. alternating laser excitation (ALEX) as described in section 2.4, new possibilities for accurate FRET measurements arise. Corrections for differing quantum yields and detection efficiencies of the fluorophores can be performed, which is often referred to as gamma-correction [34]. Applying this correction scheme enables accurate distance determination by FRET, independent of experimental factors. All distances given in associated publication P2 were determined according to the scheme outlined above [35].

4.2 Rulers used for FRET experiments

To get the most quantitative conclusions from FRET measurements and to estimate possible errors a defined and reliable FRET ruler would be a valuable tool. A defined ruler could help quantify the influences of photophysical and photochemical effects as well as instrumental factors.

The first experimental work on FRET performed by Stryer and Haugland in 1967 introduced the notion of FRET as a 'spectroscopic ruler', probing distances in the range of $1-5\,\mathrm{nm}$ [2].[1] Oligomers of poly-L-proline were used as a spacer molecule to separate a donor and an acceptor dye. The energy transfer efficiencies were determined by evaluating the donor and acceptor fluorescence spectra. In principle, the distance dependence of energy transfer from Förster theory could be validated although the experimental FRET efficiencies were generally higher than expected from rigorous calculation.

In 2005 Schuler et al. revisited the use of polyproline as spectroscopic ruler with single-

[1] Nowadays the range of $2-10\,\mathrm{nm}$ is typically seen as accessible via FRET

molecule fluorescence techniques [36]. They found that for short distances way below the Förster radius the transfer efficiencies are lower than predicted from Förster theory and assuming polyproline as a stiff rod. The authors discuss two possible contributions, namely incomplete orientational averaging during the lifetime of the donor dye and non-applicability of the point dipole approximation, due to relatively large size of the chromophores. Interestingly, the data also show a strong deviation towards higher FRET values for long polyproline residues, indicating that polyproline is more flexible than expected and cannot be readily treated as a stiff rod. Further studies of polyproline showed that a mere increase in flexibility in a worm-like chain model is not enough to fully explain the experimental deviations. Specifically, the important role of cis-trans isomerization of individual proline residues leads to a more complete picture and can explain the experimental results [37, 38, 39]. Summing up, these studies show that polyproline is not easily used as a stiff calibration ruler for FRET experiments.

As an alternative construct double stranded DNA has been used as a spacer molecule. Nowadays, this is especially convenient due to the commercial availability of DNA strands with desired sequence and fluorophore modifications. In 1993 Clegg et al. observed the helical geometry of double stranded DNA with the aid of FRET measurements [40]. A geometric model was introduced that is shown in figure 4.1 a). It includes four parameters that account for the linker lengths of the donor and acceptor dyes a and d, an offset L of the dye position along the helical axis as well as an angle θ between the dyes. The angle is

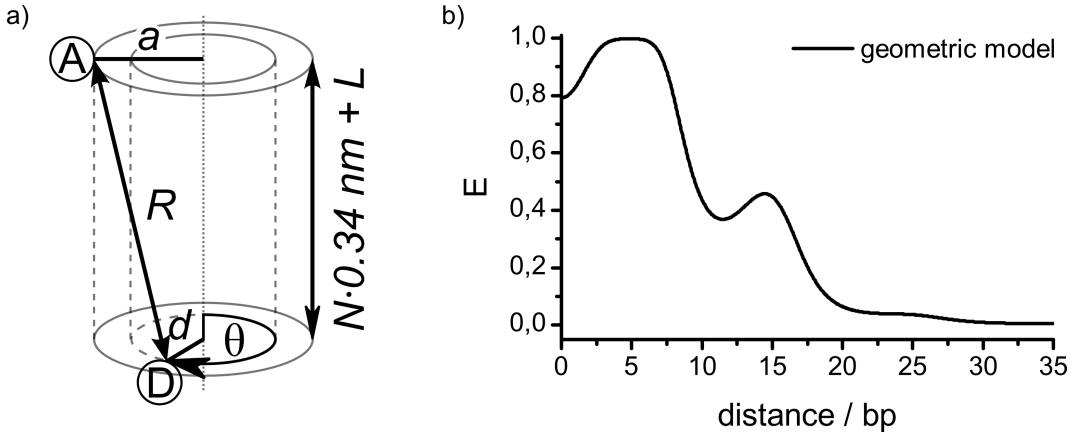

Figure 4.1: *Schematic of the geometrical model of dsDNA [40]: a) illustration of the fit parameters as described in the text b) theoretical dependence of the energy transfer efficiency on base pair separation N setting $R_0 = 5.0\,\mathrm{nm}$, $a = d = 1.5\,\mathrm{nm}$, $L = 0\,\mathrm{nm}$, $\theta = 180°$.*

given as $\theta = \frac{360°}{10.5} \cdot N + \theta_0$, assuming a helical twist of 10.5 base pairs per turn (see ref. [41]) and accounting for an angular offset θ_0 between the dyes for $N = 0$. The graph in figure 4.1 b) shows the dependence of the energy transfer efficiency E on the separation in base pairs according to the model, setting fixed values of the fit parameters as indicated in the figure caption. The behavior of the curve is more complicated and not monotonous as the dependence on physical distance (compare figure 2.1 and equation 2.1). Clegg et al. achieved a good agreement of their experimental data with the helical model of dsDNA by fitting with a fixed value for R_0 for the given dye pair [40].

However, employing dsDNA as a plain spacer molecule is hindered exactly by this helical geometry of DNA. For a FRET ruler it would be desirable to simply change the spacing of donor and acceptor dye by increments of the length of one base pair, i.e., 0.34 nm. But due to the helical turn an increase of one base pair in separation can in fact lead to a decrease in the dye to dye distance as seen in figure 4.1 b). For example, in the range between 10 and 15 base pairs, the energy transfer efficiency increases - i.e., the dyes are moving closer together - although the separation in base pairs is getting larger. In addition, the relative angle of the dyes is also changed by the turn along the helical axis with every base pair additional separation which can affect the energy transfer efficiency of the dipole-dipole interaction. The high number of fit parameters in the above mentioned helical model also has an additional adverse effect. As emphasized in associated publication P2, when fitting the experimental single-molecule data of dsDNA it is not possible to let the Förster radius R_0 vary as an additional fit parameter, as this yields results deviating strongly from expected values.

4.3 Design of a rigid DNA origami block

The DNA origami technique holds promise in circumventing a number of drawbacks of currently used molecular rulers as described in the previous section. By purposeful design tailored DNA nanostructures can be created that specifically meet the experimental requirements. In associated publication P2, the details of the design are elaborated. In brief, a three-dimensional architecture of tightly packed double helices in a square arrangement forming a rigid DNA origami block was rendered with the software caDNAno [11]. By targeted deletions of bases the global twist of the structure was removed. The resulting block-like structure is very stiff, eliminating the issue of limited persistence lengths that plagued previous rulers.

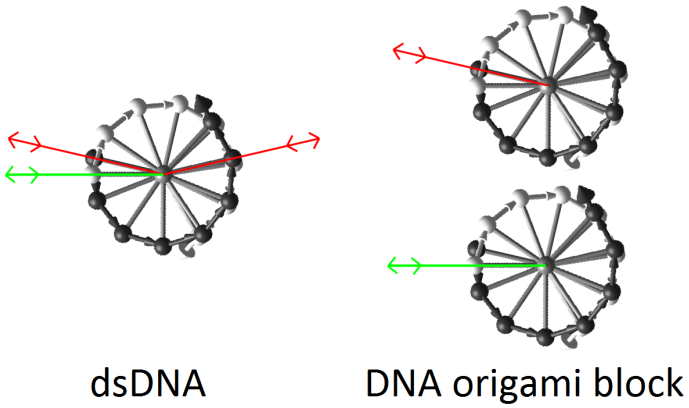

Figure 4.2: *Role of linkers for dsDNA compared to the DNA origami block: For dsDNA the linker lengths can largely contribute to the inter-dye spacing, whereas the influence is severely reduced in case of the DNA origami block as the linkers are always nearly parallel. Reprinted with permission from the supporting information of ref. [35]. Copyright 2011 WILEY-VCH.*

Additionally, the fluorophore attachment sites on the origami structure are superior for creating defined donor-acceptor separations. The influence of the linkers to the fluorophores on donor-acceptor separation is markedly reduced for the origami compared to dsDNA (see figure 4.2 and supporting information of associated publication P2, respectively). For example, for dsDNA and dye positions on opposite sides of the helical DNA, the linker lengths fully contribute to the inter-dye spacing, whereas for nearly parallel linkers on the same side the static contribution should cancel out. For the origami block all fluorophores are attached to the same surface and all linkers are oriented in nearly the same direction independent of inter-dye spacing. This leads to a minor influence of the linker lengths on the dye to dye distance. This fact is even more striking, as these linker lengths are not easily obtained, as the distance between the center of the helical DNA and the active site of the fluorophore is not readily accessible experimentally.

Single-molecule FRET measurements of a series of DNA origami blocks with varying inter-dye spacing were performed and distances were calculated based on a relatively simple geometric model of the structure. From the distance dependence of the energy transfer, the Förster radius could be directly determined, yielding $R_0 = 5.3 \pm 0.3\,\mathrm{nm}$ for the Cy3-Cy5 dye pair.

4.4 Associated publication P2

Single-Molecule FRET Ruler Based on Rigid DNA Origami Blocks

By

Ingo H. Stein, Verena Schüller, Philip Böhm, Philip Tinnefeld and Tim Liedl

published in

ChemPhysChem 2011, 12, 689–695

DOI: 10.1002/cphc.201000781

Single-Molecule FRET Ruler Based on Rigid DNA Origami Blocks

Ingo H. Stein,[a] Verena Schüller,[b] Philip Böhm,[b] Philip Tinnefeld,*[a, c, d] and Tim Liedl*[b, c]

Fluorescence resonance energy transfer (FRET) has become a work-horse for distance measurements on the nanometer scale and between single molecules. Recent model systems for the FRET distance dependence such as polyprolines and dsDNA suffered from limited persistence lengths and sample heterogeneity. We designed a series of rigid DNA origami blocks where each block is labeled with one donor and one acceptor at distances ranging between 2.5 and 14 nm. Since all dyes are attached in one plane to the top surface of the origami block, static effects of linker lengths cancel out in contrast to commonly used dsDNA. We used single-molecule spectroscopy to compare the origami-based ruler to dsDNA and found that the origami blocks directly yield the expected distance dependence of energy transfer since the influence of the linkers on the donor–acceptor distance is significantly reduced. Based on a simple geometric model for the inter-dye distances on the origami block, the Förster radius R_0 could directly be determined from the distance dependence of energy transfer yielding $R_0 = 5.3 \pm 0.3$ nm for the Cy3–Cy5 pair.

1. Introduction

The length scale below 10 nm is of profound interest for macromolecular and biomolecular interactions and structures and is accessible under biological conditions by fluorescence resonance energy transfer (FRET).[1] The use of FRET for studying biomolecular complexes began with the presentation of FRET as a spectroscopic ruler using a donor–acceptor labeled polyproline.[2] This study also experimentally demonstrated the theoretically predicted distance dependence of the energy transfer efficiency although measured FRET efficiencies were generally higher than expected.[2] Since this work, a number of approaches have been pursued to further elaborate defined donor–acceptor distances. A defined FRET ruler would be a valuable tool to estimate the accuracy of FRET-assisted distance measurements,[3] and to quantify the influence of photophysical and photochemical effects, structural flexibility and molecular heterogeneity as well as instrumental factors. Another important issue to be evaluated is the length of the linkers that are needed to attach fluorophores to the molecules of interest. With the spreading of FRET for imaging and in single-molecule spectroscopy, the interest to achieve accurate FRET measurements has further increased.

So far, the polypeptide polyproline and oligonucleotides were used to validate Förster theory and as references in biomolecular FRET studies.[3–9] Stiff organic compounds such as oligomers of *para*-phenyleneethynylene have also been suggested as FRET rulers. Such (bio-)polymers, however, exhibit a limited persistence length of ≈5–50 nm. Polyprolines had been used recently to revisit the original spectroscopic ruler and a strong deviation to expected FRET values was in particular found for larger distances.[8] This discrepancy could recently be ascribed to *cis–trans* isomerization of individual proline residues leading to a deviation from the expected stiff structure.[3,9,10] FRET as well as intramolecular quenching experiments revealed that a significant fraction of polyproline residues adopted a conformation that involved much shorter distances between donor and acceptor under relevant conditions. Due to the simplicity to produce donor- and acceptor-labeled double-stranded (ds) DNA, oligonucleotides have been used most frequently and FRET was used to illustrate the helical structure of DNA.[4–7,11–14]

On the other hand, changing the distances between donor and acceptor along DNA base-pair by base-pair does not only yield a stepwise distance change of 0.34 nm per base, but additionally goes along with a distance modulation due to the helical pitch of dsDNA, which has a diameter of ≈2 nm and a native twist of 10.5 bp per 360°. A geometric model is fre-

[a] *I. H. Stein,[+] Prof. Dr. P. Tinnefeld*
Angewandte Physik–Biophysik
Ludwig-Maximilians-Universität
Amalienstraße 54, 80799 Munich (Germany)
Fax: (+49) 89 2180 2050
E-mail: p.tinnefeld@tu-braunschweig.de

[b] *V. Schüller,[+] P. Böhm, Prof. Dr. T. Liedl*
Physik weicher Materie und Biophysik
Ludwig-Maximilians-Universität
Geschwister-Scholl-Platz 1, 80539 Munich (Germany)
Fax: (+49) 89 2180 3182
E-mail: Tim.Liedl@lmu.de

[c] *Prof. Dr. P. Tinnefeld, Prof. Dr. T. Liedl*
Center for NanoScience
Ludwig-Maximilians-Universität
Schellingstr. 4, 80799 Munich (Germany)

[d] *Prof. Dr. P. Tinnefeld*
Physical and Theoretical Chemistry-NanoBioScience
TU Braunschweig, Hans-Sommer-Str. 10, 38106 Braunschweig (Germany)

[+] *These authors contributed equally to this work.*

Supporting information for this article is available on the WWW under http://dx.doi.org/10.1002/cphc.201000781.

quently used to account for this increased complexity.[11,12] The model however, implies several fit parameters to the data and especially the role of the linkers that connect the DNA base with the dye induces considerable uncertainty because the influence of the linker length varies strongly dependent on the basepair distance between donor and acceptor. For a donor–acceptor separation of for example, 7 bps on opposite strands, the linkers should be almost parallel and on the same side of the DNA helix and their lengths (but not their dynamics) should cancel out. On the other hand, for one or twelve base pairs separation, corresponding roughly to a full turn, the dyes are on the opposite side of the DNA cylinder and the relatively undefined linker lengths largely contribute to the donor-acceptor distance (see Figure S1 in the Supporting Information). Further issues with dsDNA are the varying materials located between donor and acceptor, the anisotropic dipole–dipole orientation of molecules attached to the surface of a cylinder and the fraying and breathing of an isolated DNA double strand at a finite temperature.

DNA has long been used as a building material for nanoscale structures.[15] Herein, we introduce rigid three-dimensional DNA origami blocks as stiff FRET rulers. For DNA origami, a 8 kb-long single-stranded DNA "scaffold" is folded into shape by hundreds of short "staple" oligonucleotides.[16] This allows for the construction of arbitrarily-formed DNA objects with tunable mechanical properties.[16–20] Each position of such an object can be addressed individually, since each of the staple strands can be functionalized with (bio)chemical groups or fluorescent dyes.[21–24, 25]

We attached Cy3-donor and Cy5-acceptor dyes to the surface of an origami structure so that linkers always point in the same direction, minimizing their static influence on FRET efficiencies (Figure S1, Supporting Information). We varied the distances between the dyes and studied energy transfer efficiencies using single-molecule spectroscopy with alternating laser excitation of diffusing molecules. We compared the distance dependence of the energy transfer efficiency on the origami structure to a common double-stranded DNA FRET ruler.

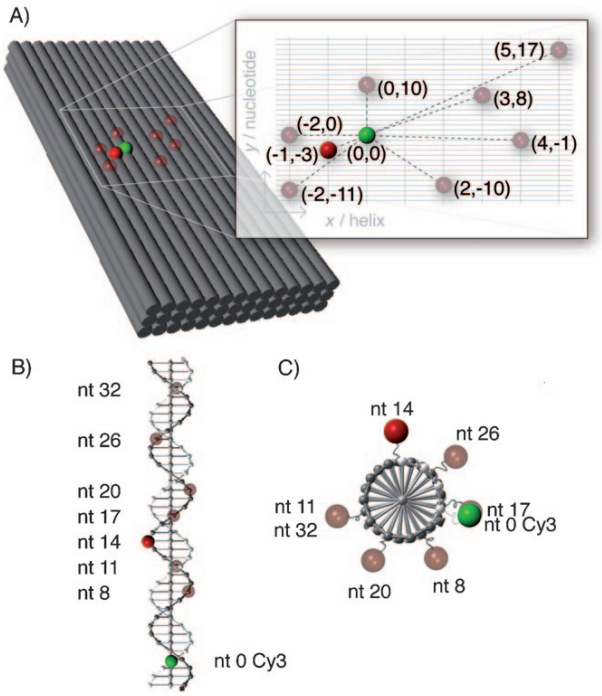

Scheme 1. Positions of the donor (green) and the acceptors (red) on the DNA FRET block and on a DNA double strand. The donor fluorophore was present in all assembled structures while only one of the acceptor dye positions was occupied in each sample.

2. Results and Discussion

2.1. DNA Origami Design

Using the software caDNAno,[17] we designed a rigid DNA origami block, which serves as a "breadboard" for the arrangement of fluorescent dyes in a single plane on top of the DNA object (Scheme 1 A). To achieve a high density of potential fluorophore sites, we chose a tightly packed square arrangement of 3×14 double helices. As scaffolding strand we used a 8064 nucleotide (nt) M13mp18-based single strand, that is arranged by 165 oligonucleotides into a plane of parallel helices that fold up to multiple layers. Each helix has a length of 168 basepairs. At the ends of the objects loops of unpaired bases (16–32 nt) are formed between each two adjacent helices (Figure S2, Supporting Information). The objects were annealed in a one-pot-reaction (Experimental Section) and analyzed with gel electrophoresis and transmission electron microscopy (TEM) (Figure 1). The measured lateral dimensions of the blocks after staining with

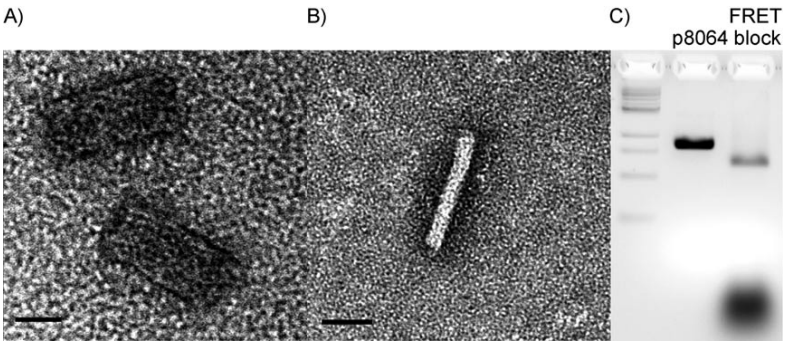

Figure 1. Electron micrograph of the DNA origami FRET blocks stained with uranyl acetate. A) Flat-lying objects. B) Standing DNA origami FRET block. The thickness of three helices is clearly visible. C) Gel analysis of assembled objects. Left to right: 2-log DNA ladder, p8064 scaffold, FRET block. The band containing the structure has been extracted and investigated with TEM. Scale bars: 20 nm.

uranyl acetate and drying are 58 nm × 30 nm, the thickness is 7 nm. These values are close to the expected values of 57 nm × 28 nm × 6 nm, if an unhydrated diameter of double-helical DNA of 2.0 nm and a spacing of 0.34 nm between two neighboring bases is assumed. However, Cryo-EM measurements of comparable objects in frozen solvent revealed an average effective diameter of 2.6 nm (±0.3 nm) for dsDNA in a square-lattice arrangement.[26] Under buffer conditions, the effective diameter is the summation of a helical diameter of 2.1 nm and an interhelical gap produced by electrostatic repulsion on the order of 0.5 nm.

The square lattice arrangement is achieved by implementing crossovers from one helix to one of its neighboring helices every eight basepairs. At a native twist of 10.5 bp per 360°,[27] eight base-pair steps along the axis of a dsDNA would correspond to a helical twist of 274.3° between two crossovers or, if a perfect square arrangement is assumed, to 10.67 bp/360° and therefore to an underwinding of the helices. To overcome the resulting global twist of the structure, we introduced targeted deletions by removing single base-pairs every 64 bp from each helix. This restores the regular 10.5 bp per 360° throughout the structure. TEM images of the corrected DNA origami FRET blocks revealed no detectable global twist (Figure 1 B).

For the donor, we chose a designated position close to the center on the "top" surface of the origami block and eight sites in close proximity in the same plane for the acceptor dyes. As donors and acceptors, we chose the well-studied Cy3 and Cy5 dyes attached to an internal thymine base via a six-carbon linker. The thymine bases were chosen such, that the dye molecules all protrude almost perpendicular out of the plane of the origami block. Thus, all dyes had approximately the same orientation—though still free to rotate and wiggle at the end of their linkers (that we refer to as dynamic heterogeneity)—and had no DNA molecule located in the direct path between them.

2.2. Double-Stranded DNA Design

For comparison, we also studied the same donor–acceptor pair with a system, where a single DNA double-helix is used as spacer between the fluorophores. The Cy3 donor was attached to a thymine close to the 5′ end of a 39 nt long oligonucleotide (Experimental Section). Each of seven complementary strands carried a Cy5 acceptor at a distance of 8, 11, 14, 17, 20, 26, and 32 base pairs from the donor (Scheme 1 B,C).

2.3. Distance Dependence of Energy Transfer

We used single-molecule fluorescence spectroscopy with alternating laser excitation (ALEX)[28] on diffusing molecules to investigate the distance dependence of FRET in our dsDNA and FRET blocks. ALEX was used to separate intact doubly-labeled populations from donor-only and acceptor-only populations and to determine correction factors (see the Experimental Section for details). Solution measurements were performed at a concentration of ≈0.1 nM such that the fluorescence bursts of diffusing molecules could be well identified by a burst search algorithm. Three consecutive measurements were taken for each sample (10 min each for the seven dsDNA samples and 15 min each for the eight FRET blocks) to obtain a total average number of bursts of 5000 (dsDNA) and 3000 (origami block) for each sample. Lower-burst yields of FRET blocks are due to their slower diffusion time. The energy transfer efficiencies E for each burst were calculated from the photon counts as described in detail in the Experimental Section. The energy transfer efficiency E for each sample as plotted in Figures 2 and 3 were determined by applying a Gaussian fit to the histogram of E values of the selected doubly-labeled population. The statistical error was determined from three separate measurements taking into account the uncertainty of the corrections for direct excitation and leakage.

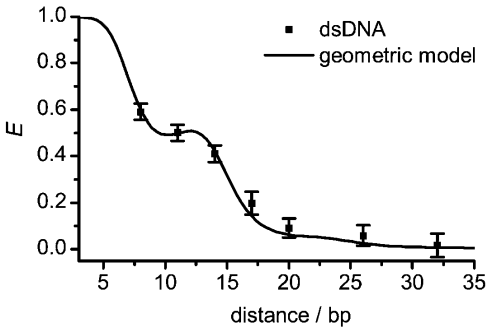

Figure 2. FRET efficiencies of dsDNA samples as a function of donor-acceptor separation in base-pairs. The solid line is a fit to the data according to a geometric model of dsDNA as described in the text.

The shape and width of the energy transfer and stoichiometry histograms of the DNA origami samples are similar to the corresponding histograms of the dsDNA samples (Figure S3, Supporting Information). Besides small donor-only and acceptor-only populations, a single homogenous FRET population is observed, indicating that correctly folded structures were obtained quantitatively without a detectable fraction of misfolded origami structures.

To compare the two systems, we used molecular models for the dsDNA as well as for the origami structures. For dsDNA we adopted the model of Clegg et al.[11] used for mapping the helical structure of double-stranded DNA via FRET. Instead of ten basepairs per helical turn of the double strand as observed in the solid state, we adjusted the value in the model to 10.5 turns—the same value we used for the origami structures—which is appropriate for dsDNA in solution.[27] The model takes into account the rotation of the dyes around the helical axis and their linker lengths. All in all, four parameters were introduced in the model: a and d, as helix radius plus individual linker lengths to donor and acceptor dyes, a displacement L along the helical axis and an angle θ_0 between the dyes for zero basepair separation. In the case of Cy3 and Cy5 as donor and acceptor pair it seems reasonable to assume equal lengths a and d, due to the similar structure and properties of the two

cyanine dyes and their identical linker length of six carbon atoms. To account for these geometrical constraints we used Equation (1):[11]

$$R = \sqrt{(0.34\text{nm}\Delta n + L)^2 + 2a^2 - 2a^2 \cos\left(\frac{360^\circ}{10.5}\Delta n + \theta_0\right)} \qquad (1)$$

The above equation together with the Förster equation [Eq. (5) with $R_0 = 5.4$ nm for the Cy3–Cy5 dye pair[29,30]] was fitted to the data using the Levenberg–Marquardt least-squares algorithm and is shown in Figure 2. The following fit parameters were obtained: $a = 18 \pm 1$ Å, $L = 9 \pm 1$ Å, $\theta_0 = 243^\circ \pm 9^\circ$. As a result of the geometrical fit of the dsDNA data, the separations in basepairs were converted to absolute distances in nm. The corrected distance dependence of the energy transfer efficiency is shown in Figure 3.

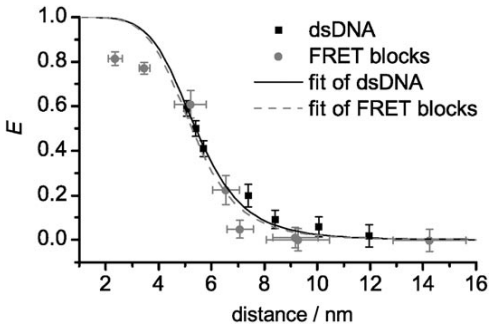

Figure 3. FRET efficiencies of dsDNA (black) and FRET block samples (grey) as a function of distance. The distances for dsDNA were calculated from the basepair separation according to the geometrical model with the prior obtained fit parameters. The FRET block data was fitted to the Förster equation [Eq. (5)] yielding $R_0 = 5.3 \pm 0.3$ nm.

Figure 3 also contains a distance-corrected plot of the origami block, which was modelled incorporating two significant corrections: 1) The position of the labeled thymine bases could not always be chosen such that each base is exactly pointing along the normal of the plane formed by the 14 parallel helices. In fact, most of the labeled bases were tilted either 17° clockwise (cw) or counter clockwise (ccw) away from this normal when the line of sight follows the axis of the respective helix. For example, an acceptor located two helices away and 10 bases downstream from the donor is tilted 17° ccw with respect to the donor, which is oriented in the plane normal. The projected shift was added (or subtracted) in the model, assuming a distance of the dye to the helix center of 2 nm. 2) Since the helices are connected through crossovers only every 31 bases, the gap between two double strands is not constant along their axis. Analyzing the cryo-electron-microscopy data of Ke et al.,[26] we estimate a minimal center-to-center distance of 2.3 nm at the crossovers sites and a maximum distance of 2.9 nm in the central position between two crossovers (Table S4, Supporting Information). These minimum and maximum values were also used for the error estimation in the distance calculation for each origami sample. The individual widths of the error bars in Figure 3 are due to different numbers of helices that are crossed between donor and acceptor. In between the extremes we interpolate the distances between neighboring helices. Based on the models used to derive the interchromophore distances, the FRET efficiency graphs are in good agreement with the values expected from Förster theory for both the dsDNA as well as for the FRET blocks (Figure 3). We ascribe deviations for the shortest distances of the FRET blocks to decreased orientational averaging at small distances due to fast energy transfer as has been suggested for polyprolines and to photophysical effects due to direct chromophore interactions.[8,12] The fit for the FRET block directly yields a Förster radius of 5.3 nm for the Cy3–Cy5 pair.

The key difference between the two discussed molecular FRET rulers is that for dsDNA a complex geometrical model with several fit parameters had to be used to translate the basepair distance into physical distance. The parameters a and L are not experimentally accessible. It was not possible to achieve an adequate fit of the data in Figure 2 with reasonable assumptions for these parameters. Specifically, the presented fit required three variable parameters and a fixed Förster radius R_0. Varying R_0 as a fourth fit parameter, for example, yields: $a = 20 \pm 1$ Å, $L = 31 \pm 5$ Å, $\theta_0 = 227^\circ \pm 7^\circ$, $R_0 = 7.5 \pm 0.4$ nm. Although the linker length a and the angle θ_0 adopt reasonable values, the displacement L along the helical axis as well as the Förster radius R_0 deviate strongly from expected values.

In contrast, our model of the origami samples directly provides interchromophore distances that allow a fit to the Förster equation yielding a reasonable R_0 value. Importantly, all assumptions of the origami structure that are the basis for the distance determination are principally accessible by other experimental methods. The inaccessible linker lengths between the DNA and the fluorophores essentially cancel out for the FRET blocks. For an interhelix spacing of 2.6 nm for example, the fitted R_0 varies by less than 0.06 nm if the dye distance to the helix center is changed from 1.7 nm to 2.3 nm. This comparison shows that the origami FRET rulers directly exhibit a distance dependence that closely resembles the predicted behavior by the Förster model.

It is worth mentioning that the presence of magnesium ions during our measurements generally increases FRET efficiencies for the FRET blocks whereas FRET values are independent of magnesium for the dsDNA (Figure S5, Supporting Information). This can be attributed to the fact that electrostatic repulsion between the negatively charged backbones of adjacent helices are screened more effectively by divalent ions which leads to smaller interhelical gaps. A thorough analysis of the influence of changing mono- and divalent ion concentrations on DNA origami geometry is currently underway. This will also reveal whether remaining deviations of energy transfer efficiencies are related to the limited structural model of the origami block and the uncertainty of the dye positions or whether for example, linker dynamics and photophysical effects are more significant.

3. Conclusions

Rigid DNA origami blocks prove to be a suitable FRET ruler with distinct advantages compared to double-stranded DNA or polyprolines. Compared to dsDNA, the influence of the linker is minimized and no multiparametric fit is required to translate the basepair separation into physical distance. By placing all dyes in a single plane on one side of the origami block, the interdye distance is known a priori and, importantly, the linker influence is reduced. Our data of eight origami blocks directly reveal the distance dependence of Förster theory and yield a reasonable R_0 value of 5.3 ± 0.3 nm well in accordance with literature values that vary between 5.4 and 6.0 nm.[14,29,30] The variation is related to the environmentally sensitive quantum yield of Cy3.[31] It will be a matter of future studies whether remaining fit uncertainties are related to the accuracy of our structural origami model or to uncertainties in the measurements related for example, to the linker dynamics. The high resolution of the method certainly shows that single-molecule FRET is well-suited to study structural and dynamic aspects in DNA origami and related nanostructures. FRET probes at sensitive positions could be used, for example, to characterize folding of highly complex three-dimensional origami constructs. Compared to AFM or TEM imaging, single-molecule FRET provides improved local resolution and the relatively non-invasive measurements are carried out in solution.

Experimental Section

Preparation of dsDNA Samples: HPLC-purified oligonucleotides were purchased from IBA GmbH (Göttingen, Germany). Sequences used to spatially separate the FRET pair: donor strand: 5′-ATC $\mathbf{T}_{Cy3}$CA CGA TTA AGA TGA GTA TAA GAA ATA GGA GCA ACA-3′-Biotin, acceptor strands: 5′-TGT $\mathbf{T}_{Cy5}$GC TCC $\mathbf{T}_{Cy5}$AT TTC $\mathbf{T}_{Cy5}$TA $\mathbf{T}_{Cy5}$AC $\mathbf{T}_{Cy5}$CA $\mathbf{T}_{Cy5}$CT $\mathbf{T}_{Cy5}$AA TCG TGA GAT-3′. The donor fluorophore ($\mathbf{T}_{Cy3}$) is fixed on the fourth base of the donor strand while the acceptor positions ($\mathbf{T}_{Cy5}$) on the acceptor strands vary from 8 nucleotides (nt) to 32 nt between donor and acceptor. In total, seven 39-basepair (bp) dsDNAs with distinct distances between donor and acceptor were tested. The DNA duplexes were formed with a molar ratio of 1:1 between each two strands at a concentration of 10 μM per oligonucleotide. Hybridization was achieved by cooling from 95 °C down to 20 °C in the course of two hours.

Preparation of DNA Origami FRET Block: The unmodified and HPSF® purified staple strands were purchased from Eurofins MWG Operon (Ebersberg, Germany) (see the Supporting Information, Tables S6 and S7 for sequences). The following fluorescently labeled and HPLC purified sequences were acquired from IBA GmbH (Göttingen, Germany): donor strand: 5′-AAT GCG CGA GTT ACA AAT CCT GAT AAA CAT AGT AGG $\mathbf{T}_{Cy3}$CT GTA AAT AAG-3′, acceptor strands: 2.4 nm: 5′-AGA GTC CAC ACA GAC AAT CCA GAA AAT CAA TAT ATC TTT AGA ATT A$\mathbf{T}_{Cy5}$C-3′, 3.5 nm: 5′-ACA AAG TTA GTC CTG AGC GCC CAA GCG TTA TAT AAG GCG TAG AGA C$\mathbf{T}_{Cy5}$A-3′, 5.2 nm: 5′-AGA GTC CAC ACA GAC AAT CCA GAA AAT CAA TAT ATC TTT AGA A$\mathbf{T}_{Cy5}$T ATC-3′, 6.5 nm: 5′-AAT AAA CAT TT$_{Cy5}$T AGC GAA ATC AGA AAA AAC AGG AAA CCG ATA ATA ACG-3′, 7.1 nm: 5′-TGC CTG AGA T$_{Cy5}$CT AAA ATC TGG TCA TCA ATA TAA ATC GCG CTA TTC ATT-3′, 9.2 nm: 5′-GCC AGA ATA AAA GAA CAA AAG GGC ATT AGA CGT TG$\mathbf{T}_{Cy5}$ TTA AGA CTT GCG-3′, 9.3 nm: 5′-AAT AGA TAA CCA GAA GGG AAG CGC GAC ATT CAT TA$\mathbf{T}_{Cy5}$ CAC CCA TAG CCC-3′, 14.2 nm: 5′-CGT ACT CAC A$\mathbf{T}_{Cy5}$C GGC AGG AAC CGC CCA AAG ACT GGC ATG AAT AGC CGA-3′. A solution containing scaffold strand (10 nM, p8064, M13mp18 phage-based), unmodified staple strands (100 nM each), fluorescently modified staple strands (500 nM each), Tris-HCl (10 mM) + EDTA (1 mM, pH 8.0 at 20 °C), $MgCl_2$ (18 mM), was heated to 80 °C for 5 min., cooled to 60 °C over the course of 80 min., and cooled further down to 24 °C in 21.6 h.

Gel Electrophoresis: 2% Agarose in Tris borate (45 mM) + EDTA (1 mM, pH 8.2 at 20 °C) was heated to boiling and cooled to 60 °C. $MgCl_2$ (11 mM) were added and filled into the gel cask for solidification. Both scaffold strands (10 μL of 20 nM, p8064, M13 mp18 phage-based) and initially annealed DNA origami structures (20 μL of 10 nM) were each mixed with 6× Agarose Gel Loading Buffer (30% glycerol weight-to-volume in water, 0.025% xylene cyanol, 0.025% bromphenol blue). Gel pockets were filled with 2-Log DNA ladder, scaffold strands (2×10^{-13} mol) and origami structures (2×10^{-13} mol). To protect structures from denaturation, the gel cask was cooled in an ice-water bath. After running for 3 h at 70 V, the gel was stained with Ethidium Bromide (0.5 μg mL^{-1}) and imaged. The origami structure band was extracted from the gel and run through spin columns (Freeze'n Sqeeze Spin Columns, Biorad) at 5000×g. The samples were then imaged using a JEM-1011 transmission electron microscope (JEOL) after negative staining with uranyl acetate for 8 s.

Purification of DNA Origami FRET Blocks for Fluorescence Measurements: To remove the excess staple strands, the samples were purified using Amicon Ultra-0.5 mL Centrifugal Filters (100,000 MWCO) 4× at 14000×g for 5 min. Between each centrifugal step 450 μL of buffer (TE with 18 mM $MgCl_2$) were added. After the last step, the filter was turned upside down and spun once more at 1000×g for 3 min to recover the samples.

Conditions for Single-Molecule Fluorescence Measurements: The single-molecule fluorescence measurements were carried out at room temperature (22 °C) in standard phosphate buffered saline (PBS) with oxygen removal using an enzymatic oxygen-scavenging system [PBS, pH 7.4, containing 10% (w/v) glucose and 12.5% (v/v) glycerine, glucose oxidase (50 μg mL^{-1}), catalase (100–200 μg mL^{-1}), and tris(2-carboxyethyl)phosphine hydrochloride (TCEP) (0.1 mM)]. Additionally, ascorbic acid (1 mM) and *N*,*N*-methylviologen (1 mM) were added to reduce blinking and bleaching according to the ROXS scheme.[32] (For the measurements with magnesium 18 mM magnesium were added.) The solution based measurements were performed on glass slides, which were prepared with perforated adhesive silicone sheets (Grace Bio-Labs, OR) to enable small sample volumes of 50 μL. To prevent DNA accumulation at the surface these custom sample chambers were incubated with BSA (1 mg mL^{-1} BSA in PBS) prior to the measurement.

Single-Molecule Fluorescence Spectroscopy: To study fluorescence and energy transfer on the level of single molecules, a custom-built confocal microscope was used as described in ref. [33]. The setup allowed alternating laser excitation of donor and acceptor fluorophores on diffusing molecules with separate donor and acceptor detection. Therefore the laser beam of a pulsed supercontinuum source (Koheras SuperK Extreme, NKT Photonics, Denmark) was coupled into a single-mode fiber and alternated on microsecond time scales by use of an acousto-optical tunable filter (AOTFnc-VIS, AA optoelectronic). Two excitation wavelengths were chosen: 533 nm (spectral width of 2 nm, excitation of Cy3) and 640 nm (spectral width of 2 nm, excitation of Cy5). The spatially filtered beam entered an inverse microscope and was coupled into a

water-immersion objective (60X, NA 1.20, UPlanSApo 60XW, Olympus) by a dual-band dichroic beam splitter for solution measurements (Dualband z532/633, AHF Analysentechnik, Germany). The light intensities were 120 μW at 533 nm for the donor Cy3 and 60 μW at 640 nm for the acceptor Cy5 for the measurements of the dsDNA samples and 15 μW (533 nm) and 10 μW at 640 nm for measurements of the origami samples. The laser alternation period between the two laser beams was fixed at 50 μs. The resulting fluorescence was collected by the same objective, focused onto a 50 μm pinhole, and split spectrally at 640 nm by a dichroic beam splitter (640DCXR, AHF Analysentechnik, Germany). Two avalanche photodiodes (SPCM-AQR-14, PerkinElmer) detected the donor and acceptor fluorescence with appropriate spectral filtering (Brightline HC582/75 and Razoredge Long Pass 647, AHF Analysentechnik, Germany). The detector signal was registered and evaluated using custom made LabVIEW software.

Data Evaluation for ALEX Measurements: In solution measurements, fluorescence bursts from single molecules diffusing through the laser focus were identified by the Seidel burst search algorithm applied to the sum of donor and acceptor photons (parameters used for origami block: $T=5$ ms, $M=60$, $L=100$, for dsDNA: $T=500$ μs, $M=40$, $L=60$).[34] Molecules are alternately excited and the fluorescence of donor and acceptor is separately detected. This defines three different photon counts: donor emission due to donor excitation F_D^D acceptor emission due to acceptor excitation F_A^A and acceptor emission due to donor excitation F_D^A. F_D^A is sometimes referred to as the FRET channel. Using these values the stoichiometry parameter S and the proximity ratio E^* are defined [see Eqs. (2) and (3)], where S describes the ratio between donor and acceptor dyes of the sample and E^* stands for the proximity ratio between the dyes in terms of energy-transfer efficiency:[28]

$$E^* = \frac{F^{FRET}}{F^{FRET} + F_D^D} \tag{2}$$

$$S = \frac{F^{FRET} + F_D^D}{F^{FRET} + F_D^D + F_A^A} \tag{3}$$

where $F^{FRET} = F_D^A - leF_D^D - dxF_A^A$.
The above equations include two additional terms apart from the photon counts, namely leakage *le* and direct excitation *dx*, which correct for crosstalk of the dyes. These parameters can be experimentally obtained by taking the ratio $le = F_D^A/F_D^D$ for a donor-only sample and $dx = F_D^A/F_A^A$ for an acceptor-only sample. Apart from the crosstalk correction, the detection correction factor γ is necessary to take into account differing detection efficiencies and quantum yields of the dyes. This enables the determination of an accurate E value that directly reports on the distance between the dyes [Eq. (4)]:

$$E = \frac{E^*}{\gamma + E^*(1-\gamma)} \tag{4}$$

This accurate E value can then be used to calculate the distances according to the Förster equation [Eq. (5)]:

$$E = \frac{1}{1 + \left(R/R_0\right)^6} \tag{5}$$

For γ calculation the method employing low- and high-FRET samples was employed,[6] that is, the measurements of the dsDNA as well as the origami samples could directly be used to calculate the corresponding γ values.

Acknowledgements

We thank Christian Steinhauer for valuable advice, Susanne Kempter and Robert Schreiber for assistance in sample preparation and Martina Bucher for assistance with the ALEX measurements. We gratefully acknowledge financial support by the DFG (TI 329/5-1 LI1743/2-1), the Volkswagen Foundation, the Nanosystems Initiative Munich, the Center for NanoScience and the Elite Network of Bavaria (International Doctorate Program NanoBioTechnology).

Keywords: DNA · FRET · nanotechnology · self-assembly · single-molecule studies

[1] T. Förster, *Ann. Phys.* **1948**, *437*, 55 – 75.
[2] L. Stryer, R. P. Haugland, *Proc. Natl. Acad. Sci. USA* **1967**, *58*, 719 – 726.
[3] R. B. Best, K. A. Merchant, I. V. Gopich, B. Schuler, A. Bax, W. A. Eaton, *Proc. Natl. Acad. Sci. USA* **2007**, *104*, 18964 – 18969.
[4] M. Antonik, S. Felekyan, A. Gaiduk, C. A. M. Seidel, *J. Phys. Chem. B* **2006**, *110*, 6970 – 6978.
[5] A. A. Deniz, M. Dahan, J. R. Grunwell, T. Ha, A. E. Faulhaber, D. S. Chemla, S. Weiss, P. G. Schultz, *Proc. Natl. Acad. Sci. USA* **1999**, *96*, 3670 – 3675.
[6] N. K. Lee, A. N. Kapanidis, Y. Wang, X. Michalet, J. Mukhopadhyay, R. H. Ebright, S. Weiss, *Biophys. J.* **2005**, *88*, 2939 – 2953.
[7] E. Nir, X. Michalet, K. M. Hamadani, T. A. Laurence, D. Neuhauser, Y. Kovchegov, S. Weiss, *J. Phys. Chem. B* **2006**, *110*, 22103 – 22124.
[8] B. Schuler, E. A. Lipman, P. J. Steinbach, M. Kumke, W. A. Eaton, *Proc. Natl. Acad. Sci. USA* **2005**, *102*, 2754 – 2759.
[9] L. P. Watkins, H. Chang, H. Yang, *J. Phys. Chem. A* **2006**, *110*, 5191 – 5203.
[10] S. Doose, H. Neuweiler, H. Barsch, M. Sauer, *Proc. Natl. Acad. Sci. USA* **2007**, *104*, 17400 – 17405.
[11] R. M. Clegg, A. I. Murchie, A. Zechel, D. M. Lilley, *Proc. Natl. Acad. Sci. USA* **1993**, *90*, 2994 – 2998.
[12] N. Di Fiori, A. Meller, *Biophys. J.* **2010**, *98*, 2265 – 2272.
[13] J. Vogelsang, S. Doose, M. Sauer, P. Tinnefeld, *Anal. Chem.* **2007**, *79*, 7367 – 7375.
[14] A. Dietrich, V. Buschmann, C. Muller, M. Sauer, *Rev. Mol. Biol.* **2002**, *82*, 211 – 231.
[15] N. C. Seeman, *Nature* **2003**, *421*, 427 – 431.
[16] P. W. Rothemund, *Nature* **2006**, *440*, 297 – 302.
[17] S. M. Douglas, H. Dietz, T. Liedl, B. Hogberg, F. Graf, W. M. Shih, *Nature* **2009**, *459*, 414 – 418.
[18] H. Dietz, S. M. Douglas, W. M. Shih, *Science* **2009**, *325*, 725 – 730.
[19] T. Liedl, B. Hogberg, J. Tytell, D. E. Ingber, W. M. Shih, *Nat. Nanotechnol.* **2010**, *5*, 520 – 524.
[20] E. S. Andersen, M. Dong, M. M. Nielsen, K. Jahn, R. Subramani, W. Mamdouh, M. M. Golas, B. Sander, H. Stark, C. L. P. Oliveira, J. S. Pedersen, V. Birkedal, F. Besenbacher, K. V. Gothelf, J. Kjems, *Nature* **2009**, *459*, 73 – 76.
[21] Y. Ke, S. Lindsay, Y. Chang, Y. Liu, H. Yan, *Science* **2008**, *319*, 180 – 183.
[22] J. Sharma, R. Chhabra, C. S. Andersen, K. V. Gothelf, H. Yan, L. Yan, *J. Am. Chem. Soc.* **2008**, *130*, 7820 – 7821.
[23] S. Pal, Z. T. Deng, B. Q. Ding, H. Yan, Y. Liu, *Angew. Chem.* **2010**, *122*, 2760 – 2764; *Angew. Chem. Int. Ed.* **2010**, *49*, 2700 – 2704.
[24] B. Ding, Z. Deng, H. Yan, S. Cabrini, R. N. Zuckermann, J. Bokor, *J. Am. Chem. Soc.* **2010**, *132*, 3248 – 3249.
[25] C. Steinhauer, R. Jungmann, T. L. Sobey, F. C. Simmel, P. Tinnefeld, *Angew. Chem.* **2009**, *121*, 9030 – 9034; *Angew. Chem. Int. Ed.* **2009**, *48*, 8870 – 8873.
[26] Y. Ke, S. M. Douglas, M. Liu, J. Sharma, A. Cheng, A. Leung, Y. Liu, W. M. Shih, H. Yan, *J. Am. Chem. Soc.* **2009**, *131*, 15903 – 15908.
[27] M. Levitt, *Proc. Natl. Acad. Sci. USA* **1978**, *75*, 640 – 644.
[28] A. N. Kapanidis, N. K. Lee, T. A. Laurence, S. Doose, E. Margeat, S. Weiss, *Proc. Natl. Acad. Sci. USA* **2004**, *101*, 8936 – 8941.
[29] A. Iqbal, S. Arslan, B. Okumus, T. J. Wilson, G. Giraud, D. G. Norman, T. Ha, D. M. Lilley, *Proc. Natl. Acad. Sci. USA* **2008**, *105*, 11176 – 11181.

[30] S. Lee, J. Lee, S. Hohng, *PLoS One* **2010**, *5*, e12270.
[31] M. E. Sanborn, B. K. Connolly, K. Gurunathan, M. Levitus, *J. Phys. Chem. B* **2007**, *111*, 11064 – 11074.
[32] J. Vogelsang, R. Kasper, C. Steinhauer, B. Person, M. Heilemann, M. Sauer, P. Tinnefeld, *Angew. Chem.* **2008**, *120*, 5545 – 5550; *Angew. Chem. Int. Ed.* **2008**, *47*, 5465 – 5469.
[33] J. Vogelsang, T. Cordes, P. Tinnefeld, *Photochem. Photobiol. Sci.* **2009**, *8*, 486.
[34] C. Eggeling, S. Berger, L. Brand, J. R. Fries, J. Schaffer, A. Volkmer, C. A. M. Seidel, *J. Biotechnol.* **2001**, *86*, 163 – 180.

Received: September 22, 2010
Revised: January 7, 2011
Published online on February 9, 2011

5 Single-Molecule Four-Color FRET Visualizes Energy-Transfer Paths on DNA Origami

Based on the design of a rigid DNA origami ruler, two fluorophores can be placed with defined spacing, as demonstrated in the previous chapter. Yet, the DNA origami technique offers the means of creating substantially more complex arrangements of incorporated molecules. Paul Rothemund already anticipated this notion of a 'nanobreadboard' when introducing the technique in 2006 [10]. In associated publication P3, a rectangular DNA origami is used to precisely arrange four individual fluorophores, creating a spectroscopic network with nanometer dimensions. Such photonic devices and light-based circuitry could help to overcome limitations of current electronics. The functionality of the assembled structures is visualized by a novel four-color FRET approach based on alternating lasers and separate excitation and detection of all fluorophores.

5.1 Spectroscopic networks

Nature's light harvesting complexes are a magnificent demonstration of directed energy transfer on the nanoscale, making use of the FRET mechanism. Inspired by these fundamental components of photosynthesis Wagner et al. synthesized a molecular photonic wire consisting of a conjugated linear array of zinc porphyrins, with fluorescent dyes as input and output. Further work on molecular wires was often based on double stranded DNA as a scaffolding material [42, 43, 44]. What is fundamentally different about this application of FRET is that it is not used as tool to report on distances or interactions, but to transport excited state energy.

An overview of techniques for light harvesting and charge separation based on DNA nanostructures is given in a review by Albinsson et al. [45]. In general, for FRET-based photonic wires there are two possible schemes for energy transfer. On the one hand, the energy can be transferred in an energetic cascade of spectrally distinct fluorophores. This creates a strong directionality with a defined input and output fluorophore. On the other hand, multiple fluorophores of the same type can be arranged in series, with the energy transfer relying on multiple homo-FRET steps. This does not define a direction, but resembles a statistical diffusion of the excited state.

For the first case outlined above, Heilemann et al. demonstrated unidirectional multi-step FRET on the single-molecule level by incorporating five spectrally distinct fluorophores along a DNA strand [42]. The second approach was shown e.g. by Hannestad et al. using dsDNA as a scaffold and an intercalating dye, YO, with transfer of energy based on homo-FRET [43]. To achieve a directionality a donor dye (pacific blue) and an acceptor dye (Cy3) were attached at the respective ends of the wire.

All the examples described so far have in common that the energy is transported simply in a linear fashion. It is not straight forward to increase the complexity to form defined branches and junctions. Especially, the energy transfer efficiency is very sensitive to minute changes in the distance - that is the property it is used for in typical FRET studies. Here the DNA origami technique offers a new dimension of complexity for designing a spectroscopic network.

In associated publication P3 a rectangular DNA origami is used as a breadboard comparable to the circuit boards in electronics. A blue dye (Atto 488) is used as input dye, whereas the energy can be transferred to either the red (Atto 647N) or IR (Alexa 750) output dye, mediated by the position of a green dye (Atto 565) (compare figure 1.1 and figure 5.1 a)). The positions of the individual fluorophores are optimized to allow minimal direct energy transfer from the input to either of the outputs in the absence of the green dye. Only in the presence of the green 'jumper' dye a two-step energy transfer gives rise to a substantial transfer efficiency that can be read out by a fluorescence signal of the respective output dye.

5.2 Improved detection scheme: four-color ALEX

Monitoring complex multi-fluorophore networks poses high demands on the experimental setup. Naturally, single-molecule methods are most suited as sample heterogeneity is expected

due to partially incomplete labeling with the fluorophores. For investigating the DNA origami FRET ruler in chapter 4 a two-color single-molecule setup with alternating laser excitation was used. This scheme had already been extended to three colors for monitoring multiple distances simultaneously (see e.g. refs. [46, 47]). In associated publication P3 these 3-color schemes were once more enhanced to enable independent excitation and detection of four spectrally distinct fluorophores.

The setup includes alternating laser excitation of four wavelengths that are optimized for individual excitation of the fluorophores, i.e. 495 nm (blue), 568 nm (green), 650 nm (red), and 725 nm (IR). The alternation was achieved with an acousto-optic tunable filter (AOTF), setting a total alternation of 100 μs. Since the diffusion time of the molecules is on the order of milliseconds, it is ensured that each molecule is cycled multiple times when passing the laser focus. The resulting bursts of fluorescence are collected on four avalanche photo diodes, spectrally separated by appropriate dichroic mirrors and filters and synchronized with the laser alternation.

The experimentally obtained photon-count streams are analyzed with a burst search algorithm (see ref. [48]) to distinguish the bursts of fluorescence caused by diffusing molecules from background fluctuations. Subsequently these bursts, containing an average of $\approx$ 500 photons, are analyzed for their dye stoichiometry as well as their energy transfer properties. Notably, stoichiometric ratios between each pair of dyes are calculated, allowing to assign the exact fluorophore composition of every diffusing molecule.

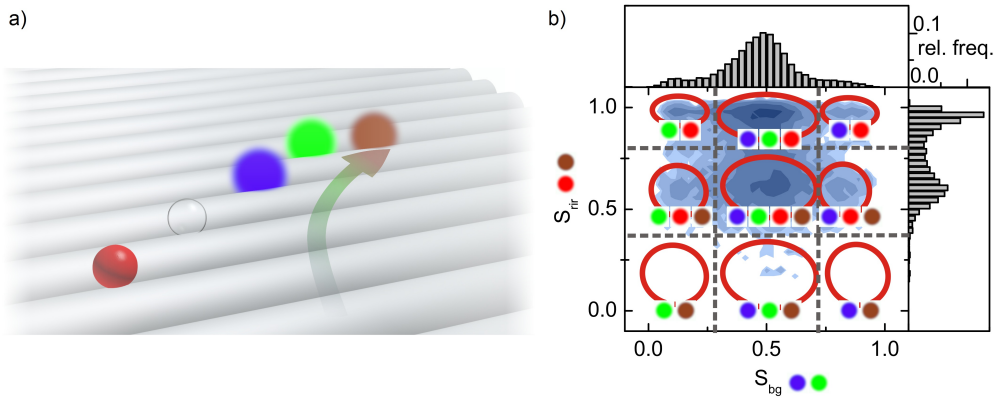

Figure 5.1: *Virtual sorting of molecules: a) schematic section of a rectangular DNA origami with the green jumper dye guiding the light towards the IR output, b) 2-dimensional histogram of the dye stoichiometry of the sample shown in a) with the partially labeled subpopulations marked in red. Adapted with permission from the supporting information of ref. [18]. Copyright 2011 American Chemical Society.*

The stoichiometry parameters allow the virtual sorting of molecules which is visualized in figure 5.1. On the left in panel a) a schematic section of a rectangular DNA origami with the green jumper dye guiding the light towards the IR output is shown. On the right in panel b) a 2-dimensional histogram of the dye stoichiometry of this sample is depicted. On the horizontal axis the parameter S_{bg} indicates the dye stoichiometry between blue and green, where $S_{bg} = 1$ corresponds to 'blue dye only', $S_{bg} = 0$ to 'green dye only' and $S_{bg} = 0.5$ to a 1:1 dye relation. Together with the ratio S_{rir} between the red and IR dye on the vertical axis, specific subpopulations can be assigned which are circled in red. The respective dye composition is indicated by the solid colored circles below each population.

From the graph in figure 5.1 b) it is clear that the incorporation of the blue, green and red dyes occurs with a very high yield. On the other hand, for a high number of origami rectangles the IR fluorophore Alexa 750 is missing. Since the general incorporation scheme for all dyes is the same, this might be ascribed to an inactive fraction of Alexa 750 as is common for cyanine dyes (see e.g. ref. [49]). For further analysis of the energy-transfer properties of the spectroscopic network only the fully labeled population was selected. The control over the alternative energy-transfer paths is demonstrated in associated publication P3.

The details of the experimental setup as well as the implementation of all crosstalk corrections are described in the supporting information of associated publication P3 (see appendix).

5.3 Associated publication P3

Single-Molecule Four-Color FRET Visualizes Energy-Transfer Paths on DNA Origami

By

Ingo H. Stein, Christian Steinhauer and Philip Tinnefeld

published in

J. Am. Chem. Soc. 2011, 133, 4193–4195

March 30, 2011
Volume 133
Number 12
pubs.acs.org/JACS

JACS

JOURNAL OF THE AMERICAN CHEMICAL SOCIETY

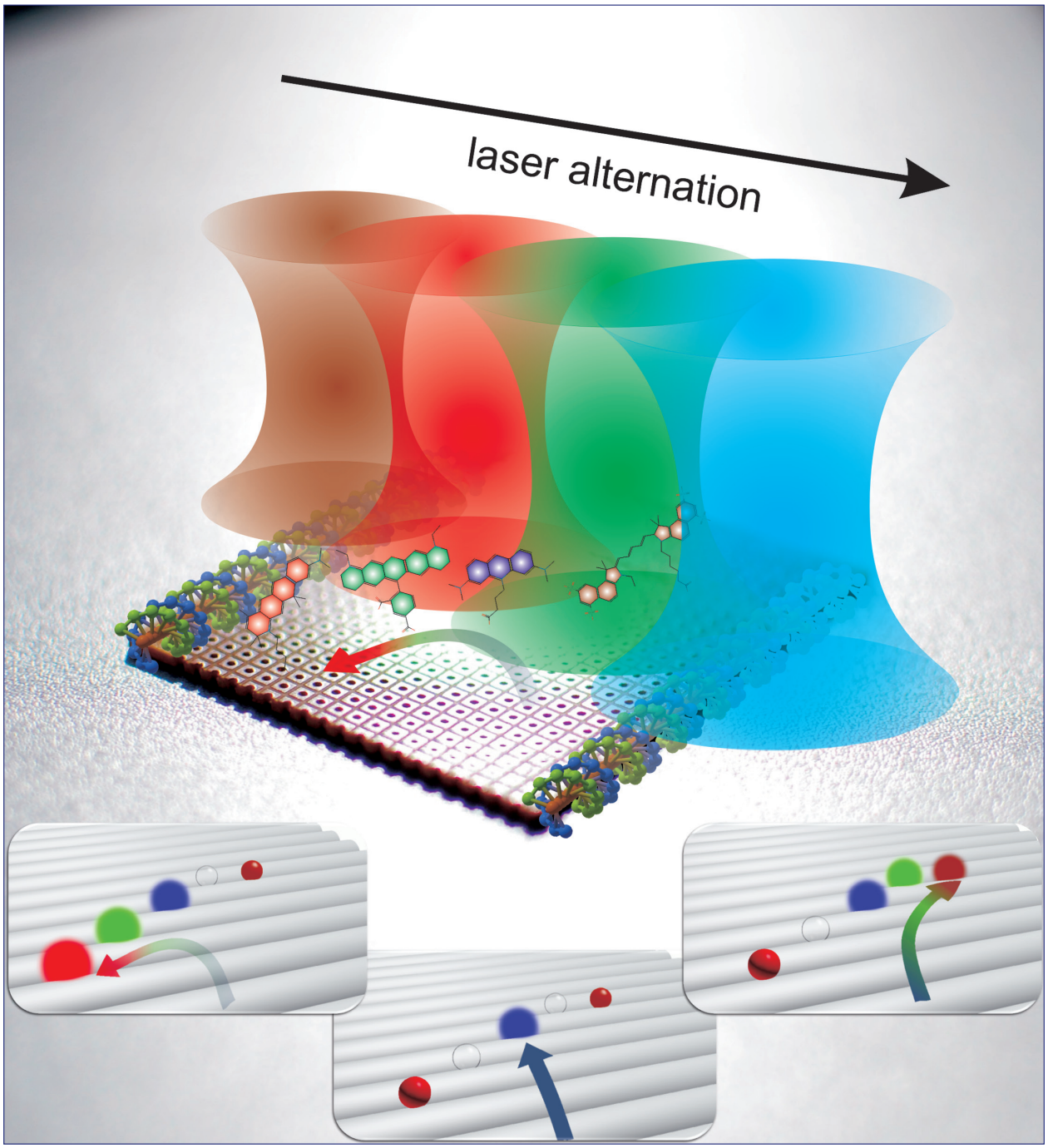

JACS
JOURNAL OF THE AMERICAN CHEMICAL SOCIETY

COMMUNICATION

pubs.acs.org/JACS

Single-Molecule Four-Color FRET Visualizes Energy-Transfer Paths on DNA Origami

Ingo H. Stein,[†,‡] Christian Steinhauer,[†,‡,§] and Philip Tinnefeld[*,‡,§]

[†]Angewandte Physik—Biophysik, Amalienstrasse 54, and [‡]Center for NanoScience, Schellingstrasse 4, Ludwig-Maximilians-Universität, 80799 Munich, Germany

[§]Physical and Theoretical Chemistry—NanoBioScience, TU Braunschweig, Hans-Sommer-Strasse 10, 38106 Braunschweig, Germany

Supporting Information

ABSTRACT: Fluorescence resonance energy transfer (FRET) represents a mechanism to transport light energy at the nanoscale, as exemplified by nature's light-harvesting complexes. Here we used DNA origami to arrange fluorophores that transport excited-state energy from an input dye to an output dye. We demonstrate that energy-transfer paths can be controlled on the single-molecule level by the presence of a "jumper" dye that directs the excited-state energy either to a red or to an IR output dye. We used single-molecule four-color FRET with alternating laser excitation to sort subpopulations and to visualize the control of energy transfer.

The size of photonic components such as fiber optic cables has hampered the development of light-based circuitry that has the potential to overcome the limitations of current electronic circuits. Today, surface plasmon-based photonics ("plasmonics") is considered a key technology to bring photonics to the nanoscale and to overcome the size compatibility problem of optics and electronics.[1] For plasmonic circuits, components such as wires, switches, and connectors are required. Since single emitters can be coupled to plasmonic devices and induce single plasmons,[2] molecular photonic devices such as wires and molecular switches might be included in nanoscale photonic circuitry and take over some of the desired functions. With respect to molecules, fluorescence resonance energy transfer (FRET) offers a means of energy transport that has led to the development of so-called photonic wires.[3−6] Furthermore, functions such as optical switching can be achieved within single molecules.[7,8]

In this Communication, we realize a combination of multistep energy transfer in a photonic wire-like structure using an energy-transfer cascade,[9,10] with the functionality of manipulating the energy-transfer path. We constructed a two-dimensional arrangement of fluorophores that allows for alternative energy-transfer pathways dependent on the incorporation of a "jumper" dye at specific positions. The construct uses two-dimensional DNA origami as a molecular breadboard that allows the precise and programmable arrangement of fluorophores in a grid-like fashion by self-assembly, similar to a circuit board for electronics (see Figure 1).[11] To create the rectangular origami, the ∼7.3k bases long single-stranded DNA genome of phage M13mp18 is folded by hybridization with ∼200 short synthetic DNA "staple" strands. Insertion of fluorophores is achieved using dye-modified staple strands that are incorporated during the self-assembly process (see Supporting Information for details on DNA sequences, modifications, and experimental methods).[11−13]

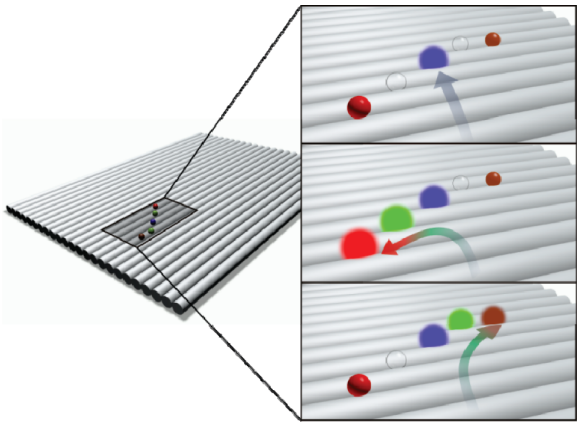

Figure 1. Arrangement of fluorophores on the DNA origami and visualization of alternative energy-transfer pathways with the "jumper" dye guiding the light from the blue input to either the red or the IR output.

On this grid we used a "blue" fluorophore (ATTO488) as the input dye. A "red" fluorophore (ATTO647N) and an "IR" fluorophore (Alexa 750) are used as alternative output dyes in this changeover switch-like arrangement (Figure 1). A "green" fluorophore (ATTO565) serves as the jumper dye that can be placed at two alternative locations, directing the excitation energy either to the red or to the IR dye (see Figure 1, magnified view). Fluorophores are spread over three helices to minimize fluorophore interactions through DNA,[14,15] and care was taken that fluorophores protrude from the same side of the DNA origami. Distances between input and output dyes are of the order of 9 nm to minimize direct FRET but to enable successive FRET with the aid of the jumper dye. We constructed origami samples without jumper dye, with jumper dye to direct the excitation energy to the red output dye, with jumper dye to direct the energy to the IR output dye, and with two jumper dyes.

To visualize the alternative energy-transfer paths, we advanced a previous four-color single-molecule FRET approach with alternating laser excitation.[4,9] This four-color setup allows studying the interaction between six energy-transfer pairs quasi-simultaneously,

Received: November 23, 2010
Published: January 20, 2011

with the potential to measure six distances within a biomolecular complex, and represents an extension of recently developed multicolor schemes.[4,16−21] The setup is based on an inverted confocal microscope and uses the combination of a supercontinuum laser for free wavelength selection with acousto-optical filters (AOTFs) and beamsplitter (AOBS) for excitation alternation and optimized detection sensitivity on all channels. The problem of decreasing transmission of the AOBS at longer wavelengths is circumvented by separating the IR fluorescence with the aid of a dichroic mirror within the microscope (see Supporting Information for details of the setup). Alternating laser excitation enables us to directly probe the stoichiometry of these complex supramolecular constructs by subsequently exciting all four fluorophores.[22]

To obtain statistics on the origami constructs, we identified single-molecule bursts of molecules diffusing through the laser focus and analyzed them with respect to their stoichiometry and energy transfer. Four-color alternating laser excitation was used to probe the presence of the respective fluorophores and to select the subpopulation of interest exhibiting all incorporated dyes. The relatively long diffusion times of about 10 ms for the focus transit allowed collecting an average of ~500 photons per burst, with ~100 photons during blue laser excitation. The extensive information content of the collected data allows discerning the possible combinations of fluorophores for every burst. This is important to exclude incompletely labeled origami structures from FRET analysis. To further refine the burst selection, ES histograms (energy transfer plotted versus dye stoichiometry) were used to exclude molecules where bleaching occurs during diffusion through the laser focus, which is particularly important for the IR dye. Singly labeled origami samples were used to determine the correction factors for leakage (le) into acceptor channels and for direct excitation (dx) of acceptors (see Supporting Information and Figure S2 for details on subpopulation selection and analysis).

Interestingly, we found that the blue, green, and red dyes were incorporated almost quantitatively, with small "donor-only" populations that can supposedly be assigned to premature bleaching. These high incorporation yields demonstrate the reliability and high yield of correctly formed structures of the origami approach. On the other hand, large fractions of missing IR dyes of >50% were detected in all samples (see Figure S2). We assign this sample heterogeneity to an inactive acceptor fraction. Inactive populations are well known for cyanine dyes such as Cy5 (see, e.g., refs 9 and 23). Notably, Alexa 750 is the only cyanine derivative of the dyes used.

To quantify the energy transfer toward a given output (red or IR), FRET-related ratios E^* were calculated as a fraction of the photon counts in the respective output channel divided by the sum of counts in the input and output channels, all during input dye excitation (see eqs S12 and S13 in the Supporting Information). These FRET-related ratios were corrected for direct excitation and leakage of the dyes, to ensure that, e.g., leaking of the red dye into the IR channel does not yield a false positive IR signal. On the other hand, corrections for differing quantum yields or detection efficiencies of the dyes were not taken into account as would be necessary for absolute distance measurements. Figure 2 shows histograms of E^* for the energy transfer from blue to red (left panel) and from blue to IR (right panel) for all of the designed origami constructs. Without the jumper dye, energy transfer from the input to the output dyes is essentially zero, as shown in Figure 2a.

Upon insertion of the jumper dye between the blue and the red dyes, the FRET-related ratio E^*_{br} increases from 0 to 0.34 ± 0.12, indicating a two-step energy transfer from blue to red enabled by the green jumper dye (see Figures 1 and 2b). The mean FRET-related ratio between the blue and IR dyes is unchanged, and the histogram is slightly broadened due to reduced photon numbers in the donor detection channel and larger correction terms in the respective acceptor channel. Alternatively, the jumper dye can be inserted between the blue and IR dyes. This causes the energy transfer to increase from blue to IR from 0 to $E^*_{bir} = 0.25 \pm 0.13$. Again, the alternative energy-transfer path remains at a mean value of zero, with a broadened histogram due to shot noise (Figure 2c). In the case of two inserted jumper dyes, both FRET-related ratios increase from 0 to $E^*_{br} = 0.36 \pm 0.17$ and $E^*_{bir} = 0.27 \pm 0.18$, respectively.

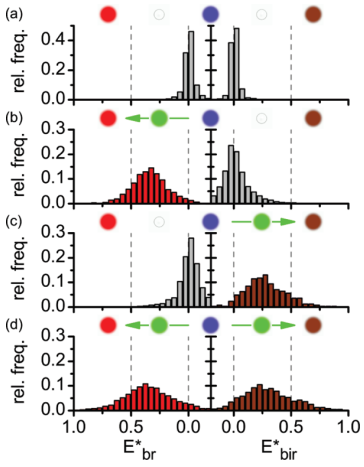

Figure 2. FRET-related ratios from blue to red, E^*_{br}, and from blue to IR, E^*_{bir}, for the four different origami samples. For each of the graphs, the colored spheres indicate the presence of the respective fluorophores on the DNA origami, and the white sphere marks the absence of the green jumper dye.

To quantify the reliability of the readout of the changeover switch, we characterized the output ratio, defined as the number of photons in the red output channel divided by the number of photons in the red and IR output channels, all during blue excitation and corrected for direct excitation and leakage (see Figure 3 and eq S17 in the Supporting Information). For the origami sample with the green jumper dye between the blue and red dyes, the histogram of the output ratio is centered at 1, indicating that photons are mainly emitted at the red output. For the sample with the jumper dye guiding the light toward the IR dye, the histogram of the output ratio is centered at 0, showing that photons are mainly emitted at the IR output. Most notably, there is almost negligible overlap between these two histograms, which are colored red and brown, respectively, in Figure 3. For an average of 82−122 collected photons during blue excitation for the different samples and a threshold of 10 photons for the sum of the output channels, the probability for correct assignment of the jumper position is >98.5%. For the origami sample with two green jumper dyes, the output ratio assumes an intermediate value of ~0.5, since light is emitted equally at both of the outputs.

In summary, our data clearly show that the energy-transfer path depends on the position of the jumper dye on the origami construct. The jumper dye determines the direction of the energy transfer, and different output dyes provide an easily read output signal. DNA origami might hence serve as a circuit board for photonic devices beyond the diffraction limit down to a molecular

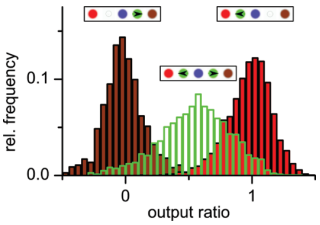

Figure 3. Histograms of the output ratios from single molecules. The number of photons in the red output channel divided by the number of photons in the red and IR output channels (all during blue excitation) are plotted for the three origami samples with jumper dyes. The fluorophore arrangement is indicated schematically above each of the histograms. Values exceeding the range of 0−1 are due to correction factors (see eq S17 in the Supporting Information).

scale. DNA nanostructures additionally offer ways for integration with other photonic structures, such as nanoscale plasmonic waveguides, since metallic nanoparticles and rods are readily modified with DNA.[24,25] The concept can also be extended to three dimensions.[26] Replacing the jumper strand by sensor strands[27] that, for example, report on binding opens interesting possibilities to exploit the control of energy-transfer paths for nanoscale sensors or molecular computing. Finally, single-molecule four-color FRET with alternating laser excitation has proven valuable to disentangle biomolecular complexes of increasing complexity.

■ ASSOCIATED CONTENT

Supporting Information. Experimental methods, data analysis, and DNA sequences. This material is available free of charge via the Internet at http://pubs.acs.org.

■ AUTHOR INFORMATION

Corresponding Author
p.tinnefeld@tu-braunschweig.de

■ ACKNOWLEDGMENT

The authors are grateful to Friedrich C. Simmel, Ralf Jungmann, and Tim Liedl for fruitful collaborations. This work was supported by the DFG (Ti329/5-1), the Center for Nano-Science Munich, and the excellence cluster Nanosystems Initiative Munich. I.H.S. and C.S. are grateful to the Elite Network of Bavaria (International Doctorate Program in NanoBioTechnology) for a doctoral fellowship.

■ REFERENCES

(1) Ozbay, E. *Science* **2006**, *311*, 189.
(2) Akimov, A. V.; Mukherjee, A.; Yu, C. L.; Chang, D. E.; Zibrov, A. S.; Hemmer, P. R.; Park, H.; Lukin, M. D. *Nature* **2007**, *450*, 402.
(3) Wagner, R. W.; Lindsey, J. S. *J. Am. Chem. Soc.* **1994**, *116*, 9759.
(4) Heilemann, M.; Tinnefeld, P.; Sanchez Mosteiro, G.; Garcia Parajo, M.; Van Hulst, N. F.; Sauer, M. *J. Am. Chem. Soc.* **2004**, *126*, 6514.
(5) Hannestad, J. K.; Sandin, P.; Albinsson, B. *J. Am. Chem. Soc.* **2008**, *130*, 15889.
(6) Vyawahare, S.; Eyal, S.; Mathews, K. D.; Quake, S. R. *Nano Lett.* **2004**, *4*, 1035.
(7) Irie, M.; Fukaminato, T.; Sasaki, T.; Tamai, N.; Kawai, T. *Nature* **2002**, *420*, 759.
(8) Heilemann, M.; Margeat, E.; Kasper, R.; Sauer, M.; Tinnefeld, P. *J. Am. Chem. Soc.* **2005**, *127*, 3801.
(9) Heilemann, M.; Kasper, R.; Tinnefeld, P.; Sauer, M. *J. Am. Chem. Soc.* **2006**, *128*, 16864.
(10) Tinnefeld, P.; Heilemann, M.; Sauer, M. *ChemPhysChem* **2005**, *6*, 217.
(11) Rothemund, P. W. *Nature* **2006**, *440*, 297.
(12) Andersen, E. S.; Dong, M.; Nielsen, M. M.; Jahn, K.; Subramani, R.; Mamdouh, W.; Golas, M. M.; Sander, B.; Stark, H.; Oliveira, C. L.; Pedersen, J. S.; Birkedal, V.; Besenbacher, F.; Gothelf, K. V.; Kjems, J. *Nature* **2009**, *459*, 73.
(13) Steinhauer, C.; Jungmann, R.; Sobey, T. L.; Simmel, F. C.; Tinnefeld, P. *Angew. Chem., Int. Ed.* **2009**, *48*, 8870.
(14) Kumbhakar, M.; Kiel, A.; Pal, H.; Herten, D. P. *ChemPhysChem* **2009**, *10*, 629.
(15) Takada, T.; Fujitsuka, M.; Majima, T. *Proc. Natl. Acad. Sci. U.S. A.* **2007**, *104*, 11179.
(16) Hohng, S.; Joo, C.; Ha, T. *Biophys. J.* **2004**, *87*, 1328.
(17) Clamme, J. P.; Deniz, A. A. *ChemPhysChem* **2005**, *6*, 74.
(18) Lee, N. K.; Kapanidis, A. N.; Koh, H. R.; Korlann, Y.; Ho, S. O.; Kim, Y.; Gassman, N.; Kim, S. K.; Weiss, S. *Biophys. J.* **2007**, *92*, 303.
(19) Ross, J.; Buschkamp, P.; Fetting, D.; Donnermeyer, A.; Roth, C. M.; Tinnefeld, P. *J. Phys. Chem. B* **2007**, *111*, 321.
(20) Person, B.; Stein, I. H.; Steinhauer, C.; Vogelsang, J.; Tinnefeld, P. *ChemPhysChem* **2009**, *10*, 1455.
(21) Lee, S.; Lee, J.; Hohng, S. *PLoS One* **2010**, *5*, e12270.
(22) Kapanidis, A. N.; Lee, N. K.; Laurence, T. A.; Doose, S.; Margeat, E.; Weiss, S. *Proc. Natl. Acad. Sci. U.S.A.* **2004**, *101*, 8936.
(23) Morgan, M. A.; Okamoto, K.; Kahn, J. D.; English, D. S. *Biophys. J.* **2005**, *89*, 2588.
(24) Ding, B.; Deng, Z.; Yan, H.; Cabrini, S.; Zuckermann, R. N.; Bokor, J. *J. Am. Chem. Soc.* **2010**, *132*, 3248.
(25) Pal, S.; Deng, Z. T.; Ding, B. Q.; Yan, H.; Liu, Y. *Angew. Chem., Int. Ed.* **2010**, *49*, 2700.
(26) Douglas, S. M.; Dietz, H.; Liedl, T.; Hogberg, B.; Graf, F.; Shih, W. M. *Nature* **2009**, *459*, 414.
(27) Jungmann, R.; Steinhauer, C.; Scheible, M.; Kuzyk, A.; Tinnefeld, P.; Simmel, F. C. *Nano Lett.* **2010**, *10*, 4756.

6 Outlook

The DNA origami method combined with fluorescence techniques holds promise for a multitude of biomolecular assays. The breadboard character of the DNA nanostructures was already demonstrated in chapter 5 with the incorporation of fluorophores. Due to the variety of possible DNA modifications a whole spectrum of biomolecules and particles can be easily attached. Specifically, this suggests further research in the following areas:

- As touched upon in associated publication P2, the structure of DNA origami objects depends on the concentration of divalent magnesium ions in solution. It is common knowledge in the field that a certain magnesium concentration is needed to allow successful folding of the structures. Typically this is in the range between 10 and 20 mM and is balanced between two effects. On the one hand a certain amount of magnesium is needed to shield the negative charge of the DNA backbone to avoid repulsion that would prevent folding. On the other hand too high concentrations lead to unspecific attraction and agglomeration that also hinder correct assembly. For future applications of DNA origami an understanding of the quantitative effect of the magnesium concentration on the assembled structures is desirable. Using the same methodology as described in chapter 4 the influence can be quantified on the single-molecule level. Together with Verena Schüller and the group of Tim Liedl a study of this dependence is currently under way.

- Gold or silver nanoparticles (NPs) can have intriguing effects on the fluorescence of single fluorophores in a strongly distance-dependent fashion. Many different geometries have been analyzed theoretically, showing the potential for strong field enhancement. So far, it has been very hard to experimentally verify this, as the positioning of NPs and fluorophores with nanometer precision and defined stoichiometry is challenging. The recent study of Acuna et al. investigating the distance-dependent quenching of single

fluorophores by gold NPs on DNA origami, points at the potential of this approach [50]. Further refinement of the technique will allow studying specific geometries of NPs and fluorophores that could dramatically enhance single-molecule fluorescence.

- The potential of the 4-color ALEX technique for virtual sorting of molecules was demonstrated in chapter 5 with the individual selection of the fully labeled subpopulation. In principle, a molecular barcode of defined stoichiometries and FRET values could be designed and experimentally read out. This might for example enable the parallel investigation of differently tagged mutations of enzymes and their interaction with a target molecule.

- The biocompatibility of DNA origami structures was recently demonstrated by Gietl et al. [51]. Extending towards more biological applications, biomolecules could be arranged on DNA origami to analyze specific interactions.

Bibliography

[1] R. Erni, M. D. Rossell, C. Kisielowski, and U. Dahmen. Atomic-resolution imaging with a sub-50-pm electron probe. *Phys. Rev. Lett.*, 102(9):096101, Mar 2009.

[2] L. Stryer and R. P. Haugland. Energy transfer: a spectroscopic ruler. *Proc. Natl. Acad. Sci. U.S.A.*, 58(2):719–726, Aug 1967.

[3] T. Ha, T. Enderle, D. F. Ogletree, D. S. Chemla, P. R. Selvin, and S. Weiss. Probing the interaction between two single molecules: fluorescence resonance energy transfer between a single donor and a single acceptor. *Proc. Natl. Acad. Sci. U.S.A.*, 93(13):6264–6268, Jun 1996.

[4] E. Betzig, G. H. Patterson, R. Sougrat, O. W. Lindwasser, S. Olenych, J. S. Bonifacino, M. W. Davidson, J. Lippincott-Schwartz, and H. F. Hess. Imaging intracellular fluorescent proteins at nanometer resolution. *Science*, 313(5793):1642–1645, Sep 2006.

[5] M. J. Rust, M. Bates, and X. Zhuang. Sub-diffraction-limit imaging by stochastic optical reconstruction microscopy (STORM). *Nat. Methods*, 3(10):793–795, Oct 2006.

[6] J. Fölling, M. Bossi, H. Bock, R. Medda, C. A. Wurm, B. Hein, S. Jakobs, C. Eggeling, and S. W. Hell. Fluorescence nanoscopy by ground-state depletion and single-molecule return. *Nat. Methods*, 5(11):943–945, Nov 2008.

[7] C. Steinhauer, C. Forthmann, J. Vogelsang, and P. Tinnefeld. Superresolution microscopy on the basis of engineered dark states. *J. Am. Chem. Soc.*, 130(50):16840–16841, Dec 2008.

[8] S. W. Hell and J. Wichmann. Breaking the diffraction resolution limit by stimulated emission: stimulated-emission-depletion fluorescence microscopy. *Opt Lett*, 19(11):780–782, Jun 1994.

[9] T. Ha and P. Tinnefeld. Photophysics of fluorescent probes for single-molecule biophysics and super-resolution imaging. *Annu Rev Phys Chem*, 63:595–617, May 2012.

[10] P. W. Rothemund. Folding DNA to create nanoscale shapes and patterns. *Nature*, 440(7082):297–302, Mar 2006.

[11] S. M. Douglas, H. Dietz, T. Liedl, B. Hogberg, F. Graf, and W. M. Shih. Self-assembly of DNA into nanoscale three-dimensional shapes. *Nature*, 459(7245):414–418, May 2009.

[12] H. Dietz, S. M. Douglas, and W. M. Shih. Folding DNA into twisted and curved nanoscale shapes. *Science*, 325(5941):725–730, Aug 2009.

[13] T. Liedl, B. Hogberg, J. Tytell, D. E. Ingber, and W. M. Shih. Self-assembly of three-dimensional prestressed tensegrity structures from DNA. *Nat Nanotechnol*, 5(7):520–524, Jul 2010.

[14] E. S. Andersen, M. Dong, M. M. Nielsen, K. Jahn, R. Subramani, W. Mamdouh, M. M. Golas, B. Sander, H. Stark, C. L. Oliveira, J. S. Pedersen, V. Birkedal, F. Besenbacher, K. V. Gothelf, and J. Kjems. Self-assembly of a nanoscale DNA box with a controllable lid. *Nature*, 459(7243):73–76, May 2009.

[15] S. M. Douglas, I. Bachelet, and G. M. Church. A logic-gated nanorobot for targeted transport of molecular payloads. *Science*, 335(6070):831–834, Feb 2012.

[16] B. Sacca and C. M. Niemeyer. DNA origami: the art of folding DNA. *Angew. Chem. Int. Ed. Engl.*, 51(1):58–66, Jan 2012.

[17] Y. Ke, S. M. Douglas, M. Liu, J. Sharma, A. Cheng, A. Leung, Y. Liu, W. M. Shih, and H. Yan. Multilayer DNA origami packed on a square lattice. *J. Am. Chem. Soc.*, 131(43):15903–15908, Nov 2009.

[18] I. H. Stein, C. Steinhauer, and P. Tinnefeld. Single-molecule four-color FRET visualizes energy-transfer paths on DNA origami. *J. Am. Chem. Soc.*, 133(12):4193–4195, Mar 2011.

[19] A. V. Pinheiro, D. Han, W. M. Shih, and H. Yan. Challenges and opportunities for structural DNA nanotechnology. *Nat Nanotechnol*, 6(12):763–772, Dec 2011.

[20] S. Weiss. Fluorescence spectroscopy of single biomolecules. *Science*, 283(5408):1676–1683, Mar 1999.

[21] Th. Förster. Zwischenmolekulare Energiewanderung und Fluoreszenz. *Ann. Physik*, 437(2):55–75, 1948.

[22] A. A. Deniz, M. Dahan, J. R. Grunwell, T. Ha, A. E. Faulhaber, D. S. Chemla, S. Weiss, and P. G. Schultz. Single-pair fluorescence resonance energy transfer on freely diffusing molecules: observation of Förster distance dependence and subpopulations. *Proc. Natl. Acad. Sci. U.S.A.*, 96(7):3670–3675, Mar 1999.

[23] M. Dahan, A. A. Deniz, T. Ha, D. S. Chemla, P. G. Schultz, and S. Weiss. Ratiometric measurement and identification of single diffusing molecules. *Chem. Phys.*, 274(1):85–106, 1999.

[24] A. N. Kapanidis, N. K. Lee, T. A. Laurence, S. Doose, E. Margeat, and S. Weiss. Fluorescence-aided molecule sorting: analysis of structure and interactions by alternating-laser excitation of single molecules. *Proc. Natl. Acad. Sci. U.S.A.*, 101(24):8936–8941, Jun 2004.

[25] K. Sanderson. Bioengineering: What to make with DNA origami. *Nature*, 464:158–159, Mar 2010.

[26] T. Ha. Single-molecule fluorescence resonance energy transfer. *Methods*, 25(1):78–86, Sep 2001.

[27] I. Rasnik, S. A. McKinney, and T. Ha. Nonblinking and long-lasting single-molecule fluorescence imaging. *Nat. Methods*, 3(11):891–893, Nov 2006.

[28] J. Vogelsang, R. Kasper, C. Steinhauer, B. Person, M. Heilemann, M. Sauer, and P. Tinnefeld. A reducing and oxidizing system minimizes photobleaching and blinking of fluorescent dyes. *Angew. Chem. Int. Ed. Engl.*, 47(29):5465–5469, 2008.

[29] I. H. Stein, S. Capone, J. H. Smit, F. Baumann, T. Cordes, and P. Tinnefeld. Linking single-molecule blinking to chromophore structure and redox potentials. *Chemphyschem*, 13(4):931–937, Mar 2012.

[30] J. Widengren and P. Schwille. Characterization of photoinduced isomerization and back-isomerization of the cyanine dye Cy5 by fluorescence correlation spectroscopy. *J. Phys. Chem. A*, 104(27):6416–6428, Jun 2000.

[31] J. Vogelsang, C. Steinhauer, C. Forthmann, I. H. Stein, B. Person-Skegro, T. Cordes, and P. Tinnefeld. Make them blink: probes for super-resolution microscopy. *Chemphyschem*, 11(12):2475–2490, Aug 2010.

[32] J. Vogelsang, T. Cordes, C. Forthmann, C. Steinhauer, and P. Tinnefeld. Controlling the fluorescence of ordinary oxazine dyes for single-molecule switching and superresolution microscopy. *Proc. Natl. Acad. Sci. U.S.A.*, 106(20):8107–8112, May 2009.

[33] Y. Sun, H. Wallrabe, S. A. Seo, and A. Periasamy. FRET microscopy in 2010: the legacy of Theodor Förster on the 100th anniversary of his birth. *ChemPhysChem*, 12(3):462–474, Feb 2011.

[34] N. K. Lee, A. N. Kapanidis, Y. Wang, X. Michalet, J. Mukhopadhyay, R. H. Ebright, and S. Weiss. Accurate FRET measurements within single diffusing biomolecules using alternating-laser excitation. *Biophys. J.*, 88(4):2939–2953, Apr 2005.

[35] I. H. Stein, V. Schüller, P. Böhm, P. Tinnefeld, and T. Liedl. Single-molecule FRET ruler based on rigid DNA origami blocks. *Chemphyschem*, 12(3):689–695, Feb 2011.

[36] B. Schuler, E. A. Lipman, P. J. Steinbach, M. Kumke, and W. A. Eaton. Polyproline and the "spectroscopic ruler" revisited with single-molecule fluorescence. *Proc. Natl. Acad. Sci. U.S.A.*, 102(8):2754–2759, Feb 2005.

[37] R. B. Best, K. A. Merchant, I. V. Gopich, B. Schuler, A. Bax, and W. A. Eaton. Effect of flexibility and cis residues in single-molecule FRET studies of polyproline. *Proc. Natl. Acad. Sci. U.S.A.*, 104(48):18964–18969, Nov 2007.

[38] L. P. Watkins, H. Chang, and H. Yang. Quantitative single-molecule conformational distributions: a case study with poly-(L-proline). *J Phys Chem A*, 110(15):5191–5203, Apr 2006.

[39] S. Doose, H. Neuweiler, H. Barsch, and M. Sauer. Probing polyproline structure and dynamics by photoinduced electron transfer provides evidence for deviations from a regular polyproline type II helix. *Proc. Natl. Acad. Sci. U.S.A.*, 104(44):17400–17405, Oct 2007.

[40] R. M. Clegg, A. I. Murchie, A. Zechel, and D. M. Lilley. Observing the helical geometry of double-stranded DNA in solution by fluorescence resonance energy transfer. *Proc. Natl. Acad. Sci. U.S.A.*, 90(7):2994–2998, Apr 1993.

[41] M. Levitt. How many base-pairs per turn does DNA have in solution and in chromatin? Some theoretical calculations. *Proc. Natl. Acad. Sci. U.S.A.*, 75(2):640–644, Feb 1978.

[42] M. Heilemann, P. Tinnefeld, G. Sanchez Mosteiro, M. Garcia Parajo, N. F. Van Hulst, and M. Sauer. Multistep energy transfer in single molecular photonic wires. *J. Am. Chem. Soc.*, 126(21):6514–6515, Jun 2004.

[43] J. K. Hannestad, P. Sandin, and B. Albinsson. Self-assembled DNA photonic wire for long-range energy transfer. *J. Am. Chem. Soc.*, 130(47):15889–15895, Nov 2008.

[44] S. Vyawahare, S. Eyal, K. D. Mathews, and S. R. Quake. Nanometer-scale fluorescence resonance optical waveguides. *Nano Lett.*, 4(6):1035–1039, Apr 2004.

[45] B. Albinsson, J. K. Hannestad, and K. Börjesson. Functionalized DNA nanostructures for light harvesting and charge separation. *Coord. Chem. Rev.*, in press, 2012.

[46] N. K. Lee, A. N. Kapanidis, H. R. Koh, Y. Korlann, S. O. Ho, Y. Kim, N. Gassman, S. K. Kim, and S. Weiss. Three-color alternating-laser excitation of single molecules: monitoring multiple interactions and distances. *Biophys. J.*, 92(1):303–312, Jan 2007.

[47] B. Person, I. H. Stein, C. Steinhauer, J. Vogelsang, and P. Tinnefeld. Correlated movement and bending of nucleic acid structures visualized by multicolor single-molecule spectroscopy. *Chemphyschem*, 10(9-10):1455–1460, Jul 2009.

[48] C. Eggeling, S. Berger, L. Brand, J. R. Fries, J. Schaffer, A. Volkmer, and C. A. Seidel. Data registration and selective single-molecule analysis using multi-parameter fluorescence detection. *J. Biotechnol.*, 86(3):163–180, Apr 2001.

[49] M. Heilemann, R. Kasper, P. Tinnefeld, and M. Sauer. Dissecting and reducing the heterogeneity of excited-state energy transport in DNA-based photonic wires. *J. Am. Chem. Soc.*, 128(51):16864–16875, Dec 2006.

[50] G. P. Acuna, M. Bucher, I. H. Stein, C. Steinhauer, A. Kuzyk, P. Holzmeister, R. Schreiber, A. Moroz, F. D. Stefani, T. Liedl, F. C. Simmel, and P. Tinnefeld. Distance Dependence of Single-Fluorophore Quenching by Gold Nanoparticles Studied on DNA Origami. *ACS Nano*, 6(4):3189–3195, Mar 2012.

[51] A. Gietl, P. Holzmeister, D. Grohmann, and P. Tinnefeld. DNA origami as biocompatible surface to match single-molecule and ensemble experiments. *Nucleic Acids Res*, published online, Apr 2012.

Appendix

Supporting information for associated publication P2

Supporting Information

Single-Molecule FRET Ruler Based on Rigid DNA Origami Blocks

By

Ingo H. Stein, Verena Schüller, Philip Böhm, Philip Tinnefeld and Tim Liedl

published in

ChemPhysChem 2011, 12, 689–695

CHEMPHYSCHEM

Supporting Information

Single-Molecule FRET Ruler Based on Rigid DNA Origami Blocks

Ingo H. Stein,[a] Verena Schüller,[b] Philip Böhm,[b] Philip Tinnefeld,*[a, c, d] and Tim Liedl*[b, c]

cphc_201000781_sm_miscellaneous_information.pdf

Figure S1: Influence of the linker lengths on donor-acceptor separation
Both images are a front view of the DNA helices with the helical axis perpendicular to the image plane.
Left: For the dsDNA the donor-acceptor separation is strongly dependent on the length of the linkers and additionally varies for different basepair separations. For a donor-acceptor separation of e.g. 7 bps on opposite strands, the linkers should be almost parallel and on the same side of the cylindrically shaped DNA helix and their lengths (but not their dynamics) should cancel out. On the other hand, for one or twelve base pairs separation, corresponding roughly to a full turn, the dyes are on the opposite side of the DNA cylinder and the relatively undefined lengths of the linkers have to be added together and largely contribute to the donor-acceptor distance
Right: On the DNA origami block, the linkers of all acceptors are almost parallel to the donor and on the same side of the origami block. The linker length itself has negligible influence on the static (averaged) donor-acceptor distance.

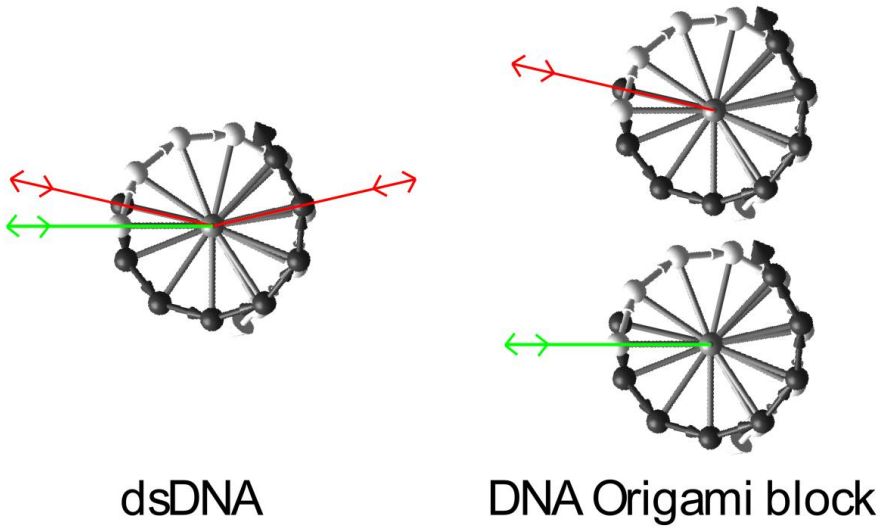

Figure S2: Design schematic of DNA origami block
Scaffold routing and staple design in two-dimensional representation. Graphics and sequences created with caDNAno.

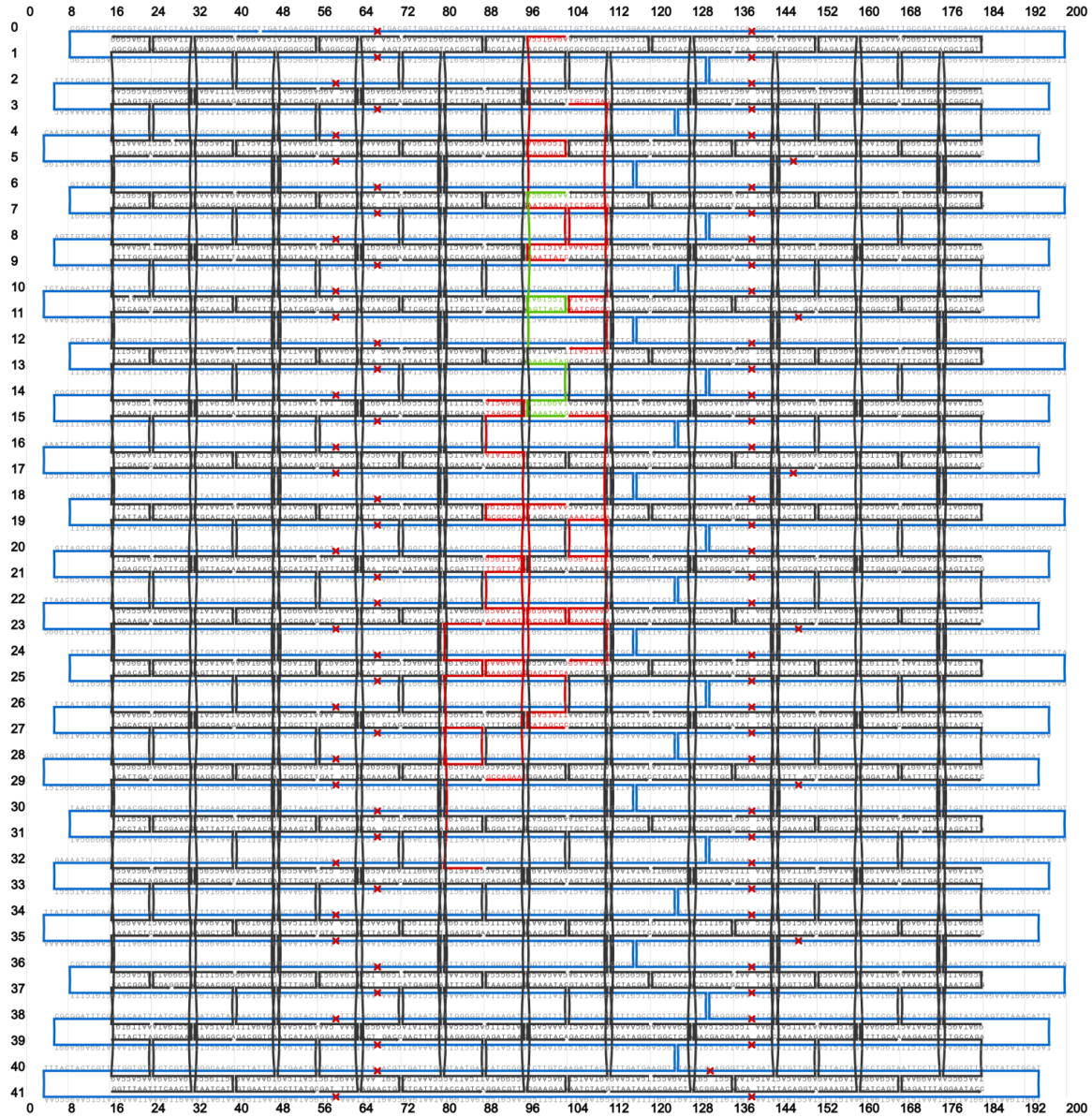

Figure S3:
Top: E-S histogram of doubly labeled dsDNA (8 bp separation)
Bottom: E-S histogram of doubly labeled DNA origami block (position of acceptor (0,10) as defined in Scheme 1A, 3.5 nm separation)
The two-dimensional histograms were obtained by 2D-binning of the E- and S-values with 40 bins each in the range of -0.1 to 1.1. Additionally one-dimensional histograms for the E- as well as the S-values are shown.
The slightly broader distribution of E- and S-histograms for the dsDNA samples is most likely due to increased shot noise. Due to longer diffusion times of the origami samples a higher number of photons could be collected per burst.

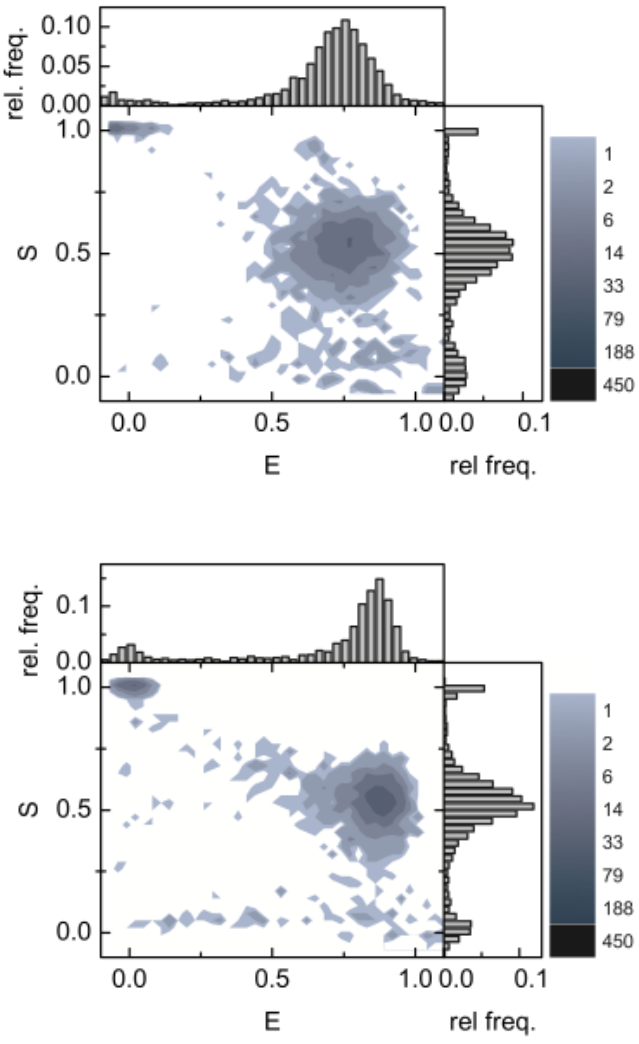

Table S4: Distance calculation between donor and acceptor dyes on DNA origami blocks
The values given in table S4 correspond to the following:
1st column: Relative positions of the fluorophores in the DNA origami block. The first value is the position of the donor, which is defined as helix 0 and base 0.
2nd column: Calculated with the simplified assumption of an average center-to-center distance of 2.6 nm between the helices.
3rd column: Differences to the original positions if the tilt of the bases to which the acceptor molecules are attached in respect to the donor molecule is taken into account.
4th column: Differences to the original positions if the model incorporates the bowing of neighboring double strands due to electrostatic repulsion.
5th column: Positions and distances between the dye molecules if all corrections are applied.

Table S4

Position (helix, nucleotide)	(x, y, distance to donor) uncorrected / nm	(Δx, Δy, distance to donor) correction i) / nm	(Δx, Δy, distance to donor) correction ii) / nm	(x, y, distance to donor) corrected / nm
(0, 0)	(0.0, 0.0, 0.0)	(0.0, 0.0, 0.0)	(0.1, 0.0, 0.0)	(0.1, 0.0, 0.0)
(-1, -3)	(-2.6, -1.0, 2.8)	(0.6, 0.0, 2.3)	(-0.0, 0.0, 3.0)	(-2.0, -1.0, 2.4)
(0, 10)	(0.0, 3.4, 3.4)	(-0.6, 0.0, 3.5)	(0.0, 0.0, 3.4)	(-0.6, 3.4, 3.5)
(-2, 0)	(-5.2, 0.0, 5.2)	(0.0, 0.0, 5.2)	(0.1, 0.0, 5.2)	(-5.1, 0.0, 5.2)
(2, -10)	(5.2, -3.4, 6.2)	(0.6, 0.0, 6.7)	(-0.1, 0.0, 6.0)	(5.7, -3.4, 6.5)
(-2, -11)	(-5.2, -3.7, 6.4)	(-0.6, 0.0, 6.9)	(-0.1, 0.0, 6.6)	(-5.9, -3.7, 7.1)
(3, 8)	(7.8, 2.7, 8.3)	(1.1, 0.0, 9.3)	(-0.1, 0.0, 8.1)	(8.8, 2.7, 9.2)
(4, -1)	(10.4, -0.3, 10.4)	(-1.1, 0.0, 9.3)	(0.1, 0.0, 10.4)	(9.4, -0.3, 9.3)
(5, 17)	(13.0, 5.8, 14.2)	(0.0, 0.0, 14.2)	(0.1, 0.0, 14.2)	(13.1, 5.8, 14.2)

Figure S5: Measurements of dsDNA and FRET blocks with Magnesium
Top: FRET efficiencies of dsDNA samples in absence and presence of 18 mM magnesium as a function of donor-acceptor separation in basepairs. The solid line is a fit to the data according to a geometric model as described in the main text. The fitting parameters of both measurements agree within measurement uncertainty:
without magnesium: $a = 17.8 \pm 0.9$ Å, $L = 9.4 \pm 1.0$ Å, $\theta_0 = 243.3° \pm 9°$;
18mM magnesium: $a = 17.8 \pm 1.3$ Å, $L = 7.2 \pm 1.4$ Å, $\theta_0 = 232° \pm 11°$
Bottom: FRET efficiencies of FRET blocks in absence and presence of 18 mM magnesium as a function of distance. The pair of data points for each origami sample was marked according to the nomenclature given in Scheme 1A of the main text (i.e. (Δ helix, Δ nucleotide)). To illustrate the shift of E-values with and without magnesium the same distances for identical acceptor positions on the origami block were used as in Figure 3 of the main text. The increased energy transfer values in the presence of magnesium are explained by the reduced DNA repulsion in the presence of divalent kations, which leads to shorter inter-helix distances.

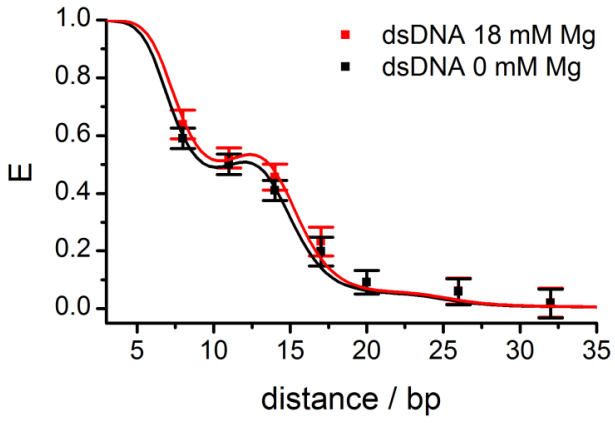

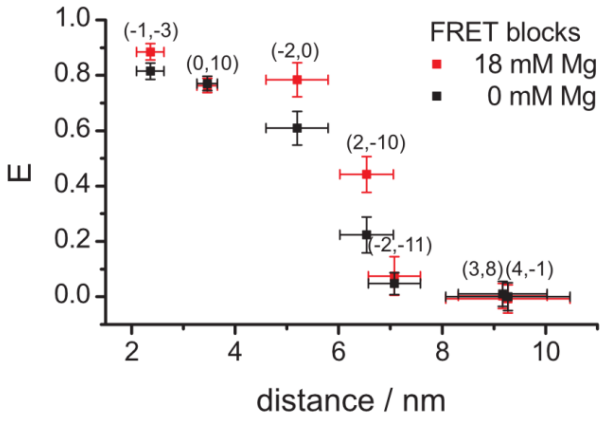

Table S6: Staple sequences with optional dye modification
Each fully assembled structure contains the donor sequence with the donor attached to a designated thymine base and all of the following oligonucleotides except for one. This particular sequence is replaced by an oligonucleotide labeled with the acceptor at a given Thymine base (cf. Experimental Section).

Donor	AATGCGCGAGTTACAAATCCTGATAAACATAGTAGGT$_{Cy3}$CTGTAAATAAG
Acc 2.4 nm	AGAGTCCACACAGACAATCCAGAAAATCAATATATCTTTAGAATTAT$_{Cy5}$C
Acc 3.5 nm	ACAAAGTTAGTCCTGAGCGCCCAAGCGTTATATAAGGCGTAGAGACT$_{Cy5}$A
Acc 5.2 nm	AGAGTCCACACAGACAATCCAGAAAATCAATATATCTTTAGAAT$_{Cy5}$TATC
Acc 6.5 nm	AATAAACATTT$_{Cy5}$TAGCGAAATCAGAAAAAACAGGAAACCGATAATAACG
Acc 7.1 nm	TGCCTGAGAT$_{Cy5}$CTAAAATCTGGTCATCAATATAAATCGCGCTATTCATT
Acc 9.2 nm	GCCAGAATAAAAGAACAAAAGGGCATTAGACGTTGT$_{Cy5}$TTAAGACTTGCG
Acc 9.3 nm	AATAGATAACCAGAAGGGAAGCGCGACATTCATTAT$_{Cy5}$CACCCATAGCCC
Acc 14.2 nm	CGTACTCACAT$_{Cy5}$CGGCAGGAACCGCCCAAAGACTGGCATGAATAGCCGA

Table S7: Unmodified staple sequences of DNA origami blocks

Oligo1	GCCCCCGAAAAAGGGATTGACGCTAGAGCCAGTAGAAGTATTAATTTT
Oligo2	GTCAAAGCCCTTCTGCAGGAAAACACCTTGGAGCCGTCTTGCGGA
Oligo3	AGCCCGAGATAGGGTATCATGGTGCGTTGCGTTGAGTGT
Oligo4	AAATCCCTTGTTATCCTGCCTAATGGTGCTGCCGGTGCCGCATCCCTT
Oligo5	TCACCGCATTAATTCATAGCTGCAGTTGA
Oligo6	AGGCCGATTAAAGGGAGAAAGGAGCCTACATTCATTCTGGCAGCAGAA
Oligo7	CTCGTTAGAATCAGAGGTAGCGGTCATTGCAAACCTGAAAACATCGCC
Oligo8	GACGAGCACGCCGCGCCTGGTAATATATTTTTGAATGTCG
Oligo9	GAGACGGGCAACAGCTGATTCGCGCCCGCTT
Oligo10	AGTCTGTCTGAGGATTCAGCAAATTCAAAATTTACCTTTTTTACATTT
Oligo11	GCAATACTATAGATTACTGAACCTCTGAATAATTCGCCTGGATGAAAC
Oligo12	TCCAGTCACGATCCAGCGCAAAAATGGGTA
Oligo13	TTAATGAAGCAGCCAGGGCCAGAATCCGCCGGAGGTGTCCCGGACTTG
Oligo14	CGGCCTTGTTAATGCGGTTCCAGTTTGGAACA
Oligo15	CCAGTAATTTTAGAGCAGGAAGGGAAGAAAGCTTTTAGACAGTAAAAG
Oligo16	GATAGAAGGCGAAAAAGGGCGCTGGCAAGTCGGGAGCTCGTTGTA

Oligo17	ATACGTGGCTATTAAAGCGTAACCACCACACCCGTATAACACATCACT
Oligo18	AATTCGTATGAGTGTTCCGCTACAGGGGCCCT
Oligo19	TGTGAAATTATAAATCGAGAGAGTTGCAGCAATTTTCTTTCAGCTGCA
Oligo20	GATAAAACAGTAACAGATTTGCACTGAGTGAAGCTGATGCTAATTTCA
Oligo21	ATTAAAAATAACGGATGGAAGGGCTATTAACTTAGGTTTGAAATA
Oligo22	GGATCCCCCGTCGGTGGCCCTGCGGAAGATGC
Oligo23	TCTTCGCGACGGCTGGGCGCGGTTGTCCGTTTACAGGCGGTCATTTGC
Oligo24	CACTGCGCACTGTTGTGCCATCTGGTCAG
Oligo25	AATACATTCATCACGCTGGAAATACGGGCGCTACCGTCTATCAAGGGA
Oligo26	AACAACTATCTTTGATCCGCCAGCCACGCTGCGAACGTGGACTCCAAC
Oligo27	GGAAGGTTTAGAAGAACTCAAACTGTACTATGGTTGCTTT
Oligo28	TGCATCAGGGGAAACCTAACTCACCTGGCCCTAAAAGAAT
Oligo29	AAAAGTTTATGTAAATTAACCTTGGCTTAATTAAAGTACCAGAAACCA
Oligo30	ACAAAGAAACCTCCGGTTAATTTTTACCAGTACCAGACGAAATAATAT
Oligo31	ATCATATTCAAAATCACGATAGCTCTGTTTAGAATGCAGATTATCAAC
Oligo32	AAGGTTTGTAAAGTTAAACGAGCAGAAACA
Oligo33	ACACTGGTAAAGCCGCTTTCGTCTGAGAGATAAATCGGCGAAGTTGGG
Oligo34	GCAATTCAGTTGGCAAAGCGCTATTAGTCTTT
Oligo35	GAATATACAGAGGTGACCACGCTGCAAT
Oligo36	AGAAACAATACCGAATAAAGCATACGCTCAAAATTAACAAACAGG
Oligo37	GAATACCAAACTGATAAAACCCTCCAATATTATAGTAATAGTGCTTTC
Oligo38	GGCAGCACGGGTACCGATCAACAGCTCACTAT
Oligo39	ACCAGCTTTCCGTGAGCACTCTGTGAGTGAGCTGTCGTGCTCACCAGT
Oligo40	AACAATTTGAGAATATGAGAATCGCGCACTCAGCTACAATAGTTACAA
Oligo41	AAACATCAATTCTGTTAAAGCCATTTTCATTAAATCAACAATCCA
Oligo42	CAGCAACCGGTGGAGCCGGAAAAAGGTTTCAG
Oligo43	TAGAACGTCCGGAAACGACTTTCTGATCGGTGTCTGGTGCTTTGAGGG
Oligo44	TGATTGCGCTCTCACGCCACGGGACGTTG
Oligo45	ATAACTATGAGTAACACTACCATAGAAAAATCCGAACCACCCAACAGA
Oligo46	CCTTTTTAACCACCAGTTATACTTCAAATATCGCCCTAAAGCGTAAGA
Oligo47	ATTTATCCTGATTATCAGAGGTGGAATTGA
Oligo48	GATGAAGGCTTTGCTCAGCCGGGTCGCCTGTGCCTCCTCATTTCCTG

Oligo49	TCTTCTGATGCACCCATCGAGAACATTGAGCGAGCTATCTAACGTAGA
Oligo50	CCGACCGTTGAAGCCTCGTAGGAAAACTGAACGTAAGCAGTTAAGACT
Oligo51	GCGGATCCGCCATTCGCCAATTGATGGGCG
Oligo52	CGCCAGCAGCACCGCTCGGGCCTCTCCGTGGGGCTTTCATACGTTAAT
Oligo53	GAAAAAGCTAGATTAAGCCCGAATAGAGGAAC
Oligo54	AGTAATAACATTTGAAAATATATGGTAAAACAGAACGTTATTAGACTT
Oligo55	GTAAAGTAAGAAAACAATCGTCGTTAGAACTTATCATTAATAGAT
Oligo56	AACAACATCTGAGCAAATCCTTGATGTTTGGAAAGGAGCGGGAGCACT
Oligo57	CTTTCAGAGCAAGAATGACGCTGAGCTTGATG
Oligo58	TAACCTCACAGCGTGGCAAACGCGGCGGTATGGTCATAAAGTGCCCCC
Oligo59	ATCAATAAATAGCAATCTAATATCAGTTTATTTTACCATTAGCGACAG
Oligo60	CCCATCCTAAGAAAAACCCTGATATGGTTATTAGAGCACTGTAG
Oligo61	TAAAACGAGCCATCAAGTCACGTTTATTAAAA
Oligo62	TAACGCCATGTAGCCAAACAAACGCCGGTTGATCTGGAGCATTAATGC
Oligo63	GCTGCGCGGGATAGAAATAATTTTTTGTT
Oligo64	TGCTATTTCCTAAATTACAGTAGGCTTCTGTAAAAATTAAACATCGGG
Oligo65	GGAGGTTTGTGATAAACAAATTCTCCCTTAGAAAGAAGATATTGCTTT
Oligo66	AGGCAAAGAAACTTAAAAGGGATACGTTCCGGTGCTGGTCCCACGCA
Oligo67	AATAAACATAGCACCATTGTCACAACCCTCAGTCAGACGAGGGTCAGT
Oligo68	AATAAGAAATTTGGGATACCAGCGCTCCCTCAATAAATCCTACAGGAG
Oligo69	ATGAAAATAAGGTGAAACCGATTGATCACCGGCAGTCTCTTTCCAGTA
Oligo70	CATCGTAGAACGGTAATCGTGACAATATGA
Oligo71	GACGACGACCTGAGAGTAATCAGATGTAGGTAAATTTTTAAATTAAGC
Oligo72	AATAACATTATAGAAGGCCCCTGTACGCGAAG
Oligo73	ACAATGAATCGGCTGTCCAAGTACCCATATTTATTTTAGTAAATCCAA
Oligo74	CCCTTTTTAATTTACCGTTTTTAACGCTCATAATGGTTGGGTTAT
Oligo75	ATAGGAACCGGCCAGTGCTTATCCGAGTACTA
Oligo76	GGCCTTCCGGGTTTTCGGAAGGGCCCGTGGTGATTTCTGCCCTTTAGT
Oligo77	AAATACATGAGGCAGGAGCCACCATATTATTCGAACCGCCTGTACCGT
Oligo78	CCTTATTACAAACAAGAGCCGCCTGAGACTAGTACCGCAAACTAC
Oligo79	GAATACCCGGAAAGCGAACCAGAGCGGGGTTTGGAATAGGGCCCTCAT
Oligo80	AAATCAGCCTTTTGCGAGTCAAATCCGTGGGG

Oligo81	ATTTTGTTAGGATAAAAAGATTCAATTCTACTCAAATGGTCCATATAA
Oligo82	CTAGCATCGGAGACGGAGAAGCAAATCGG
Oligo83	ATCACCAGGCCATATTAGAGGGTAAAGCAAGCGAGCATGTGACAAAAG
Oligo84	CTTGAGCCACGATTTTGGAGAATTTCATTACCACAAGAAACGACAATA
Oligo85	ATTCATTAAGCAGCCTTTACAGTACTAAGAAC
Oligo86	GAATCGATACCGTGCAACCGTAATAACTGTTGCCAGTCACGAACGGA
Oligo87	AATCAAGTCACCCTCATGAAACATGGAGTGAGAAAGGAGCGTTAAAGG
Oligo88	CGCGTTTTGGAGGTTTCCTCAAGAATTTTGCTCTTGCTTTCGATATAT
Oligo89	CCTTATTATATAGCCCTGCTCAGTCCAGACGTGATACCGAGACAATGA
Oligo90	TATTCAATATATTTTCATTTCGCAACTAAA
Oligo91	CGGAGAGGACATTTCGAATA
Oligo92	AGGAGGTTACATAAAGACGGAATAAGAGAGATAATTTGCCTTTATCCT
Oligo93	GATATTCACGCAGTAAAAATTCAACAAAGTCATTTATCCGATTAGT
Oligo94	CTGTAATATCATTTTTAAGGTAAAGGTGAGAG
Oligo95	TCAACGCAAAAATTCGTATGTACCGCGGATTGTCTGCCAGCGGAAACC
Oligo96	GCCTTGAGAGGCTCCAAATAGAAAGCAACGGCGTATCATCGAGGCGCA
Oligo97	TGTACTGTTTATCAGAAACAACTCTTTTTCCCAAGCGCACTGACC
Oligo98	AGCGTCATAACAGCTTTAGTAAATTAAAATACAAAACACTGGTGTACA
Oligo99	TTGTACCACCAGACCGATGTTTTACCTAAATG
Oligo100	AATAAAGCATTAGAGATTAATTGCAATGACCATGCGGAATTTTTGCAA
Oligo101	CGCGAGCGCTCAACGAAGCAAATTCAAAT
Oligo102	AGAACCGCTTGCCTTTGAACCGCCATCAATAGTGTTAGCATACCGAAG
Oligo103	GATATAAGGCGTTTGCCATCTCATCGGAAATT
Oligo104	TGTTTAGCCCGTTCTAAGAAAGGCGTCAATCACATTAAATCGCGTCT
Oligo105	AACACTGAGGAGATTTTACAGAGGTGAATAAGGTGAATTACCTTATGC
Oligo106	AACGCCTGCGATTATAATGAGGAACCAAATCACTCATTATACCAGTCA
Oligo107	AGTTAGCGAATACACTGTAATGCCAGTAATCTAATCTACG
Oligo108	GTACGGTTGAATCCCCCTCAAAGACGACGATAAAAAC
Oligo109	TCGTCTTTACCAGGCGATGTACCGGAATTACC
Oligo110	CAAAAAAATAACAGTGTCGGAACCCCCTCAGATAATCAGTAGCAAGGC
Oligo111	GTATCGGGTAATAAGTAAGAGGCACCCTCAAGCGTCAGCAGCAAA
Oligo112	AAAGCGAAAAAACATTGATAAGTGCACTTTCA

Oligo113	AGGTCAGGCTCAGAGCTGGCATCAAAAGGGTGGCTGATAAAAACAAGA
Oligo114	CCGCTTTTTAATCATTGCTTGCCCTGACGAGAGCCGGAACGCCTGATA
Oligo115	TCGGTCGAGAACTGGACGTAACAAAGCTGCGGAACCGAGAAACAA
Oligo116	CAACAACCGGAAGAAATGACAAGAACCGGATAAGATGAACCATCTTTG
Oligo117	ATCGCGTTACGGAACACCCTCGTTTAGACCT
Oligo118	AGATTAAGCATCAGTTTACGAGGCATAGTAAGCGAGAGGCCGTCATAA
Oligo119	GGTAGGAACAACGGAACCCAACCCTCAG
Oligo120	CTTTAAATATCATAAACATTATTACAGGTA
Oligo121	AGTACAACGTTTCGTCGTTTCAGCGAAAGTATTTTTAACGTTGGCCTT
Oligo122	ACCCCCAGTAGCATTCTGTATGGGGAAGGATTTTTGATGATCATTAAA
Oligo123	GGCAAAAGTAACGATCTAAAGATGAGAGGGTT
Oligo124	ATATTCATGTCTGGAAATGCTGTATGAAAAGGATAAAGCTCTTTATT
Oligo125	GACGGTCAATCATAAGTCATTCAGCTTTGAGGTGCAGGGACTTTAATT
Oligo126	AACTTTGAAAGAGGACTTCATTACGTTTCCATCGCATAACCGAGGTGA
Oligo127	GACCAGGCGCATAGGCTGGCTCCAACGAAAGA
Oligo128	CAAAATAGAGCAACACCAGTTCAGCGAAAGACCTCCAAC
Oligo129	TCATCAAGACTACGAAAGCGCGCCTAGTTTTC
Oligo130	GATTTTACTGAGGCTACTAAAGATTCAACAACCAGTACCACCCTC
Oligo131	GGACGTTGATCGCCCATAAACGGGGAATTTTCCACAGACATGTATCAC
Oligo132	TTAATAAAACGAACTATTAATTCGGGCACCAAAATTTTTG
Oligo133	GAAAGATTAGGAAGCCAAAACGAGTGAATATAGTTTCATTCAATAACC
Oligo134	TGGGCGCCAGGGTGGTGCGGTCCAGCCTGGGGGCTCACAAGTGCCTGT
Oligo135	CGTCGGCCACCGAGGAACGGTACGCCAG
Oligo136	TACAAACAATCAGTGATGAAATGGGGCGAGAATTGACGGG
Oligo137	GGTTACCTTCGGCCAAAGTGTAAACGCTGGTTGGTTCCGAAATCGGCA
Oligo138	TCGCAAGACTTTGCCCGAAA
Oligo139	CCGTAAAAGTGTTCAGGCACTCAATGCGGCGGCAGCACGCTTCCACAC
Oligo140	GAATCTTATCAAATATAACAACGCCATAAATCTTACCTTTCGTCAGAT
Oligo141	GCTTTCCGGTTGGGCGGAATTTGTCGTCGCTGGAACGTGCAGCATCAG
Oligo142	CGGAAACGCAGAGCCTAACCCACAGTATTAAACTTTCCTTTTCGAGCC
Oligo143	GGTCATTGCAGTATCGTCGGATTCTTCGCTATAGGCGATTAAACGTAC
Oligo144	AGCCACCACAGCACCGGCCGCCACAAGACACCGTGGCAACAGCAAGAA

Oligo145	CATTAGATGTAGCTATGAGTAATGAAAGCCCCAATTGTAACAACATTA
Oligo146	CAGTTGATTCCAATACTAAATCAAAAAGGAATGAGATTTAGGAATACC
Oligo147	AATTGTGTGCCCAATATAAAGGAATGCCTATTCCCGTATAGCATTGAC
Oligo148	GGATAGCGTCCCAATTGCGGATGGTAGCATTAATTAGCAAGAACCCTC
Oligo149	GTTACTTAAACACCAGCATCGGAAGTCACCCTAAAATCTC
Oligo150	AAGAAGTTTTGCCAGATAACGCCAAAATCAGGGCGGATTGAATTGCTC
Oligo151	GGTTTAATTTCAACTTGCGGGATCCGAG
Oligo152	ATTTCTTAACATGGCTAGGATTAGCCACCACCTTTTCGGTGTCACCGA
Oligo153	TCAATTACGTTCAGCTTATCATATTAGCAAGCAACCTCCCCGTCAAAA
Oligo154	GCGAGGCGCCGGAATCATAATACGTCAATAGTGA
Oligo155	TAAACAACAGTGGGCGGTCATCACACGA
Oligo156	TAATCAAAAGGGAGGGTAACGCAAGGAAACCA
Oligo157	GTAGCTTAGAGCGTACCTTTCATCAAAA

Supporting information for associated publication P3

Supporting Information

Single-Molecule Four-Color FRET Visualizes Energy-Transfer Paths on DNA Origami

By

Ingo H. Stein, Christian Steinhauer and Philip Tinnefeld

published in

J. Am. Chem. Soc. 2011, 133, 4193–4195

Supporting Information

Single-Molecule Four-Color FRET Visualizes Energy Transfer Paths on DNA Origami

Ingo H. Stein[†‡], Christian Steinhauer[†‡], Philip Tinnefeld[‡§] *

[†]Angewandte Physik – Biophysik, Ludwig-Maximilians-Universität, Amalienstraße 54, 80799 Munich, Germany, [‡]Center for NanoScience, Ludwig-Maximilians-Universität, Schellingstr. 4, 80799 Munich, Germany, [§]Physical and Theoretical Chemistry, NanoBioScience, TU Braunschweig, Hans-Sommer-Str. 10, 38106 Braunschweig, Germany

*To whom correspondence should be addressed;

Email: p.tinnefeld@tu-braunschweig.de

1 Experimental setup

To study the energy transfer pathways of four interacting dyes, a custom built confocal setup was used as shown in Figure S1. It represents a four-color extension of the setup described previously in ref. [1] and allows performing alternating laser excitation (ALEX)[2] and independent detection of four spectrally separated fluorophores. Excitation was carried out by a pulsed supercontinuum laser (Koheras SuperK Extreme, NKT Photonics, Denmark) with the following four wavelengths that were selected with the provided AOTF: 495 nm (blue), 568 nm (green), 650 nm (red) and 725 nm (IR). The laser was alternated on the microsecond timescale by a second acousto-optical tunable filter (AOTFnc-VIS, AA optoelectronic) with a total alternation period of 100 µs (blue: 0 - 30 µs, green: 30 - 50 µs, red: 50 - 70 µs, IR: 70 – 100 µs). The laser was coupled into a polarization maintaining single mode fiber. The AOBS (provided by Leica Microsystems) was used to spectrally separate the excitation light from the fluorescence light. After passing the AOBS the light beam is expanded to match the rear aperture of the objective (60X, NA 1.20, UPlanSApo 60XW, Olympus) by an achromatic telescope and guided to the microscope (Olympus IX70) (see Figure S1).

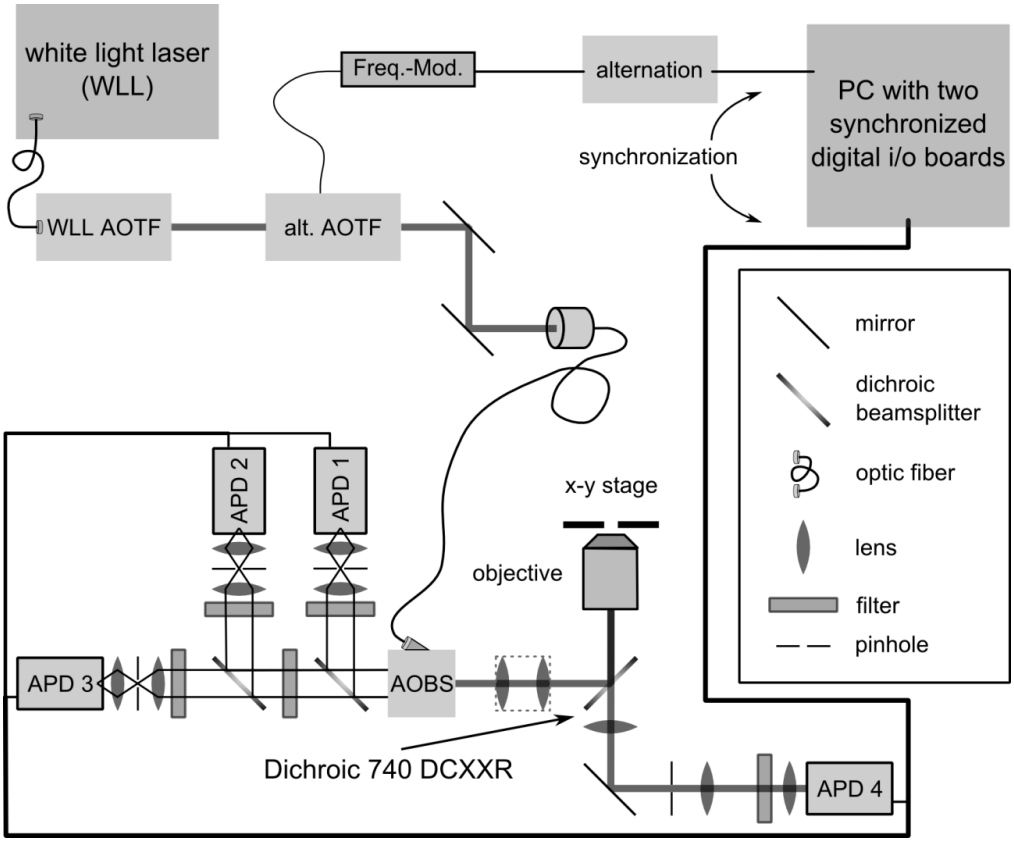

Figure S1: Confocal single-molecule 4-color ALEX setup

The fluorescence light is collected by the same objective and split by a dichroic mirror (740 DCXXR, AHF Analysentechnik). Thus the fluorescence of the IR-dye passes the dichroic and is coupled out from the bottom port of the microscope. The blue, green and red fluorescence light is reflected back to the left detection arm, where fluorescence light is separated into the respective detection channels for blue (APD1), green (APD 2) and red (APD 3) as described previously.[1] IR light is filtered by an emission filter (Brightline HC 785/62, AHF Analysentechnik) in front of APD 4.

Synchronization between excitation and detection is carried out by employing two coupled PC boards (PXI-6602, National Instruments) that are used to collect the data from the four avalanche photo diodes (SPCM, AQR 14, Perkin Elmer) and which trigger each alternation cycle in combination with two pulse/delay generators (DG535, Stanford Research Systems).

2 Sample preparation

The rectangular DNA origami design from Rothemund's original publication was used for all experiments.[3] Modifications to the design are shown in the table below.

Table S1: Modifications to DNA origami staple strands

Original staple name	Original sequence	Modification
r3t10e	TATTTTGCTCCCAATCCAAATAAGTGAGTTAA	Atto647N at position 3
r5t8f	ATACCCAAGATAACCCACAAGAATAAACGATT	Atto565 at position 26
r5t10f	TTTTGTTTAAGCCTTAAATCAAGAATCGAGAA	Atto488 at position 8
r5t10e	AGGTTTTGAACGTCAAAAATGAAAGCGCTAAT	Atto565 at position 30
r7t8f	TTATTACGGTCAGAGGGTAATTGAATAGCAGC	Alexa750 at position 21

Unmodified staple strands were supplied by DNA Technology A/S (Risskov, Denmark) and used without further purification. Fluorescently labeled staple strands (HPLC grade) were purchased from IBA (Göttingen, Germany). For folding the DNA origami, 3nM M13mp18 viral DNA (NEB, Ipswish, USA) 30nM unmodified staples and 300nM labeled staples were heated in a thermocycler (Eppendorf, Germany) to 95°C and cooled down to 20°C within 1.5 hours in the presence of 12.5 mM $MgCl_2$.
After folding, excess staple strands were removed using Amicon Ultra-0.5 mL Centrifugal Filters (100,000 MWCO) according to manufacturer's instructions.

Single-molecule fluorescence measurements were carried out at room temperature (22° C) in standard phosphate buffered saline (PBS) with oxygen removal using an enzymatic oxygen-scavenging system (PBS, pH = 7.4, containing 10% (w/v) glucose and 12.5% (v/v) glycerine, 50 µg ml^{-1} glucose oxidase, 100–200 µg ml^{-1} catalase, and 0.1 mM tris(2-carboxyethyl)phosphine hydrochloride (TCEP)). Additionally, 2 mM Trolox were added to reduce blinking and bleaching according to the ROXS scheme.[4-5] The solution based measurements were performed on glass-slides, which were prepared with perforated adhesive silicone sheets (Grace Bio-Labs, OR) to enable small sample volumes of 50 µl. To prevent DNA accumulation at the surface these custom sample chambers were incubated with BSA (1 mg ml^{-1} BSA in PBS) prior to measurements.

3 Analysis of 4c-ALEX measurements

3.1 Experimental photon counts

Applying alternating laser excitation, ten distinct photon-count streams are recorded corresponding to four different excitation wavelengths and the respective detection channels (see Table S2). In solution measurements, fluorescence bursts from single molecules diffusing through the laser focus are identified by a burst search algorithm applied to the sum of all photons (parameters used: T = 5 ms, M = 90, L = 150).[6]

Table S2: matrix of the photon-streams obtained in 4c-ALEX

	detection channel			
excitation ↓	blue	green	red	IR
blue	F_b^b	F_b^g	F_b^r	F_b^{ir}
green	-	F_g^g	F_g^r	F_g^{ir}
red	-	-	F_r^r	F_r^{ir}
IR	-	-	-	F_{ir}^{ir}

Here F_X^Y stands for the photon counts detected in channel Y due to excitation at wavelength X. Taking a measurement solely with buffer the photon counts F_X^Y can be individually corrected for background; this yields photon counts $F_{X,bkg}^Y$.

In Figure S2 a section of a time transient of origami constructs diffusing through the laser focus is shown for the origami sample with the green jumper dye between the blue and IR dye. The highlighted diffusion events in the figure represent subpopulations with the following composition: i) missing green dye, ii) missing blue and IR dye, iii) missing IR dye and iv) intact.

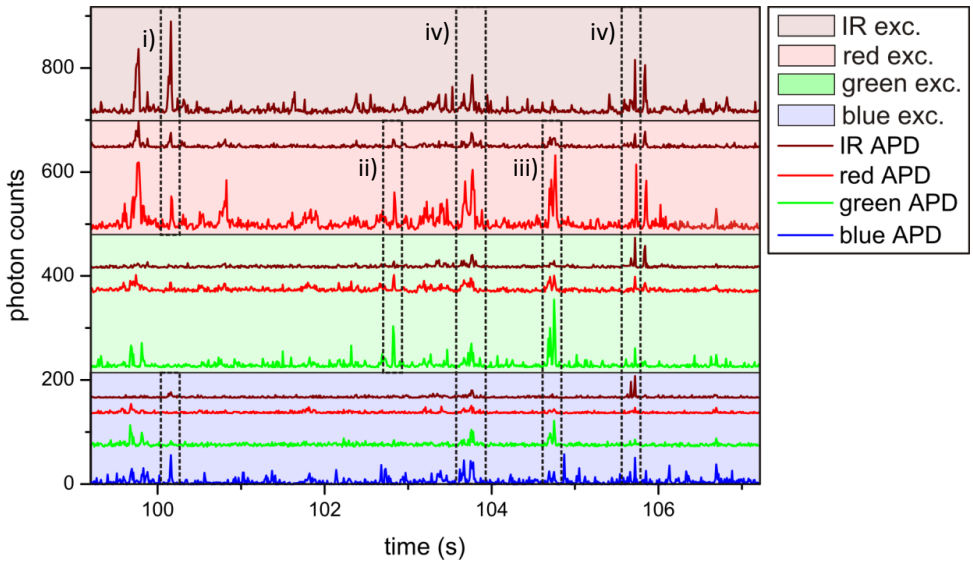

Figure S2: Single-molecule time transient of origami molecules diffusing through the laser focus (10 ms binning). Five events of diffusing molecules with different compositions are highlighted for discussion in the text.

3.2 Direct excitation and leakage

Direct excitation and leakage corrections were performed as described in detail in ref.[1]. Extending to the four-color scheme a total of six leakage and six direct excitation factors have to be taken into account. For the respective measurements, origami constructs with only a single fluorophore attached were prepared.

Table S3: Determination of direct excitation and leakage

	Ratio*	**measurement of**	**obtained value**
dx_b^g	F_b^g/F_g^g	green dye only	6.5%
dx_b^r	F_b^r/F_r^r	red dye only	2.0%†

dx_b^{ir}	F_b^{ir}/F_{ir}^{ir}	ir dye only	1.2%
dx_g^r	F_g^r/F_r^r	red dye only	10.2%
dx_g^{ir}	F_g^{ir}/F_{ir}^{ir}	ir dye only	2.7%
dx_r^{ir}	F_r^{ir}/F_{ir}^{ir}	ir dye only	14.1%
le_b^g	F_b^g/F_b^b	blue dye only	8.6%
le_b^r	F_b^r/F_b^b	blue dye only	1.6%
le_b^{ir}	F_b^{ir}/F_b^b	blue dye only	0.0%
le_g^r	F_g^r/F_g^g	green dye only	22.3%
le_g^{ir}	F_g^{ir}/F_g^g	green dye only	4.4%
le_r^{ir}	F_r^{ir}/F_r^r	red dye only	18.9%

** For notational simplicity "bkg" was omitted here, although background corrected photon counts were used.*
†The value for the measurement of the origami sample with solely a red dye attached yielded $dx_b^r = 4.7\%$. This value led to negative mean FRET related ratios of E_{br}^* for the origami sample with r-b-g-ir stoichiometry that are physically not reasonable (distance blue-red is approx. 9.3nm, which theoretically implies E_{br}^*= 0.03). Since the value of E_{br}^* is very sensitive to minute changes in the value of direct excitation of the red dye by the blue laser we set E_{br}^* to zero and used this value to calibrate dx_b^r. This procedure has no influence on the relative positions of peaks in the histograms and is likely related to small setup (laser) instabilities.

3.3 Crosstalk corrected photon-counts

Utilizing the experimentally obtained direct excitation and leakage values the crosstalk corrected photon-counts are calculated as follows:

S1) $$ {}^{b}F_b^b = F_{b,bkg}^b $$

S2) $$ {}^{g}F_g^g = F_{g,bkg}^g $$

S3) $$ {}^{r}F_r^r = F_{r,bkg}^r $$

S4) $$ {}^{ir}F_{ir}^{ir} = F_{ir,bkg}^{ir} $$

S5) $$ {}^{r\to ir}F_r^{ir} = F_{r,bkg}^{ir} - le_r^{ir}\,{}^{r}F_r^r - dx_r^{ir}\,{}^{ir}F_{ir}^{ir} $$

S6) $$ {}^{g\to r}F_g^r = F_{g,bkg}^r - le_g^r\,{}^{g}F_g^g - dx_g^r\,{}^{r}F_r^r $$

S7) $$ {}^{b\to g}F_b^g = F_{b,bkg}^g - le_b^g\,{}^{b}F_b^b - dx_b^g\,{}^{g}F_g^g $$

S8) $$ {}^{g\to ir}F_g^{ir} + {}^{g\to r\to ir}F_g^{ir} = F_{g,bkg}^{ir} - le_g^{ir}\,{}^{g}F_g^g - dx_g^r le_r^{ir}\,{}^{r}F_r^r - dx_g^{ir}\,{}^{ir}F_{ir}^{ir} - le_r^{ir}\,{}^{g\to r}F_g^r - $$
$$ - dx_g^r\,{}^{r\to ir}F_r^{ir} $$

S9) $$ {}^{b\to r}F_b^r + {}^{b\to g\to r}F_b^r = F_{b,bkg}^r - le_b^r\,{}^{b}F_b^b - le_g^r\,{}^{b\to g}F_b^g - dx_b^r\,{}^{r}F_r^r - dx_b^g le_g^r\,{}^{g}F_g^g - dx_b^g\,{}^{g\to r}F_g^r $$

S10) $$ {}^{b\to FRET\to ir}F_b^{ir} = F_{b,bkg}^{ir} - le_b^{ir}\,{}^{b}F_b^b - le_g^{ir}dx_b^g\,{}^{g}F_g^g - dx_b^r le_r^{ir}\,{}^{r}F_r^r - dx_b^{ir}\,{}^{ir}F_{ir}^{ir} - $$
$$ - le_g^{ir}\,{}^{b\to g}F_b^g - le_r^{ir}\left({}^{b\to r}F_b^r + {}^{b\to g\to r}F_b^r + dx_b^g\,{}^{g\to r}F_g^r\right) - dx_b^g\left({}^{g\to ir}F_g^{ir} + $$
$$ + {}^{g\to r\to ir}F_g^{ir}\right) - dx_b^r\,{}^{r\to ir}F_r^{ir} $$

Here, ${}^{Z}F_X^Y$ represents the sub-photon-counts originating from source Z upon excitation of laser X and detection by detector Y. Z can either stand for one of the four fluorophores (b, g, r or ir) or for a FRET-related source (b→g, b→r, b→ir, g→r, g→ir, r→ir, b→g→r, b→g→ir, b→r→ir, g→r→ir or b→g→r→ir). In formula S10) b→FRET→ir stands for all four FRET related sources where blue excitation leads to infrared fluorescence emission.

3.4 FRET related ratios

With the crosstalk corrected photon counts six FRET-related ratios E* are obtained which approximate the corresponding values of E:

S11) $$E^*_{bg} = \frac{{}^{b\rightarrow g}F_b^g}{{}^{b\rightarrow g}F_b^g + {}^{b}F_b^b}$$

S12) $$E^*_{br} = \frac{{}^{b\rightarrow r}F_b^r + {}^{b\rightarrow g\rightarrow r}F_b^r}{{}^{b\rightarrow r}F_b^r + {}^{b\rightarrow g\rightarrow r}F_b^r + {}^{b}F_b^b}$$

S13) $$E^*_{bir} = \frac{{}^{b\rightarrow FRET\rightarrow ir}F_b^{ir}}{{}^{b\rightarrow FRET\rightarrow ir}F_b^{ir} + {}^{b}F_b^b}$$

S14) $$E^*_{gr} = \frac{{}^{g\rightarrow r}F_g^r}{{}^{g\rightarrow r}F_g^r + {}^{g}F_g^g}$$

S15) $$E^*_{gir} = \frac{{}^{g\rightarrow ir}F_g^{ir} + {}^{g\rightarrow r\rightarrow ir}F_g^{ir}}{{}^{g\rightarrow ir}F_g^{ir} + {}^{g\rightarrow r\rightarrow ir}F_g^{ir} + {}^{g}F_g^g}$$

S16) $$E^*_{rir} = \frac{{}^{r\rightarrow ir}F_r^{ir}}{{}^{r\rightarrow ir}F_r^{ir} + {}^{r}F_r^r}$$

FRET related ratios are not corrected for different dye quantum yields and detection sensitivities.

3.5 The output ratio

To quantify the switching readout reliability of the designed origami constructs the following output ratio was used. It is defined as the corrected photon counts in the red output channel divided by the corrected photon counts in the red and IR output channels, all during blue excitation (see formulas S9 and S10):

S17) $$output\ ratio = \frac{{}^{b\rightarrow r}F_b^r + {}^{b\rightarrow g\rightarrow r}F_b^r}{{}^{b\rightarrow r}F_b^r + {}^{b\rightarrow g\rightarrow r}F_b^r + {}^{b\rightarrow FRET\rightarrow ir}F_b^{ir}}$$

3.6 Stoichiometries

In complex systems, sample heterogeneity with various subpopulations that do not exhibit all dyes has to be considered. With the aid of stoichiometric ratios and corresponding S-S-histograms,[2] the subpopulations of interest were identified and selected for further analysis.[7-8] The following definitions for S were used:

S18) $$S_{XY} = F_X/(F_X + F_Y)$$

where X and Y stand for the same pairs of b, g, r and ir as in equations S11) – S16) and $F_b = F^b_{b,bkg} + F^g_{b,bkg} + F^r_{b,bkg} + F^{ir}_{b,bkg}$, $F_g = F^g_{g,bkg} + F^r_{g,bkg} + F^{ir}_{g,bkg}$, $F_r = F^r_{r,bkg} + F^{ir}_{r,bkg}$ *and* $F_{ir} = F^{ir}_{ir,bkg}$

To calibrate the setup, such that an S value of approximately 0.5 is achieved for a sample with 1:1 fluorophore stoichiometry, the intensities of the corresponding laser wavelengths had to be adjusted.

3.7 Population selection

An exemplary workflow for the final selection of the correct species for further data analysis is shown in Figure S3 for the origami construct with the green jumper dye between the blue and the IR dye.

In the upper left of Figure S3 the E*S-histogram for the energy transfer from blue to IR is shown for all acquired bursts. The desired population in the center of the histogram is smeared out by

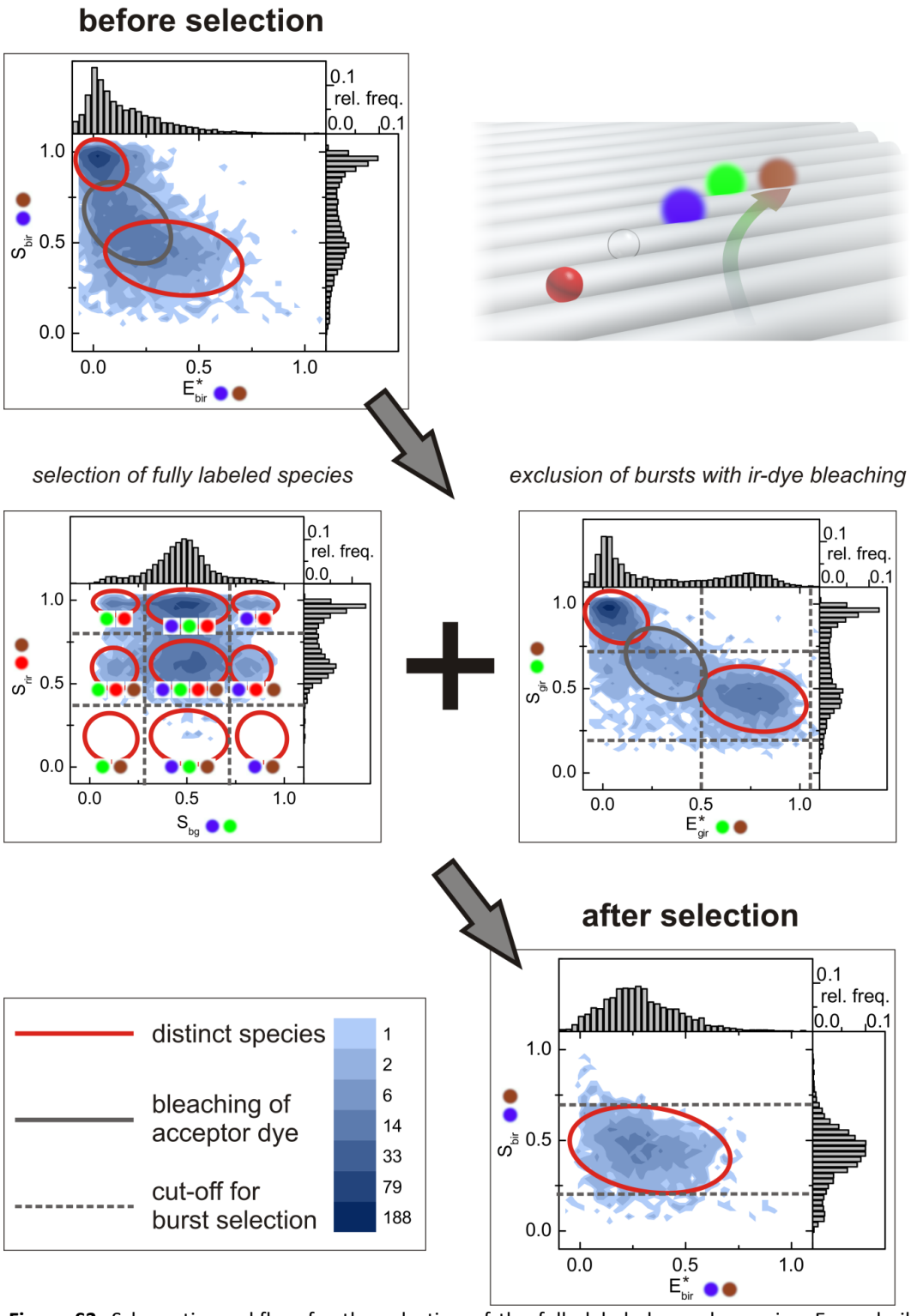

Figure S3: Schematic workflow for the selection of the fully labeled sample species. Exemplarily, species selection is shown for the origami construct with the green jumper dye placed between the blue and IR dye.

bleaching of the IR dye (marked by the grey ellipse). Especially, the E^*_{bir}-histogram plotted at the top is dominated by the sample species with no active IR-dye attached.

In the second row two histograms are shown that enable the selection of the desired bursts. The SS-histogram on the left shows distinct dye configurations for the measured sample that are a result of incomplete labeling, incomplete sample formation or premature photobleaching. The desired central population was selected by applying the appropriate thresholds for the stoichiometry parameters indicated by dashed grey lines. The absence of bursts in the lower third of this histogram indicates that the presence of the IR dye Alexa Fluor 750 is significantly lower than that of all other dyes used. This is related to an inactive fraction of this fluorophore as discussed in the main text. The E*S-histogram for the energy transfer from green to IR can be used to further refine the burst selection, especially to exclude those bursts where IR-dye bleaching occurs, for further analysis. This selection is applied with the indicated thresholds for E^*_{gir} and S_{gir}.
The resulting E*S-histogram for blue-IR after this selection is plotted in the lower right of Figure S3. The desired population is now clearly visible in the center of the histogram, and the E^*_{bir}-histogram shows the familiar Gaussian shape. Finally, the indicated thresholds for S_{bir} are applied to the remaining bursts to finalize the selection process.
For the other origami samples, the population selection was performed accordingly by applying appropriate thresholds.

References:

(1) Person, B.; Stein, I. H.; Steinhauer, C.; Vogelsang, J.; Tinnefeld, P. *ChemPhysChem* **2009**, *10*, 1455.
(2) Kapanidis, A. N.; Lee, N. K.; Laurence, T. A.; Doose, S.; Margeat, E.; Weiss, S. *Proc. Natl. Acad. Sci. U. S. A.* **2004**, *101*, 8936.
(3) Rothemund, P. W. *Nature* **2006**, *440*, 297.
(4) Cordes, T.; Vogelsang, J.; Tinnefeld, P. *J Am Chem Soc* **2009**, *131*, 5018.
(5) Vogelsang, J.; Kasper, R.; Steinhauer, C.; Person, B.; Heilemann, M.; Sauer, M.; Tinnefeld, P. *Angew Chem Int Ed* **2008**, *47*, 5465.
(6) Eggeling, C.; Berger, S.; Brand, L.; Fries, J. R.; Schaffer, J.; Volkmer, A.; Seidel, C. A. M. *J. Biotechnol.* **2001**, *86*, 163.
(7) Lee, N. K.; Kapanidis, A. N.; Koh, H. R.; Korlann, Y.; Ho, S. O.; Kim, Y.; Gassman, N.; Kim, S. K.; Weiss, S. *Biophys J* **2007**, *92*, 303.
(8) Ross, J.; Buschkamp, P.; Fetting, D.; Donnermeyer, A.; Roth, C. M.; Tinnefeld, P. *J Phys Chem B* **2007**, *111*, 321.

Full list of publications

G. P. Acuna, M. Bucher, **I. H. Stein**, C. Steinhauer, A. Kuzyk, P. Holzmeister, R. Schreiber, A. Moroz, F. D. Stefani, T. Liedl, F. C. Simmel, and P. Tinnefeld. Distance dependence of single-fluorophore quenching by gold nanoparticles studied on DNA origami. *ACS Nano*, 6(4):3189–3195, Mar 2012.

I. H. Stein, S. Capone, J. H. Smit, F. Baumann, T. Cordes, and P. Tinnefeld. Linking single-molecule blinking to chromophore structure and redox potentials. *ChemPhysChem*, 13(4):931-937, Mar 2012 (incl. cover feature).

I. H. Stein, P Tinnefeld. Single-molecule FRET and super-resolution: DNA nanostructures organize dyes for nanophotonic apps. *GIT Imaging and Microscopy*, 3, Jun 2011.

I. H. Stein, C. Steinhauer, and P. Tinnefeld. Single-molecule four-color FRET visualizes energy-transfer paths on DNA origami. *J. Am. Chem. Soc.*, 133(12):4193-4195, Mar 2011 (incl. cover feature).

I. H. Stein*, V. Schüller*, P. Böhm, P. Tinnefeld, and T. Liedl. Single-molecule FRET ruler based on rigid DNA origami blocks. *ChemPhysChem*, 12(3):689-695, Feb 2011. *equal contribution

J. Vogelsang, C. Steinhauer, C. Forthmann, **I. H. Stein**, B. Person-Skegro, T. Cordes, and P. Tinnefeld. Make them blink: probes for super-resolution microscopy. *Chemphyschem*, 11(12):2475-2490, Aug 2010.

B. Person, **I. H. Stein**, C. Steinhauer, J. Vogelsang, and P. Tinnefeld. Correlated movement and bending of nucleic acid structures visualized by multicolor single-molecule spectroscopy. *ChemPhysChem*, 10(9-10):1455-1460, Jul 2009.

T. Cordes, **I. H. Stein**, C. Forthmann, C. Steinhauer, M. Walz, W. Summerer, B. Person, J. Vogelsang and P. Tinnefeld. Controlling the emission of organic dyes for high sensitivity and super-resolution microscopy. *Proc SPIE*, 7367:73671D, Jun 2009.

Acknowledgement

Many people contributed to the success of this thesis and without them the last years wouldn't have been half the fun. I would especially like to thank a number of people:

- Philip Tinnefeld for the opportunity to work in his group and on this exciting topic, for his professional support and great discussions. Philip, I really had a great time!
- Christian Steinhauer for fruitful collaboration in the four-color project, assistance with all types of LabVIEW issues and as a valuable discussion partner.
- Verena Schüller for making the extra hours during the FRET ruler project in the lab and in Venice more enjoyable. I will never forget the submission process together with Philip directly from the island San Servolo.
- Tim Liedl and his group for advice in DNA origami related topics and excellent collaboration.
- Thorben Cordes for the successful cooperation and valuable discussions, not just on the nature of blinking molecules.
- Jan Vogelsang for setting up the basis for the confocal setup that all the measurements of this thesis rely upon.
- Phil Holzmeister for his tireless support with LabVIEW-based issues and as challenging discussion partner for confocal measurements.
- Angelika Kardinal and Thomas Nicolaus for advice and assistance in the chemistry lab.
- CeNS and the IDK-NBT for providing a remarkable scientific atmosphere and for making the Junior Nanotech Network with Urbana-Champaign possible, especially Marilena Pinto, Marie-Christine Blüm and Susanne Hennig.
- The excellence cluster NIM for funding and contributing to the exceptional scientific environment in Munich, especially Peter Sonntag, Birgit Gebauer and Christoph Hohmann.
- Dieter Braun and his group for scientific discussions, movies in the lab and the amazing espresso, especially Christof Mast and Hubert Krammer.
- Hermann Gaub and the entire LS Gaub for the great research conditions and a very inspiring working atmosphere. Stefan Stahl, Stephan Heucke, Philip Severin, Mathias Strackharn, Marcus Otten, Daniela Aschenbrenner, Martin Benoit, Stefan Scheuer, ...
- All former and current members of the AG Tinnefeld for the amazing team spirit including Andreas Gietl, Guillermo Acuna (Amazing Asados!), Fabian Baumann, Martina Bucher, Sarah Schulz, Dina Grohmann, Carsten Forthmann, Jürgen Schmied, Stella Capone, Philipp Schwarz...

Finally, I would like to thank my parents Jutta and Lothar for their financial support and great encouragement during my whole education. And last but not least I thank Steffi for her personal support, encouragement and understanding.